Spring 2012

HVAC system study: a data-driven approach

Guanglin Xu
University of Iowa

HVAC SYSTEM STUDY: A DATA-DRIVEN APPROACH

by

Guanglin Xu

A thesis submitted in partial fulfillment
of the requirements for the Master
of Science degree in Industrial Engineering
in the Graduate College of
The University of Iowa

May 2012

Thesis Supervisor: Professor Andrew Kusiak

Graduate College
The University of Iowa
Iowa City, Iowa

CERTIFICATE OF APPROVAL

_____

MASTER'S THESIS

_____

This is to certify that the Master's thesis of

Guanglin Xu

has been approved by the Examining Committee
for the thesis requirement for the Master of Science
degree in Industrial Engineering at the May 2012
graduation.

Thesis Committee: _____
Andrew Kusiak, Thesis Supervisor

_____
Yong Chen

_____
Pavlo Krokhmal

To My Father

And most important, have the courage to follow your heart and intuition

- Steve Jobs

ACKNOWLEDGMENTS

First of all, I would like to express my special thanks to my advisor, Prof. Andrew Kusiak, for his continuous devotion, great motivation, invaluable support, and intellectual guidance to this research. He has been the most instrumental person for my academic research achievements which have prepared me for the challenges of future life. I think that this invaluable experience has allowed me to maintain a balance between theory and practice leading to realistic solutions.

I would like to acknowledge Prof. Yong Chen and Prof. Pavlo Krokhmal for serving on my Thesis Committee and providing invaluable suggestions and feedback on my research.

I would like to thank my parents and my wife, Shuai Shi, who have solidly supported me with love and advices in my academic pursuing over years.

I am also grateful for the financial support from Iowa Energy Center. The energy experts from Iowa Energy Center have extended invaluable information and effort for this research.

Finally, but most importantly, I thank all the members of the Intelligent Systems Laboratory who have worked with and supported me through kinds of ways. I would like to thank (soon to be Dr.) Zijun Zhang for sharing his successful experience on research. I thank (soon to be Dr.) Anoop Verma for discussing with me my research. I would like to thank Fan Tang for providing me with valuable suggestions for my research. I thank Xiupeng Wei and Maciej Rysz for motivating my research directions. I also thank Yaohui Zeng, a talented person, for working with me on the same project.

ABSTRACT

The energy consumed by heating, ventilating, and air conditioning (HVAC) systems has been increasing over the last decades. Thus, improving efficiency of HVAC systems has gained attention of industry and academia. This concern has posed challenges for modeling and optimizing HVAC systems. The traditional methods, such as analytical and statistical approaches, usually involve assumptions that may not hold in practice since HVAC systems are complex, nonlinear, and dynamic.

Data-mining is a novel science aiming at extracting system characteristics, identifying models and recognizing patterns from large-size data sets. It has proved its power in modeling complex and nonlinear systems through various effective and successful applications in industrial, business, and medical areas. Applications of classical data-mining approaches, such as neural networks and boosting tree have been reported in the HVAC literature. Evolutionary computation, including swarm intelligence, have rapidly developed in the past decades and then applied to improving the performance of HVAC systems.

This research focuses on modeling, optimizing, and controlling HVAC systems. Data-mining algorithms are utilized to extract predictive models from experimental data sets provided by the Energy Resource Station located in Ankeny, IA. Evolutionary algorithms are employed to optimize models formulated based on the data-driven approach. In the optimization process, two set points of the HVAC system, supply air duct static pressure set point and supply air temperature set point, are controlled aiming at improving energy efficiency and maintaining thermal comfort.

The methodology presented in this Thesis is applicable to various industrial processes other than HVAC systems.

TABLE OF CONTENTS

LIST OF TABLES viii

LIST OF FIGURES x

CHAPTER1. INTRODUCTION 1

1.1 Review of simulation models of HVAC systems 3
1.2 Review of analytic models of HVAC systems 4
1.3 Review of data-driven models of HVAC systems 6
1.4 Computational intelligence and optimization 7
1.5 Thesis structure 8

CHAPTER 2. OPTIMIZATION OF HVAC SYSTEMS WITH AN INTERIOR-POINT METHOD 9

2.1 Introduction 9
2.2 Problem description 9
2.3 Data description 11
2.4 Parameter selection 12
2.5 HVAC system modeling 14
2.5.1 Model formulation 14
2.5.2 Model validation 16
2.6 Model optimization 20
2.6.1 Optimization model formulation 20
2.6.2 Nonlinear interior-point algorithm 21
2.6.3 Case study 23
2.7 Summary 29

CHAPTER 3. MODELING AND OPTIMIZATION OF HVAC SYSTEM USING A DYNAMIC NEURAL NETWORK 30

3.1 Introduction 30
3.2 Solution methodology 30
3.2.1 Nonlinear autoregressive with external inputs 30
3.2.2 Problem formulation 31
3.3 HVAC predictive model 32
3.3.1 Data description 32
3.3.2 Parameter selection 33
3.3.3 Model construction 37
3.3.4 Model validation 39
3.4 Model Optimization 40
3.4.1 Optimization model formulation 40
3.4.2 Multi-objective particle swarm optimization algorithm 42
3.4.3 Optimization results and analysis 45
3.5 Model implementation and result analysis 51
3.6 Summary 54

CHAPTER 4. CONTROLLING AN HVAC SYSTEM WITH SWARM INTELLIGENCE AND DATA-DRIVEN APPROACH 56

4.1 Introduction....56
4.2 Data description....57
4.3 Control of the HVAC system....58
4.4 Model development....62
4.4.1 Parameter selection....62
4.4.2 Predictive model formulation....62
4.4.3 Model validation....64
4.5 Multi-objective optimization model....68
4.5.1 Optimization model formulation....68
4.5.2 Multi-objective rule-based particle swarm optimization algorithm....71
4.6 Computational results....73
4.6.1 Representative points used in optimization....73
4.6.2 Optimization of multiple data points....76
4.7 Summary....79

CHAPTER 5. CONCLUSION....81

REFERENCES....83

LIST OF TABLES

Table 2.1 Description of data sets 12

Table 2.2 Parameters selected for building HVAC system energy consumpiton model 13

Table 2.3 Parameters selected for building HVAC system indoor temperature model 14

Table 2.4 Parameters selected for modeling energy consumpiton at time stamp *t* 15

Table 2.5 Parameters selected for modeling indoor temperature at time stamp *t* 16

Table 2.6 Peformance of the models predicting HVAC system energy consumption and indoor temperature 18

Table 2.7 Performance of the simulation models of energy consumption and indoor temperature 18

Table 2.8 The simulated internal heating load of the HVAC system 26

Table 3.1 Description of data sets 33

Table 3.2 Candidate parameters selected based on domain knowledge 34

Table 3.3 The parameters selected for building energy consumption model at time $t + d$ 37

Table 3.4 The parameters selected for building the indoor temperature model at time $t + d$ 38

Table 3.5 Prediction accuracy of the MLP ensemble algorithm of energy consumption and room temperature 39

Table 3.6 Settings for the three multi-objective PSO variants 47

Table 3.7 Two scenarios involving different weight values 47

Table 3.8 Performance of the three multi-objective PSO variants 48

Table 4.1 Description of data sets. 57

Table 4.2 Rules for deciding the intervals of the supply air temperature set point 61

Table 4.3 Parameters selected for building the energy consumption model 62

Table 4.4 Parameters selected for building the indoor temperature model 64

Table 4.5 Performance of the MLP ensemble models of energy consumption and indoor temperature 65

Table 4.6 Nine representative points selected from the validation data set.....75

Table 4.7 Three weight scenarios for energy consumption and indoor temperature preference.....75

LIST OF FIGURES

Figure 1.1 The schematic diagram for a typical air handling unit system 1

Figure 1.2 The schematic diagram for a typical single-room variable-air-volume box.....2

Figure 2.1 The schematic diagram of a typical HVAC system.....10

Figure 2.2 The correlation coefficient of the observed and predicted values of HVAC system energy consumption.....18

Figure 2.3 The correlation coefficient of the observed and predicted values of indoor temperature 19

Figure 2.4 Observed and predicted values of HVAC system enregy consumption 19

Figure 2.5 Observed and predicted values of HVAC system indoor temperature 20

Figure 2.6 Simulated value of energy consumption in the period 07/15/2011 – 07/16/2011 24

Figure 2.7 Simulated value of indoor temperature in the period 07/15/2011 – 07/16/2011 25

Figure 2.8 Comparison between the optimized and simulated HVAC system energy consumption 27

Figure 2.9 Comparison between the optimized and simulated HVAC system inoor temperature 27

Figure 2.10 Comparison between optimized and observed values for supply air duct static pressure set point 28

Figure 2.11 Comparison between optimized and observed values for supply air temperature set point.....28

Figure 2.12 Comparison between the optimized and simulated total energy consumption based on the 48 data points 29

Figure 3.1 The correlation coefficient between energy consumption and its previous values at different time steps.....35

Figure 3.2 The correlation coefficient between room temperature and its previous values at different time steps.....35

Figure 3.3 The correlation coefficient between energy consumption and room temperature at different time steps.....36

Figure 3.4 The correlation coefficient between energy consumption and supply air fan speed at different time steps.....36

Figure 3.5 Validation of the energy consumpiton model with 442 data instances 40

Figure 3.6 Validation of the room temperature model with 442 data instances 40

Figure 3.7 The flow chart of multi-objective particle swarm optimization algorithm 46

Figure 3.8 Comparison between the observed and optimized energy consumption in Scenario 1 49

Figure 3.9 Comparison between the observed and optimized energy consumption in Scenario 2 49

Figure 3.10 Comparison between the observed and optimized room temperature in Scenario 1.....50

Figure 3.11 Comparison between the observed and optimized room temperature in Scenario 2.....50

Figure 3.12 Recommended supply air temperature set point compared to the observed value in Scenario 1 51

Figure 3.13 Recommended supply air duct static pressure set point compared to the observed value in Scenario 1 51

Figure 3.14 Energy consumption of AHU-A and AHU-B at the first stage 53

Figure 3.15 Room temperature of AHU-A and AHU-B at the first stage.....53

Figure 3.16 Comparison of energy consumption of AHU-A and AHU-B for the same set points at the second stage 54

Figure 3.17 Comparison of the bias-adjusted energy consumption of AHU-A and AHU-B.....54

Figure 4.1 The schematic diagram of a typical HVAC system.....56

Figure 4.2 Set point and actual supply air temperatue 58

Figure 4.3 Set point and actual static pressure in suppy air duct 59

Figure 4.4 Diagram of the HVAC system control.....60

Figure 4.5 The membership function of the supply air temperature set point 61

Figure 4.6 The membership function of the indoor temperature 61

Figure 4.7 The correlation coefficient between predicted and observed values for 1-increment ahead prediction of energy consumption.....66

Figure 4.8 The correlation coefficient between predicted and observed values for 2-increment ahead prediction of energy consumption.....66

Figure 4.9 The correlation coefficient between predicted and observed values for 1-increment ahead prediction of indoor temperature 67

Figure 4.10 The correlation coefficient between predicted and observed values for 2-increment ahead prediction of indoor temperature 67

Figure 4.11 The observed and optimized energy consumption for the three scenarios 74

Figure 4.12 The observed and optimized indoor temperature at time $t + T$ for the three scenarios 76

Figure 4.13 The observed and optimized indoor temperature at time $t + 2T$ for the three scenarios 76

Figure 4.14 The sum of the observed and optimized energy consumption of the 100 points for the three scenarios 77

Figure 4.15 The observed and optimized indoor temperature at time $t + T$ for the three scenarios 78

Figure 4.16 The observed and optimized indoor temperature at time $t + 2T$ for the three scenarios 78

Figure 4.17 The recommended set point of the supply air static pressure at $t + T$ and $t + 2T$ 79

Figure 4.18 The recommended set point of the supply air temperature at $t + T$ and $t + 2T$ 79

CHAPTER 1

INTRODUCTION

Heating Ventilating and Air Conditioning (HVAC) systems are designed to control the indoor environment including indoor air quality and thermal comfort for occupants. HVAC systems are used in residential and commercial buildings worldwide. Figures 1.1 -1.2 illustrate schematic diagrams of a typical air handling unit (AHU) system and a typical single-room variable-air-volume box. According to the literature [1, 2], HVAC systems account for over 60% of the energy consumed by buildings and this number is likely to grow in the future. From the efficiency perspective, it is crucial to maintain a healthy and a comfortable indoor environment for occupants since people spend large portion of their time in buildings. Therefore, balancing the energy efficiency and effectiveness of HVAC systems has drawn attentions of the research community.

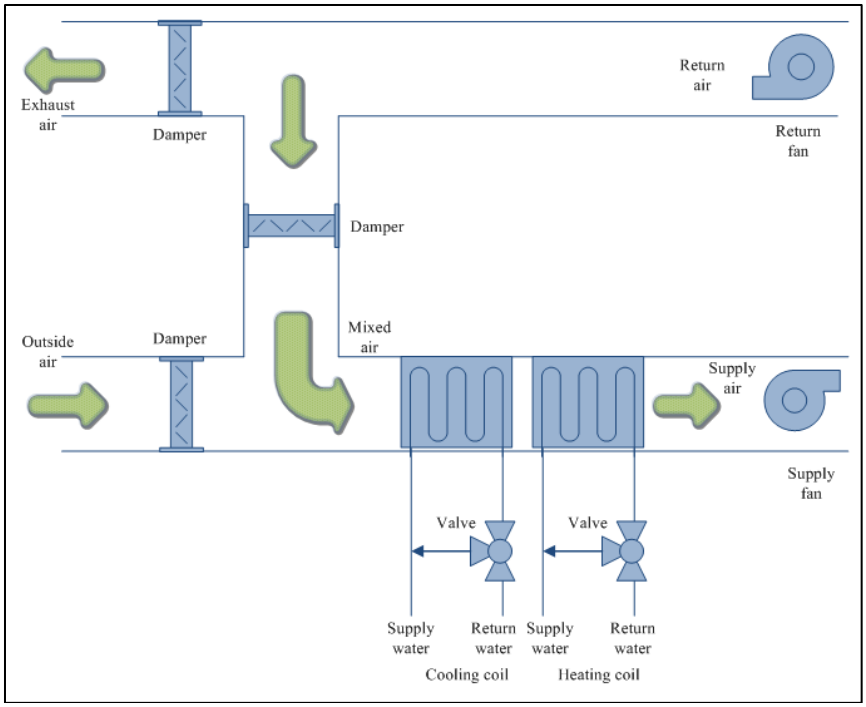

Figure 1.1 Schematic diagram of a typical air handling unit system

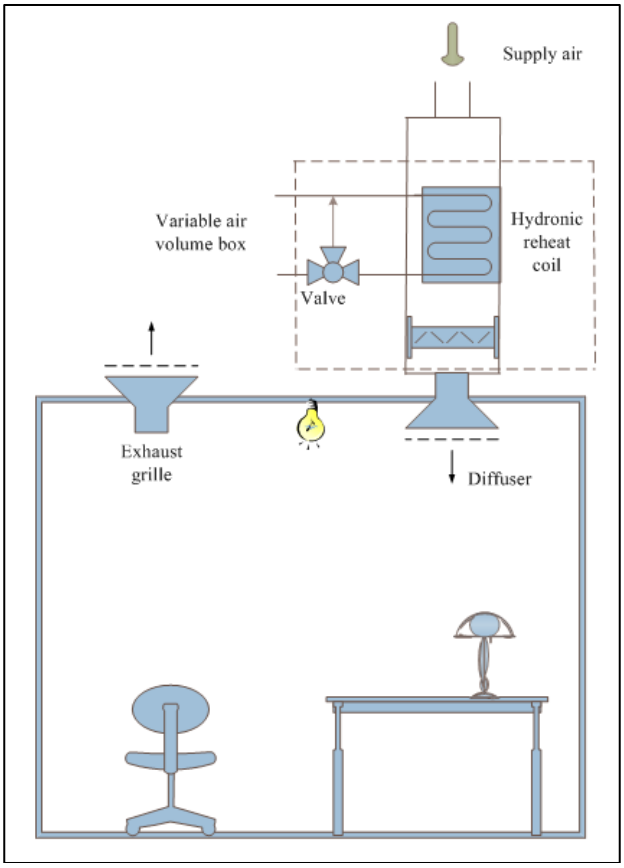

Figure 1.2 Schematic diagram of a typical single-room variable-air-volume box

Previous research has introduced numerous simulation models for analysis of different operational scenarios of HVAC systems. A typical commercial HVAC system includes a large number (hundreds) of variables with static and dynamic characteristics most of which are neglected by simulation models. Therefore, simulation models cannot be used in practical to control the HVAC systems, especially when a rapid response needed.

Analytical or mathematical models of HVAC systems have been extensively investigated in the literature. Although such models can accurately describe the physical properties of HVAC systems, they could be computationally expensive due to the complex, nonlinear, and dynamic characteristics of the system. Analytical models can only be reliable and practical when appropriate assumptions or simplifications are made.

Data-driven models have gained attention in the recent years and applied to modeling HVAC systems. The data-driven models are derived from empirical behavior and heuristic searching process [3]. They have proven to be powerful in capturing complex, noisy, and imprecise data collected from various nonlinear and large-scale systems.

1.1 Review of Simulation Models of HVAC Systems

The simulation models depend mostly on simulation software and a few are derived from physics-based equations.

Winkelmann *et al.* [4] employed DOE-2 building energy analysis computer program to simulate hourly-varying interior illuminance, management of windows for sun and glare control, and the operation of electric lighting control systems. They presented sample DOE-2 day-lighting output reports and relevant results analysis in their research. Cui *et al.* [5] utilized HVACSIM+ environment to establish a simulation model for a hybrid ground-coupled heat pump (HGCHP) with domestic hot water (DHW) supply system. A case study showed that the HGCHP system can effectively alleviate the imbalanced loads of the ground heat exchanger and can offer almost 95% DHW demand. Aiming at evaluating the energy performance of the variable-refrigerant-volume air-conditioning system, Zhou *et al.* [6] developed and validated a simulation module on the simulation program, EnergyPlus. McDowell *et al.* [7] integrated the CONTAM air flow modeling tool into the TRNSYS energy analysis program in order to address an issue that commonly used programs for estimating the energy use of buildings do not incorporate the inter-zonal airflow modeling techniques required to adequately account for the effect of these factors on energy usage. Sowell *et al.* [8] presented direct comparisons between the Simulation Problem Analysis and Research Kernel (SPARK) and the HVACSIM+ programs and an indirect comparison between SPARK and the IDA program. An

overview of twenty major building energy simulation programs was proposed by Crawley *et al.* [9].

Yu *et al.* [10] developed a mathematical model for simulating an operating strategy of regulating the set point of condensing temperature based on the outdoor temperature as well as enhancing the efficiency of air-cooled chillers used in air-conditioned buildings. Huang *et al.* [11] proposed a system level dynamic model as simulation platform that integrated five energy management control functions such as outside air economizer cycle, programmed start and stop lead time, load reset and occupied time adaptive control strategy.

Although they are free of the spatial and temporal limit, simulation models have the following drawbacks [12]:

- They require significant look-ahead time intervals.
- They can only be involved in high-level supervisory control.
- The building use varies or changes (e.g. large variations in occupancy or significant change in weather condition) which are not known in advance.

1.2 Review of Analytical Models of HVAC Systems

The analytical approaches are usually applied to model individual components or overall HVAC system.

He *et al.* [13] presented a new lumped-parameter model for describing the dynamics of vapor compression cycles. Particularly the dynamics associated with the two heat exchangers, i.e., the evaporator and the condenser, are built based on a moving-interface approach by which the position of the two-phase/single-phase interface inside the one-dimensional heat exchanger can be properly predicted. Wang *et al.* [14] developed a simple, yet accurate cooling coil unit engineering model that yielded better real time control and optimization of HVAC systems. They used a technique that is based on an energy balance and heat transfer principles to build the model. Jin *et al.* [15]

proposed a new, simple, yet accurate mechanical cooling tower model for the purpose of energy conservation and management that is on the basis of Merkel's theory and effectiveness-NTU method. Yu *et al.* [16] applied mathematical modeling with two different approaches, block-wise Simulink and bond graph. Results from their research indicated that combination with two approaches to realize complicated models of building HVAC system for the application of model-based fault detection and diagnosis is a realistic solution. Sen *et al.* [17] developed a comprehensive numerical study of the performance of a capacitive humidity sensor for HVAC applications.

Liu *et al.* [18] employed a calibrated simplified engineering modeling method to optimize HVAC system operation. The method can be utilized to optimize operating strategies and control schedules. Zheng [19] presented a comprehensive modeling and optimization methodology for global multiple-stage optimal operation of HVAC and building systems. Two different dynamic models of a multi-zone variable air volume system had been developed using two approaches respectively: bottom-up and top-down approaches. Kulkarni *et al.* [20] proposed a proportional control system for the residential building by setting up the dynamic simulation for the building and the control system. They used state-space method to model the building system and the corresponding code was implemented on MATLABTM. Platt *et al.* [21] focused on real-time HVAC zone model fitting and prediction techniques based on physical principles. Their proposed approach was validated by comparing real-time HVAC zone model fitting and prediction against the corresponding experimental measurements. Tashtoush *et al.* [22] designed a procedure for deriving a dynamic model of HVAC system that consists of a zone, heating coil, cooling and dehumidifying coil, humidifier, ductwork, fan, and mixing box. Their focus was centered on control strategies to reduce energy consumption and improvement of the quality of indoor environment.

Although the analytical approaches can offer benefits, such as the ability to address cause and effect scenarios, they have the following disadvantages:

- They can be computationally expensive, especially for solving complex systems.
- Some analytical approaches can only be suitable for component level. It is inapplicable to apply them into system-level.
- Many approaches can be employed to system level application only when assumptions and simplifications are made.

1.3 Review of Data-driven Models of HVAC Systems

In the past decade, data-driven approaches have been extensively applied to model HVAC systems along with the development of novel data-mining algorithms [23, 24].

Katipamula *et al.* [25] developed multiple linear regression (MLR) models that were applied to derive baseline models and detect deviations in energy consumption resulting from major operational changes. Compared to single-variable model, MLR models showed a decrease in coefficient of variation which is between 10 percentage to 60 percentage and with an average decrease of about 33%. Abbassi *et al.* [26] utilized artificial neural network to construct thermodynamic modeling of an evaporative condenser under steady state and transient state conditions for establishing control of thermal capacity. Teeter *et al.* [27] applied a functional link neural network approach to performing the HVAC thermal dynamic system identification. In their research, they presented methodologies to reduce inputs of the functional link network, to degrade the complexity, and to speed up the training speed. Soyguder *et al.* [28] utilized artificial neural fuzzy interface system method to predict the damper gap rates of a HVAC system with only one zone. Xi *et al.* [29] employed support vector regression (SVR) to build the 2-by-2 nonlinear dynamic model of a HVAC system. Based on the model, a nonlinear model predictive controller was then designed. Kumar *et al.* [30] demonstrated application of least square support vector machines (LS-SVM) to estimate the predicted

mean vote for thermal comfort and the generation of psychometric chart. Kusiak *et al.* [31] proposed a data-driven approach for the development of a daily steam load model that is realized by a neural network ensemble with five multi-layer perceptron (MLPs). Kusiak *et al.* [32-35] applied neural network to model the air handling unit, variable-air-box, and overall HVAC system and to develop virtual models of indoor air quality sensors.

1.4 Computational Intelligence and Optimization

New theories and techniques in computational intelligence [36-38] offer alternatives to solve problems in HVAC systems.

Wright *et al.* [39] designed a multi-objective genetic algorithm search method in the identification of the optimum pay-off characteristic between the energy cost of a building and the occupant thermal discomfort. Lu *et al.* [40] first formulated a mix-integer nonlinear constraint optimization of system energy and then employed a modified genetic algorithm to solve the optimization problem. Fong *et al.* [41] proposed a meta-heuristic simulation – evolutionary programming coupling approach developed by evolutionary programming to effectively handle the discrete, nonlinear and highly constrained optimization problem for HVAC systems. Hadjiski *et al.* [42] presented a new hybrid intelligent system for HVAC system control by integration of multi-agent system, dynamic ontology, and colony optimization. Fong *et al.* [43] designed a robust evolutionary algorithm to efficiently solve the simulation model of a HVAC system that is a time consuming problem. Ardakani *et al.* [44] employed continuous genetic algorithm and particle swarm optimization to solve an optimal chiller loading problem.

The goal of this thesis is to analyze an HVAC system and develop nonlinear, nonparametric, and dynamic models to optimize the system performance in two objectives, minimizing the energy consumed by components, and maintaining the thermal

comfort of the inside environment. Intelligent optimization algorithms are applied to solve the models derived by data-driven approaches.

1.5 Thesis Structure

The structure of the Thesis is organized as follows. Chapter 1 reviews the research of HVAC systems. In chapter 2, a predictive model and simulation model are built based on data mining approach and then an interior-point method is applied to solve the data-driven model. In chapter 3, a dynamic neural network is proposed to build a dynamic HVAC model and then a multi-objective particle swarm optimization algorithm is applied to solve the model. In chapter 4, a data-driven approach is adopted to build an HVAC model and fuzzy logic and multi-objective particle swarm optimization are employed to solve the model.

CHAPTER 2

OPTIMIZATION OF HVAC SYSTEMS WITH AN INTERIOR-POINT METHOD

2.1 Introduction

In this chapter, a time-series-based model is extracted by a data-driven approach to predict energy consumption and indoor temperature of an HVAC system. A simulation model is also built based on the same data-driven approach to simulate energy consumption and indoor temperature of the HVAC system. The effectiveness of the data-driven approach has been demonstrated in the literature [32-33]. Poisson and uniform distributions are applied to simulate the behavior of the occupants impacting the internal heat balance. An optimization model is developed from the predictive model to minimize energy consumption while maintaining the indoor air temperature within a desirable range. The supply air static pressure and the supply air temperature set points are generated by this optimization model by applying a nonlinear interior-point algorithm to solve it. The interior-point method was originally developed for linear programming optimization and then extended to non-convex nonlinear programming [45-47]. A case study is presented to validate the effectiveness of the proposed approach.

2.2. Problem Description

A typical variable air volume (VAV) heating, ventilating, and air conditioning (HVAC) system includes a chiller, pumps, a supply fan, a return fan, and VAV boxes. A schematic diagram of such a system is shown in Figure 2.1. The chiller, pumps, supply fan, return fan, and VAV reheating coils are the main consumers of the energy. In the HVAC system considered in this chapter, the chillers, pumps, supply fan, and return fan consume electricity, while the VAV reheating coils consume natural gas. In total, the energy consumed by the HVAC system can be expressed by Equation (2.1):

$$E_{Total} = E_{Electricity} + E_{Gas} \tag{2.1}$$

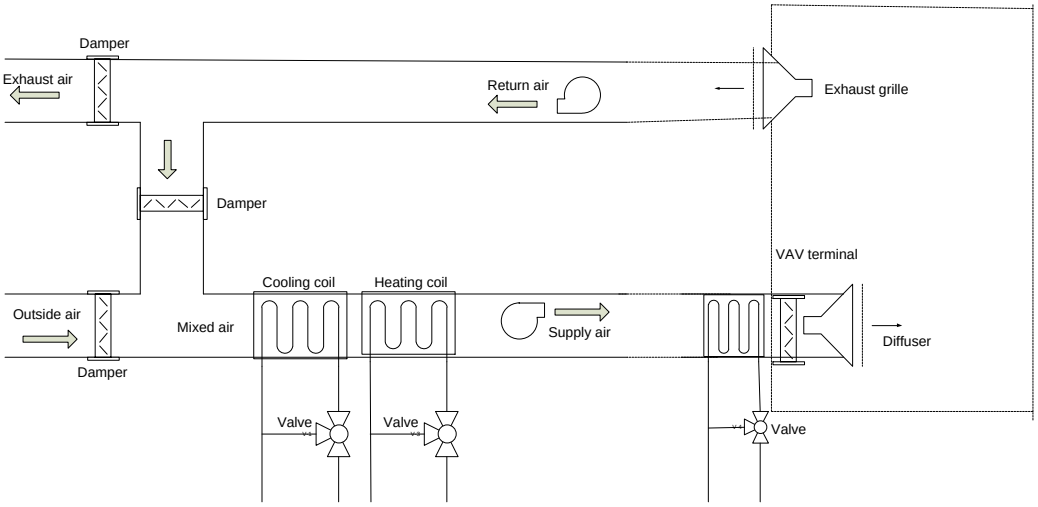

Figure 2.1 Schematic diagram of a typical HVAC system

The goal of the research reported in this Chapter is to minimize the total energy consumption, while maintaining the indoor temperature (thermal comfort) at a desirable level by adjusting two controlling set points: the supply air static pressure and the supply air temperature set point. In this research, the indoor humidity is not considered since the relevant data in the experimental building cannot be obtained. Another reason is due to the average humidity in our experimental location that falls in the desirable range most of the time. Therefore, humidity is not necessary to be considered in the model proposed in this research. Thus, in constructing the energy consumption predictive model and the indoor temperature predictive model, it is necessary to include the two set points as parameters (see Equations (2.2) – (2.3)).

$$y_1(t+d) = f_1(\cdot) \tag{2.2}$$

$$y_2(t+d) = f_2(\cdot) \tag{2.3}$$

where $y_1\ (t+d)$ and $y_2\ (t+d)$ represent the energy consumption and indoor temperature at time $t+d$, t current time, d time increment.

A nonlinear autoregressive time-series model with external input (NARX) is used to capture the dynamic behavior of the system as shown in Equations (2.4) – (2.5):

$$y_1(t+d) = f_1(y_1(t), y_1(t-d), \dots, y_1(t-n_{11}d), x_1(t), x_1(t-d), \dots, x_1(t-n_{12}d)) \quad (2.4)$$

$$y_2(t+d) = f_2(y_2(t), y_2(t-d), \dots, y_2(t-n_{21}d), x_2(t), x_2(t-d), \dots, x_2(t-n_{22}d)) \quad (2.5)$$

Two models for simulating energy consumption and indoor temperature at time t are also considered and expressed in Equations (2.6) - (2.7):

$$y_3(t) = f_3(y_3(t-d), \dots, y_3(t-n_{31}d), x_3(t), x_3(t-d), \dots, x_3(t-n_{32}d)) \quad (2.6)$$

$$y_4(t) = f_4(y_4(t-d), \dots, y_4(t-n_{41}d), x_4(t), x_4(t-d), \dots, x_4(t-n_{42}d)) \quad (2.7)$$

where $n_{ij}$is the time increment for each input in the time series model. The internal heat gain has a significant impact on the HVAC energy consumption. In commercial buildings, the number of occupants is a random variable. Thus, it is necessary to model activities of the occupants. In this research, considering its successful application in simulating discrete occurrences, a Poisson process is applied to model arrival of the occupants, and a uniform distribution is used to model their departure. Assume the occupants arrive at the conditioned zone in accordance with a Poisson distribution with rate λ. Each occupant's departure time is assumed to be independent and modeled with a uniform distribution $U(0, a)$. Based on these assumptions, the number of occupants remaining in the conditioned zone at time t is expressed in Equation (2.8):

$$E[N(t)] = \lambda \int_0^t (1 - P\{U < y\})dy \quad (2.8)$$

where N(t) is the number of occupants staying in the conditioned zone at time t.

2.3 Data Description

The HVAC system discussed in this Chapter is operated by the Energy Resource Station in Ankeny, Iowa, which is an energy laboratory for testing and demonstrating commercial HVAC systems. The system includes two independent identical air handling

units (AHUs) and thermal zones. The data set in this research was obtained from an experiment designed to investigate the impacts of two AHU set points, the supply air static pressure (SA-SPSPT) and the supply air temperature set point (SAT-SPT) on the total energy consumption and the indoor temperature. The set points of both air handling units were adjusted during the experiment. In particular, the SA-SPSPT varied from 0.4 in. WG (0.1 kPa) to 1.8 in. WG (0.45 kPa) with 0.2 in. WG (0.05 kPa) increments; whereas the SAT-SPT varied from 50 ℉ (10 ℃) to 65 ℉ (18.33 ℃) at 1 ℉ (0.556 ℃) increments. To simulate the internal heating load of occupants, electric energy was used. In total, more than 300 parameters, including weather conditions, energy consumption, and indoor temperature, was recorded at 1-minute intervals by the sensors. The data was collected from June 22 to July 16, 2011. The original data set at 1-min frequency has been transformed into to 1-h data by averaging the 1-min data. In total, 789 data instances (from June 22 to July 14, 2011) were used for training and testing, while 96 data instances (from July 15 to July 16, 2011) were used as a validation set. Table 2.1 presents details of the data.

Table 2.1 Description of data sets

No.	Data Set Type	Time Period	Number of Instances
1	Entire data set	06/22 – 07/16/2011	885
2	Training data set	Randomly selected from 06/22 to 07/14/2011	670
3	Test data set	Randomly selected from 06/22 to 07/14/2011	119
4	Validation data set	07/15 – 07/16/2011	48

2.4 Parameter Selection

The original data set includes almost 400 data points (parameters), most of which are irrelevant to the modeled phenomena. The presence of unimportant parameters may negatively impact the accuracy of the models derived from the data. Therefore, it is

essential to select the parameters used to develop accurate, scalable, and comprehensive models [48]. A boosting tree is a learning algorithm for ranking the importance of parameters for prediction. According to [49, 50], the boosting tree algorithm has demonstrated good performance in parameter selection, and therefore it is used in this chapter for selecting parameters. Tables 2.2 - 2.3 list all the final inputs for building predictive models of energy consumption and indoor temperature. Based on the parameter selection for building predictive models, Tables 2.4-2.5 list the inputs for building identification models that are used to simulate energy consumption and indoor temperature at time stamp *t*.

Table 2.2 Parameters selected for building HVAC system energy consumption model

Input	Description	Remark
x_{1a}	Supply air duct static pressure set point at time *t* + *d*	Controlled input
x_{1b}	AHU supply air temperature set point at time *t* + *d*	Controlled input
x_{1c}	Internal heating load at time *t* + *d*	Predicted input
x_{1d}	Chilled water coil mixed water temperature at time *t*	Observed input
x_{1e}	Chilled water coil valve position at time *t*	Observed input
x_{1f}	Mixed air temperature at time *t*	Observed input
x_{1g}	Outside air flow rate at time *t*	Observed input
x_{1h}	Outside air inlet temperature at time *t*	Observed input
x_{1i}	Outside air inlet temperature at time *t* - *d*	Observed input
x_{1j}	Return air temperature at time *t*	Observed input
x_{1k}	Return fan VFD speed at time *t*	Observed input
x_{1l}	Supply air flow rate at time *t*	Observed input
x_{1m}	Supply fan pressure differential at time *t*	Observed input
x_{1n}	Infrared radiation at time *t*	Observed input
x_{1o}	Infrared radiation at time *t* - *d*	Observed input
x_{1p}	Outside air temperature at time *t*	Observed input
x_{1q}	Solar normal flux at time *t*	Observed input
x_{1r}	Solar normal flux at time *t* - *d*	Observed input
x_{1s}	Variable air volume box damper position at time *t*	Observed input
x_{1t}	Variable air volume box velocity pressure differential at time *t*	Observed input
x_{1u}	Indoor temperature at time *t*	Observed input
x_{1v}	HVAC system energy consumption at time *t*	Observed input

Table 2.3 Parameters selected for building HVAC system indoor temperature model

Input	Description	Remark
x_{2a}	Supply air duct static pressure set point at time *t* + *d*	Controlled input
x_{2b}	AHU supply air temperature set point at time *t* + *d*	Controlled input
x_{2c}	Internal heating load at time *t* + *d*	Predicted input
x_{2d}	Mixed air temperature at time *t*	Observed input
x_{2e}	Outside air inlet temperature at time *t*	Observed input
x_{2f}	Return air flow rate at time *t*	Observed input
x_{2g}	Return air temperature at time *t*	Observed input
x_{2h}	Supply fan air flow rate at time *t*	Observed input
x_{2i}	Infrared radiation at time *t*	Observed input
x_{2j}	Outside air temperature at time *t*	Observed input
x_{2k}	Solar normal flux at time *t*	Observed input
x_{2l}	Solar normal flux at time *t* - *d*	Observed input
x_{2m}	Variable air volume box damper position at time *t*	Observed input
x_{2n}	Variable air volume box velocity pressure differential at time *t*	Observed input
x_{2o}	HVAC system energy consumption at time *t*	Observed input
x_{2p}	HVAC system indoor temperature at time *t*	Observed input
x_{2q}	HVAC system indoor temperature at time *t* - *d*	Observed input

2.5 HVAC System Modeling

2.5.1 Model formulation

Multilayer perceptron (MLP) [51] is a feed-forward neural network model that maps input data onto an output. An MLP consists of multiple layers of nodes in a directed graph, with each layer fully connected to the next. With the exception of the input layer, each node is a neuron with a nonlinear activation function. Note that all nodes in one layer use the same activation function. Normally, the activation functions used in MLP include hyperbolic tangent function, logistic function, exponential function, and identification function, as shown in Equations (2.9) – (2.12):

$$g(a) = \tanh(a) = \frac{e^{a}-e^{-a}}{e^{a}+e^{-a}} \tag{2.9}$$

$$g(a) = \frac{1}{1+e^{-a}} \tag{2.10}$$

$$g(a) = e^{a} \tag{2.11}$$

$$g(a) = \text{a} \tag{2.12}$$

Table 2.4 Parameters selected for modeling energy consumption at time stamp *t*

Input	Remark
Supply air duct static pressure set point at time *t*	Observed input
AHU supply air temperature set point at time *t*	Observed input
Internal heating load at time *t*	Observed input
Chilled water coil mixed water temperature at time *t*	Observed input
Chilled water coil valve position at time *t*	Observed input
Mixed air temperature at time *t*	Observed input
Outside air flow rate at time *t*	Observed input
Outside air inlet temperature at time *t*	Observed input
Outside air inlet temperature at time *t* - *d*	Observed input
Return air temperature at time *t*	Observed input
Return fan VFD speed at time *t*	Observed input
Supply air flow rate at time *t*	Observed input
Supply fan pressure differential at time *t*	Observed input
Infrared radiation at time *t*	Observed input
Infrared radiation at time *t* - *d*	Observed input
Outside air temperature at time *t*	Observed input
Solar normal flux at time *t*	Observed input
Solar normal flux at time *t* - *d*	Observed input
Variable air volume box damper position at time *t*	Observed input
Variable air volume box velocity pressure differential at time *t*	Observed input
Indoor temperature at time *t*	Observed input
HVAC system energy consumption at time *t* - *d*	Observed input

In this chapter, a three-layer MLP with one output unit is utilized to describe the HVAC systems. The Broyden–Fletcher–Goldfarb–Shanno (BFGS) method is used to train the network. Thus, an explicit expression for the energy consumption and the indoor temperature predictive models is represented in Equations (2.13) – (2.14):

$$y_1(t+d) = \tilde{g}_1\left(\sum_{j=0}^{M_1} w_j^{(2)} g_1\left(\sum_{i=a}^{v} w_{ji}^{(1)} x_{1i} + w_{j0}^{(1)}\right)\right) \quad (2.13)$$

$$y_2(t+d) = \tilde{g}_2\left(\sum_{j=0}^{M_2} m_j^{(2)} g_2\left(\sum_{i=a}^{q} m_{ji}^{(1)} x_{2i} + m_{j0}^{(1)}\right)\right) \quad (2.14)$$

where $w_{ji}^{(1)}$ and $m_{ji}^{(1)}$ are the elements of input-hidden weight matrices for y_1 and y_2 respectively, $w_{j0}^{(1)}$ and $m_{j0}^{(1)}$ are the hidden bias for y_1 and y_2 respectively, $w_j^{(2)}$ and $m_j^{(2)}$ are the elements of hidden-output weight matrices for y_1 and y_2 respectively. In order to obtain the functions $y_1(t+d)$ in Equation (2.15) and $y_2(t+d)$ in Equation (2.16), data

set 2 (670 instances) and data set 3 (119 instances) of Table 1 are used as a training set and a testing set, respectively.

Table 2.5 Parameters selected for modeling indoor temperature at time stamp *t*

Input	Remark
Supply air duct static pressure set point at time *t*	Observed input
AHU supply air temperature set point at time *t*	Observed input
Internal heating load at time *t*	Observed input
Mixed air temperature at time *t*	Observed input
Outside air inlet temperature at time *t*	Observed input
Return air flow rate at time *t*	Observed input
Return air temperature at time *t*	Observed input
Supply fan air flow rate at time *t*	Observed input
Infrared radiation at time *t*	Observed input
Outside air temperature at time *t*	Observed input
Solar normal flux at time *t*	Observed input
Solar normal flux at time *t - d*	Observed input
Variable air volume box damper position at time *t*	Observed input
Variable air volume box velocity pressure differential at time *t*	Observed input
HVAC system energy consumption at time *t*	Observed input
HVAC system indoor temperature at time *t - d*	Observed input
HVAC system indoor temperature at time *t - 2d*	Observed input

$$y_1(t+d) = \sum_{j=0}^{9} w_j^{(2)} \frac{1}{1+e^{-(\sum_{i=a}^{v} w_{ji}^{(1)} x_{1i} + w_{j0}^{(1)})}} \tag{2.15}$$

$$y_2(t+d) = \sum_{j=0}^{12} m_j^{(2)} e^{(\sum_{i=a}^{q} m_{ji}^{(1)} x_{2i} + m_{j0}^{(1)})} \tag{2.16}$$

In this research, the three-layer MLP is also applied to extract the concrete expression for the two identification models for simulating energy consumption and indoor temperature in Equations (2.6) – (2.7).

2.5.2 Model validation

To evaluate performance of the predictive models built by the MLP ensemble algorithm, four metrics are used: the mean absolute error (MAE) (Equation (2.18)), the standard deviation of absolute error (Std_AE) (Equation (2.21)), the mean absolute

percentage error (MAPE) (Equation (2.20)), and the standard deviation of absolute percentage error (Std_APE) (Equation (2.22)) [52]. In Equation (2.17), AE represents the absolute error, while in Equation (2.19) represents the absolute percentage error.

$$AE = |\tilde{y} - y| \tag{2.17}$$

$$MAE = \frac{\sum_{i=1}^{N} AE_i}{N} \tag{2.18}$$

$$APE = \left|\frac{\tilde{y}-y}{y}\right| \tag{2.19}$$

$$MAPE = \frac{\sum_{i=1}^{N} APE_i}{N} \tag{2.20}$$

$$Std\_AE = \sqrt{\frac{\sum_{i=1}^{N}(AE_i - MAE)^2}{N-1}} \tag{2.21}$$

$$Std\_APE = \sqrt{\frac{\sum_{i=1}^{N}(APE_i - MAPE)^2}{N-1}} \tag{2.22}$$

where, $\tilde{y}$ is the predicted value, y is the actual observed value, and n is the number of data instances used for training and testing. The data in Table 2.6 shows the performance of the MLP-developed predictive models. Figures 2.2-2.3 present the correlation coefficient between the observed and the predicted values. Figures 2.4-2.5 compare the predicted and observed values of the energy consumption and indoor temperature on 119 1-h data instances drawn from data set 3. As shown in Figures 2.4-2.5, the predicted values of the energy consumption and the indoor temperature closely follow the observed values. Performance of the two predictive models is summarized in Table 2.6 showing the accuracy of the model predicting energy consumption on the test data set as 90%, while the accuracy for the indoor temperature is 99.7%. Table 2.7 lists the performance for the two identification models for simulating energy consumption and indoor temperature.

Table 2.6 Performance of the models predicting HVAC system energy consumption and indoor temperature

Objective	Data Set	MAE	MAPE	Std_AE	Std_MAPE
Energy consumption	Training	0.362	6.6%	0.353	5.5%
	Testing	0.454	10.0%	0.452	19.4%
Indoor temperature	Training	0.157	0.2%	0.159	0.2%
	Testing	0.210	0.3%	0.218	0.3%

Table 2.7 Performance of the simulation models of energy consumption and indoor temperature

Objective	Data Set	MAE	MAPE	Std_AE	Std_MAPE
Energy consumption	Training	0.214	4.3%	0.176	4.1%
	Testing	0.247	5.4%	0.205	5.2%
Indoor temperature	Training	0.091	0.13%	0.085	0.12%
	Testing	0.114	0.16%	0.11	0.16%

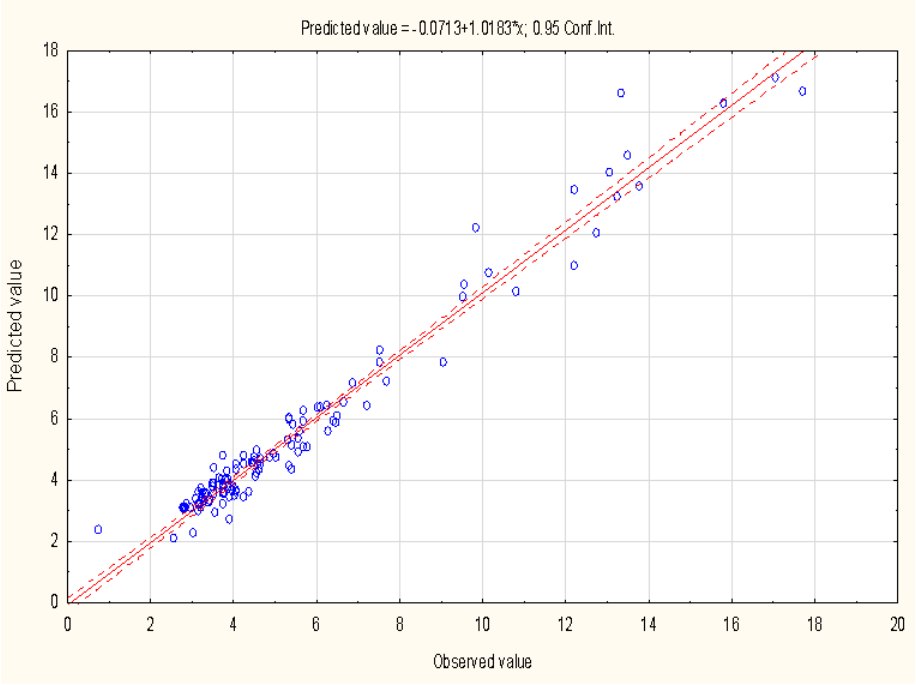

Figure 2.2 The correlation coefficient of the observed and predicted values of HVAC system energy consumption

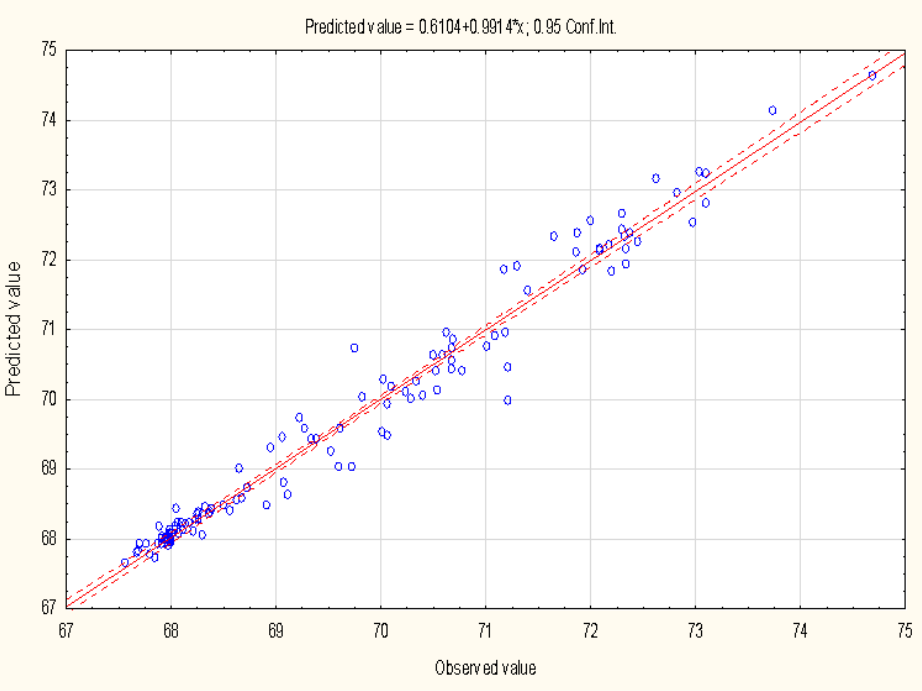

Figure 2.3 The correlation coefficient of the observed and predicted values of indoor temperature

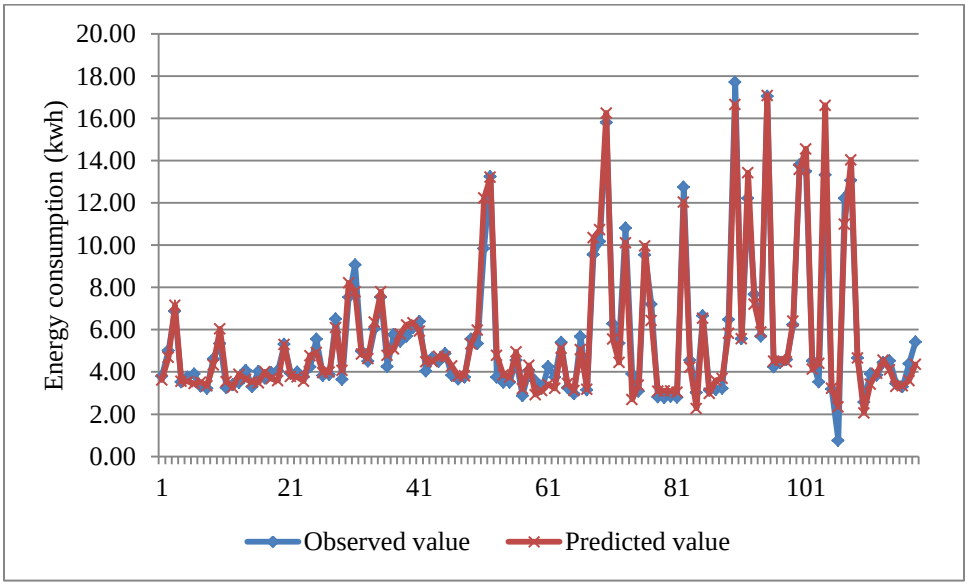

Figure 2.4 Observed and predicted values of HVAC system energy consumption

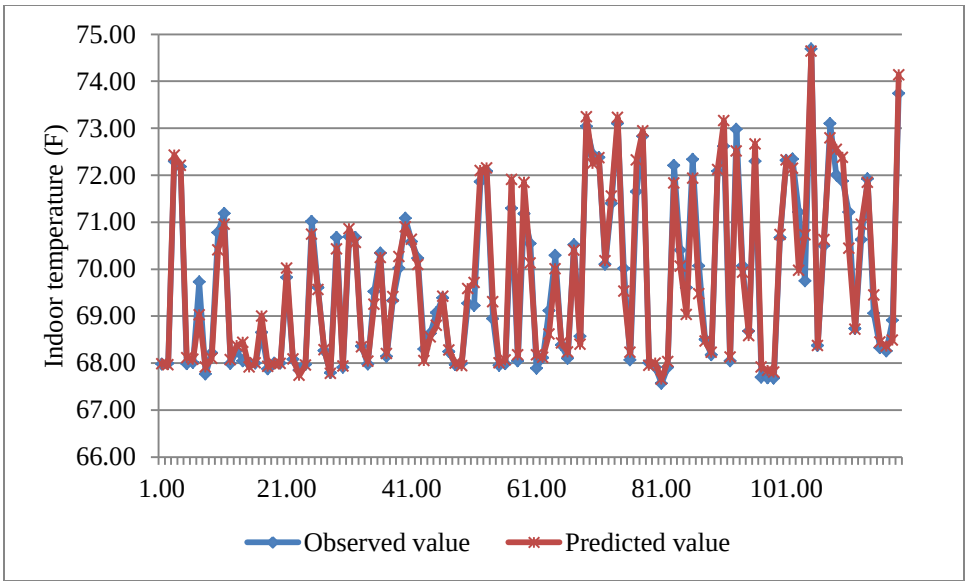

Figure 2.5 Observed and predicted values of HVAC system indoor temperature

2.6 Model Optimization

2.6.1 Optimization model formulation

To optimize the energy consumption of the HVAC system, the objective function $y_1(t+d)$ in Equation (2.15) is minimized while maintaining the value of $y_2(t+d)$ in Equation (2.16) within an acceptable range. Optimal values of the supply air temperature and the supply air duct static pressure set points at time $t + d$ are computed. The observed indoor temperature is measured by the sensors while the observed energy consumption is computed from Equation (2.1). The constraints in the model are established by setting lower and upper bounds of the control parameters and assigning an acceptable range for indoor temperature as follows:

- The supply air temperature set point varies from 50 ℉ (10 ℃) to 64 ℉ (17.7 ℃).
- The supply air duct static pressure set point varies between 0.4 in. WG (0.1 kPa) to 1.8 in. WG (0.45 kPa).

- The indoor temperature is maintained between 68 ℉ (20.0 ℃) and 73 ℉ (22.8 ℃).

These three limits are determined by the design of the HVAC system and preferences of the occupants. The optimization model is formulated in Equation (2.23):

$$\begin{gathered}\min_{x_{1a}(t+d),x_{1b}(t+d),x_{2a}(t+d),x_{2b}(t+d)} y_1(t+d) \\ \text{subject to:} \\ y_1(t+d)=\sum_{j=0}^{9} w_j^{(2)} \frac{1}{1+e^{-(\sum_{i=a}^{v} w_{ji}^{(1)} x_{1i}+w_{j0}^{(1)})}} \\ \mathrm{y}_2(t+d)=\sum_{j=0}^{12} m_j^{(2)} e^{(\sum_{i=a}^{q} m_{ji}^{(1)} x_{2i}+m_{j0}^{(1)})} \\ 68 \le y_2(t+d) \le 73 \\ 0.4 \le x_{1a}(t+d)=x_{2a}(t+d) \le 1.8 \\ 50 \le x_{1b}(t+d)=x_{2b}(t+d) \le 65\end{gathered} \tag{2.23}$$

Where $y_2(t+d)$ is the value of indoor temperature predicted by applying the original supply air duct static pressure set point $x_{1a}(t+d)$ and $x_{2a}(t+d)$ and the supply temperature set point $x_{1b}(t+d)$ and $x_{2b}(t+d)$. In minimizing the energy consumption at time stamp $t + d$, the room temperature is maintained within a predetermined range.

2.6.2 Nonlinear interior-point algorithm

The interior-point method was initially proposed by John von Neumann for linear programming optimization and was then extended to nonlinear programming. Consider the general nonlinear programming model [53]:

$$\begin{gathered}\min_{x,s} f(x) \\ \text{subject to:} \\ \mathrm{c_E}(x)=0 \\ c_I(x)-s=0 \\ s \ge 0\end{gathered} \tag{2.24}$$

where $c_E(x)$ is an equality constraint, while $c_I(x)$ is an inequality constraint. The Karush–Kuhn–Tucker (KKT) conditions for the model in (2.24) are formulated in (2.25) – (2.28):

$$\nabla f(x) - A_E^T(x)y - A_I^T(x)z = 0 \tag{2.25}$$

$$Sz - \mu e = 0 \tag{2.26}$$

$$c_E(x) = 0 \tag{2.27}$$

$$c_I(x) - s = 0 \tag{2.28}$$

Applying Newton's method [53] to the nonlinear system in the variables x, s, y and z, the Equation in (2.29) is obtained:

$$\begin{bmatrix} \nabla^2_{xx}L & 0 & -A_E^T(x) & -A_I^T(x) \\ 0 & Z & 0 & S \\ A_E(x) & 0 & 0 & 0 \\ A_I(x) & -I & 0 & 0 \end{bmatrix} \begin{bmatrix} p_x \\ p_s \\ p_y \\ p_z \end{bmatrix} = - \begin{bmatrix} \nabla f(x) - A_E^T(x)y - A_I^T(x)z \\ Sz - \mu e \\ c_E(x) \\ c_I(x) - s \end{bmatrix} \tag{2.29}$$

Where L is the Lagrangian of model (2.24),

$$L(x, s, y, z) = f(x) - y^T c_E(x) - z^T(c_I(x) - s) \tag{2.30}$$

After the values (p_x, p_s, p_y, p_z) have been determined, new values of (x^+, s^+, y^+, z^+) in (2.31) are computed:

$$x^+ = x + \alpha_s^{max} p_x, s^+ = s + \alpha_s^{max} p_x \text{ , and}$$

$$y^+ = y + \alpha_z^{max} p_y, z^+ = z + \alpha_z^{max} p_z \tag{2.31}$$

where $\alpha_s^{max} = \max\{\alpha \in (0,1]: s + \alpha p_s \geq (1-\tau)s\}$, and

$$\alpha_z^{max} = \max\{\alpha \in (0,1]: z + \alpha p_z \geq (1-\tau)z\} \tag{2.32}$$

with $\tau \in (0,1)$.

In the algorithm, the following function based on the perturbed KKT system in Equations (2.25) - (2.28) is used:

$$E(x, s, y, z; \mu) = \max\{\|\nabla f(x) - A_E^T(x)y - A_I^T(x)z\|, \|Sz - \mu e\|, \|c_E(x)\|, \|c_I(x) - s\|\}$$

Where $\|\cdot\|$ is the vector norm.

Algorithm 1, borrowed from [53], shows the basic interior-point algorithm for nonlinear programming:

Algorithm 1

Choose x_0 and $s_0 > 0$, and compute initial values for the multipliers y_0 and $z_0 > 0$. Select an initial barrier parameter $\mu_0 > 0$ and parameters $\sigma, \tau \in (0,1)$. Set $k = 0$.

while a stopping criterion for the nonlinear problem in Eq. (2.24) is not satisfied,

while $E(x_k, s_k, y_k, z_k, \mu_k) \leq \mu_k$

Solve (2.26) to obtain the search direction (p_x, p_s, p_y, p_z);

Compute $\alpha_s^{max}, \alpha_z^{max}$ using (2.29);

Compute $(x_{k+1}, s_{k+1}, y_{k+1}, z_{k+1})$ using (2.32);

Set $\mu_{k+1} = \mu_k and\ k = k + 1$

endwhile

Choose $\mu_k \in (0, \sigma\mu_k)$;

endwhile

2.6.3 Case study

In the case study presented in this section, the data set 4 (from 07/15/2011 – 07/16/2011) of Table 2.1 is used. The following assumptions are made:

- The occupied schedule is from 8:00 am to 12:00 am;

- The mean inter-arrival time of the occupants is $\lambda = 15$ per hour;
- Occupants' stay in the conditioned space follows uniform distribution $U(0\text{h}, 1\text{h})$;
- The arrival and leaving processes are independent;
- Each occupant produces 400 BTU (421,740 Joules) heating load per hour, including sensible and latent heating load.

The occupants' arrival and staying is simulated by using MATLAB, and the internal heating load results for 07/15/2011 – 07/16/2011 are shown in Table 2.8:

Using the simulated internal heating load together with the observed supply air duct static pressure set point and supply air temperature set point as inputs for simulation models, the energy consumption and indoor temperature from 07/15/2011 – 07/16/2011 can be simulated in Figures 2.6-2.7.

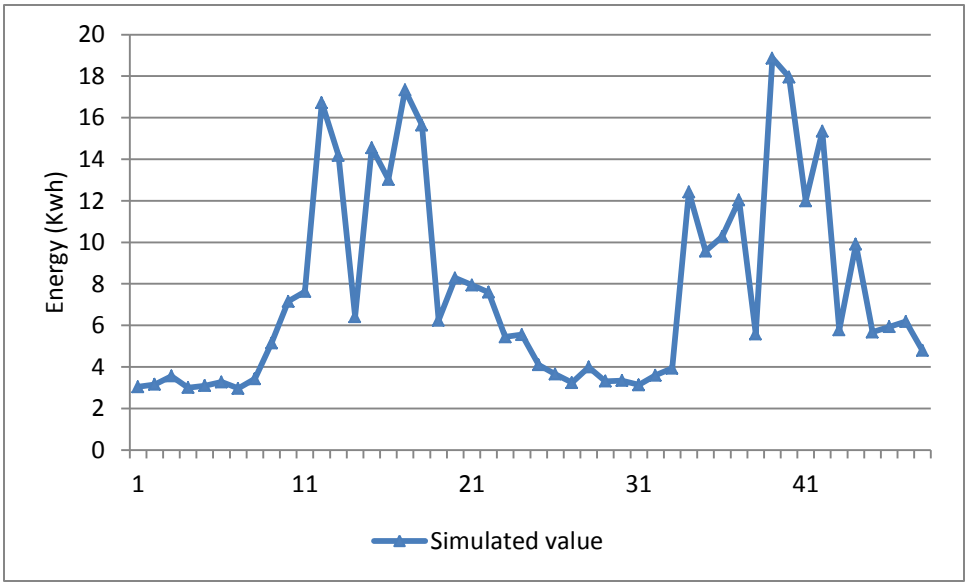

Figure 2.6 Simulated value of energy consumption in the period 07/15/2011 – 07/16/2011

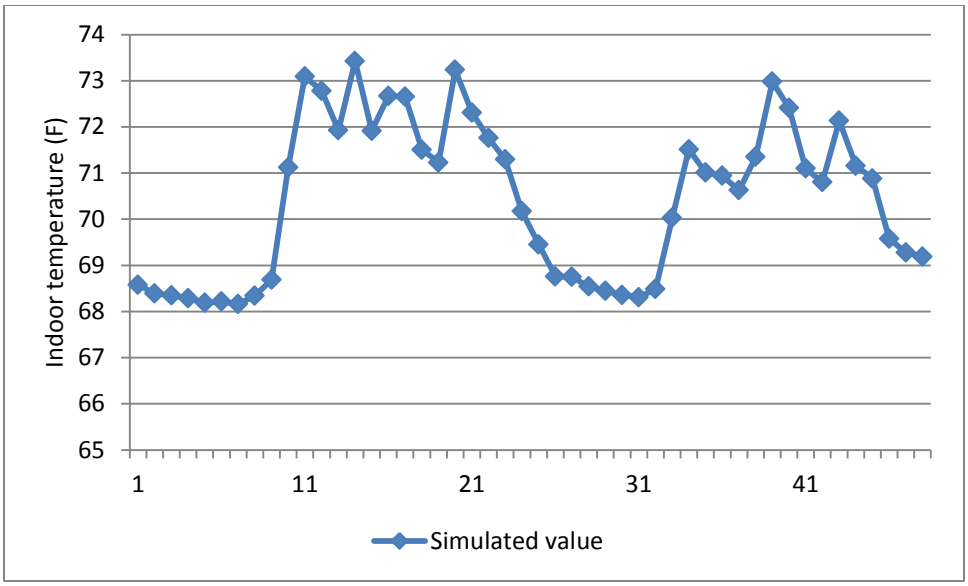

Figure 2.7 Simulated value of indoor temperature in the period 07/15/2011 – 07/16/2011

Using Equation (2.8), the average number of occupants at any time period is computed as:

for $0 \le t \ll 1$, $E[N(t)] = \lambda \int_0^t (1 - P\{U < y\})dy = \lambda t - \frac{1}{2}\lambda t^2$

for $1 \le t \le 16$,

$$E[N(t)] = \lambda \int_0^t (1 - P\{U < y\})dy = \lambda t - \lambda(t-1) - \int_0^1 y dy = \frac{1}{2}\lambda$$

Thus, the expected number of occupants in [8:00am, 9:00am] is $\int_0^1 (\lambda t - 1/2 * \lambda t^2)dt$ = 5, while the expected number of occupants in [9:00am, 10:00am], …, [11:00pm, 12:00am] is 7.5.

Using the above expected values as internal heating load, the optimization model (2.21) is solved. The energy consumption before and after optimization for 48 data points is shown in Figure 8, while the indoor temperature is illustrated in Figure2. 9. Figures 2.10-2.11 compare the observed and optimized set points for supply air duct static pressure set point and supply air temperature set point based on the same 48 data points.

Table 2.8 The simulated internal heating load of the HVAC system

Time	Avg. No. of Occupants	Occupants' Heating (Wh)	Lighting (Wh)	Total Internal Heating Load (Wh)
0:00--8:00 7/15/2011	0	0	0	0
8:00--9:00 7/15/2011	4.68	524.55	1000	1524.55
9:00--10:00 7/15/2011	8.97	1004.25	1000	2004.25
10:00--11:00 7/15/2011	5.95	666.9	1000	1666.9
11:00--12:00 7/15/2011	9.35	1047.15	1000	2047.15
12:00--13:00 7/15/2011	9.09	1017.9	1000	2017.9
13:00--14:00 7/15/2011	7.47	836.55	1000	1836.55
14:00--15:00 7/15/2011	10.79	1209	1000	2209
15:00--16:00 7/15/2011	6.27	702	1000	1702
16:00--17:00 7/15/2011	10.36	1160.25	1000	2160.25
17:00--18:00 7/15/2011	10.01	1121.25	1000	2121.25
18:00--19:00 7/15/2011	9.21	1031.55	1000	2031.55
19:00--20:00 7/15/2011	6.42	719.55	1000	1719.55
20:00--21:00 7/15/2011	5.75	643.5	1000	1643.5
21:00--22:00 7/15/2011	10.38	1162.2	1000	2162.2
22:00--23:00 7/15/2011	9.47	1060.8	1000	2060.8
23:00--0:00 7/15/2011	6.86	768.3	1000	1768.3
0:00--8:00 7/16/2011	0.00	0	0	0
8:00--9:00 7/16/2011	3.05	341.25	1000	1341.25
9:00--10:00 7/16/2011	7.61	852.15	1000	1852.15
10:00--11:00 7/16/2011	14.56	1630.2	1000	2630.2
11:00--12:00 7/16/2011	11.40	1277.25	1000	2277.25
12:00--13:00 7/16/2011	6.06	678.6	1000	1678.6
13:00--14:00 7/16/2011	7.23	809.25	1000	1809.25
14:00--15:00 7/16/2011	6.51	729.3	1000	1729.3
15:00--16:00 7/16/2011	8.67	971.1	1000	1971.1
16:00--17:00 7/16/2011	11.93	1335.75	1000	2335.75
17:00--18:00 7/16/2011	7.56	846.3	1000	1846.3
18:00--19:00 7/16/2011	7.82	875.55	1000	1875.55
19:00--20:00 7/16/2011	10.06	1127.1	1000	2127.1
20:00--21:00 7/16/2011	7.70	861.9	1000	1861.9
21:00--22:00 7/16/2011	7.66	858	1000	1858
22:00--23:00 7/16/2011	8.62	965.25	1000	1965.25
23:00--0:00 7/16/2011	9.96	1115.4	1000	2115.4

Figure 2.6 shows that the optimized energy consumption is reduced over the simulated energy. Figure 2.9 illustrates that the optimized indoor temperature is constrained in the range between 68 F and 73 F in most cases. Figure 2.12 indicates that the optimized model provides 20% energy savings based on the 48 validation data points of Table 2.1.

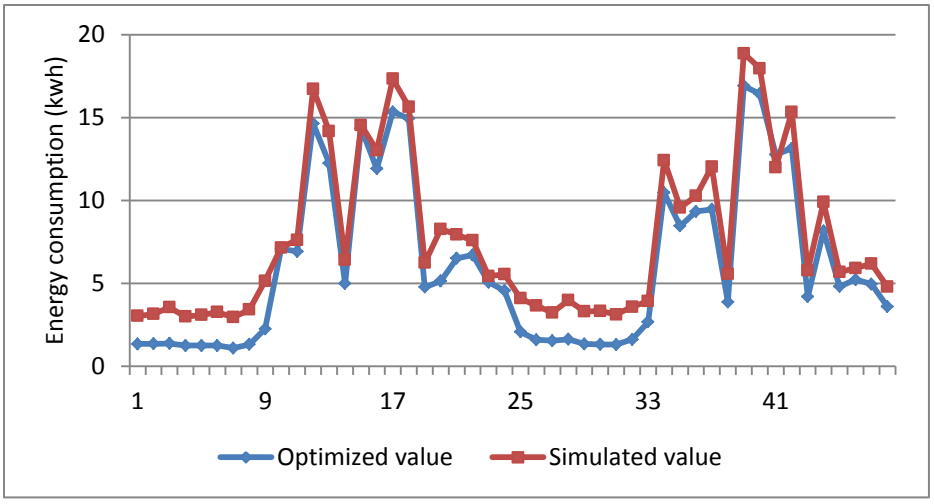

Figure 2.8 Comparison between the optimized and simulated HVAC system energy consumption

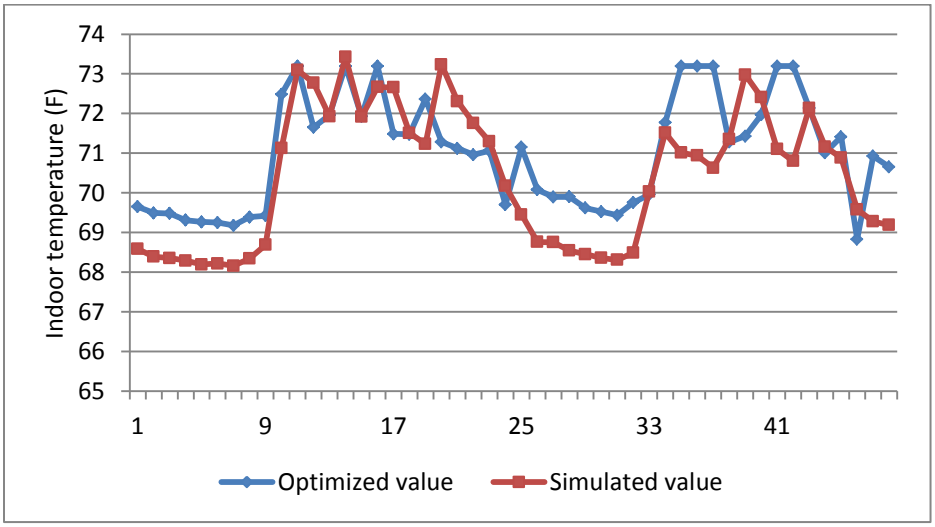

Figure 2.9 Comparison between the optimized and simulated HVAC system indoor temperature

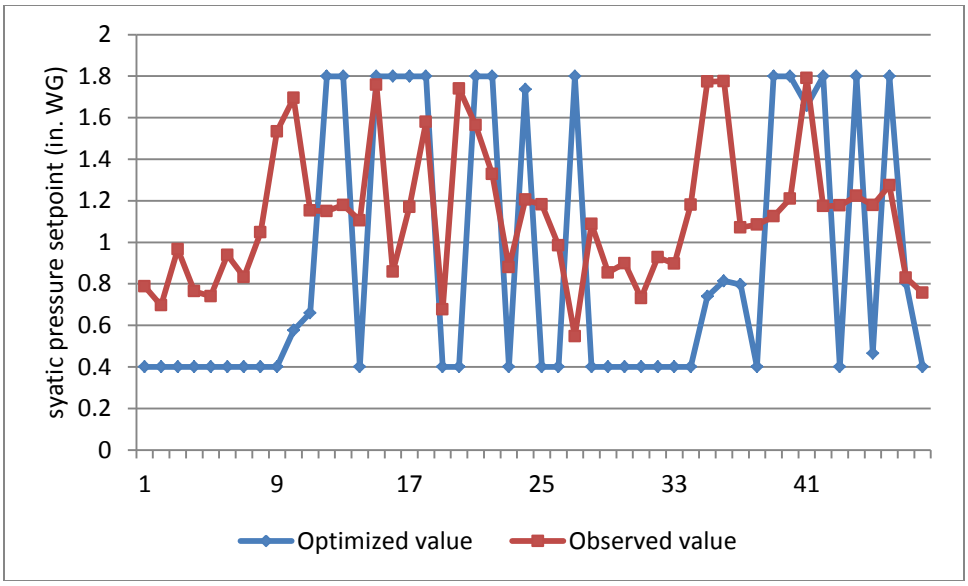

Figure 2.10 Comparison between optimized and observed values for supply air duct static pressure set point

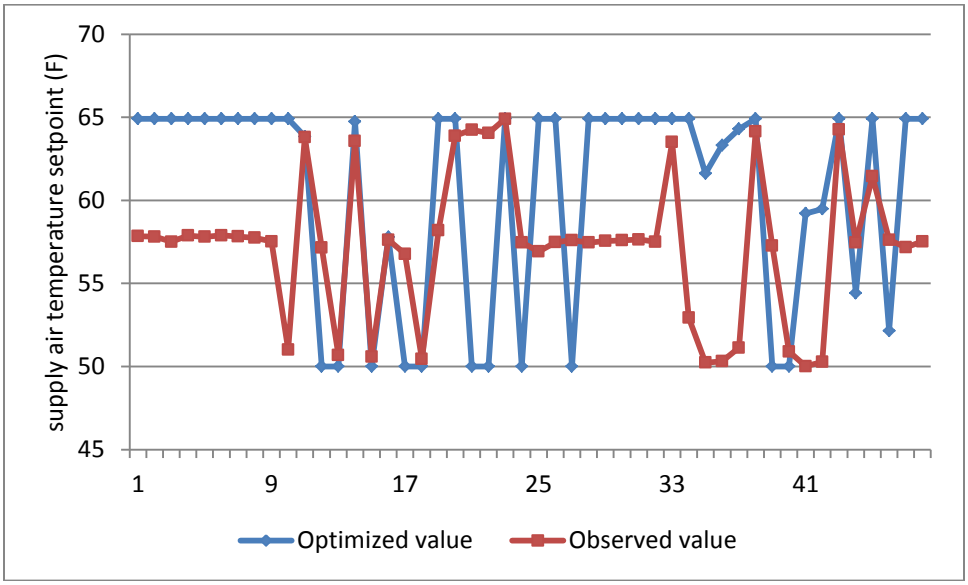

Figure 2.11 Comparison between optimized and observed values for supply air temperature set point

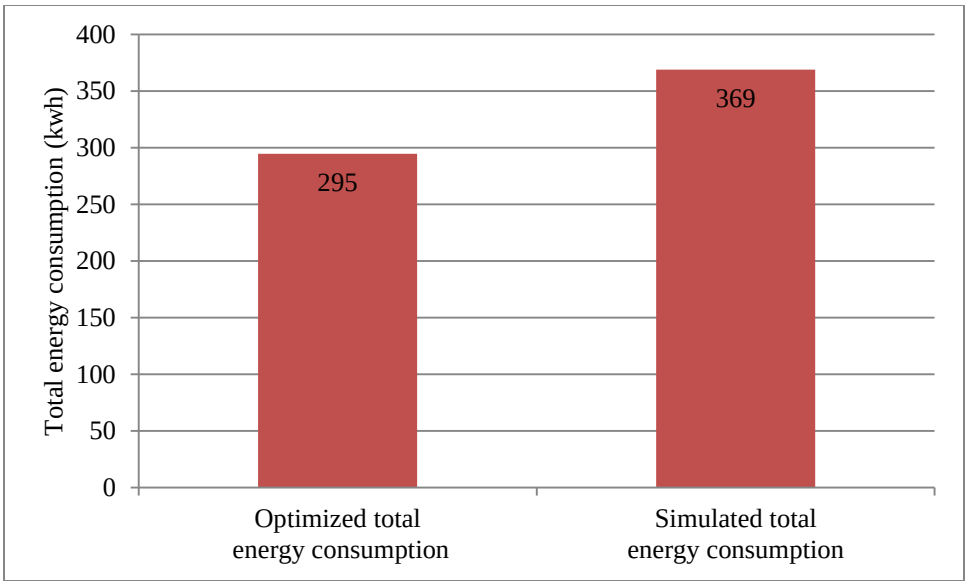

Figure 2.12 Comparison between the optimized and simulated total energy consumption based on the 48 data points

2.7 Summary

In this chapter, a data-driven model was built using a time-series approach, and then it was validated with a historical data set. The stochastic arrival of the occupants was considered in order to simulate the internal heating load. The data-driven model was solved by an interior-point method. A case study illustrating the model and the algorithm was presented. Numerical results indicated that the proposed approach is effective in optimization of the HVAC system energy consumption. Energy savings of 20% were accomplished based on a validation data set. Future research will focus on improving the model accuracy and better handling of user preferences.

CHAPTER 3

MOELDING AND OPTIMIZATION OF AN HVAC SYSTEM USING A DYNAMIC NEURAL NETWORK

3.1 Introduction

As HVAC systems exhibit dynamic and nonlinear characteristics, a nonlinear autoregressive with external inputs (NARX) model can capture its properties and states. Many studies have focused on applying neural networks to identify and control dynamic systems based on NARX [54-57].

This Chapter proposes an optimization model derived by a dynamic neural network based on the concept of a nonlinear autoregressive with external input (NARX). This model is then optimized by three variants of the multi-objective particle swarm optimization (MOPSO) algorithm. The optimization model and the MOPSO algorithm have been implemented at an industrial test laboratory setting. The results from the comparative experiment are reported.

3.2 Solution Methodology

3.2.1 Nonlinear autoregressive with external inputs

The approach known as the nonlinear autoregressive with external input (NARX) is an important modeling of discrete non-linear systems. The NARX model is expressed in Equations (3.1) - (3.2).

$$\hat{x}(t+d) = f_1(x(t), x(t-d), \dots, x(t-m_x d), u_x(t), u_x(t-d), \dots, u_x(t-n_x d)) \quad (3.1)$$

$$\hat{y}(t+d) = f_2(y(t), y(t-d), \dots, y(t-m_y d), u_y(t), u_y(t-d), \dots, u_y(t-n_y d)) \quad (3.2)$$

Where x and y are the system outputs, u_x the input of x, u_y the input of y, d the time delay, $\hat{x}(t+d)$ is the predicted value x at time $t+d$, and $\hat{y}(t+d)$ is the predicted value y at time $t+d$.

In the NARX model, $\hat{x}(t+d)$ together with $x(t), x(t-d), \ldots, x(t-md)$ can be the inputs of the function of $f_2(\cdot)$ when they have significant impact on the output of $\hat{y}(t+d)$. Equation (3.2) can be modified to Equation (3.3) under this situation.

$$\hat{y}(t+d) = f_2(y(t), y(t-d), \ldots, y(t-m_y d), \hat{x}(t+d),\ x(t), x(t-d), \ldots, x(t-md), u_y(t), u_y(t-d), \ldots, u_y(t-n_y d)) \quad (3.3)$$

3.2.2 Problem formulation

From the designer's perspective, the HVAC system should satisfy the peak load of a building. However, usually the system delivers a partial load. It may operate at its full capacity for a limited time only. In this chapter, the HVAC system consumed energy includes electricity ($E_{Electricity}$) and natural gas (E_{Gas}). The electricity is used to power a supply fan (E_{SF}), return fan (E_{RF}), outside air injection fan (E_{OAF}), chillers (E_{CHL}), and pumps (E_{PUMP}). Natural gas is used as reheating source by the variable air volume boxes. Therefore, the total HVAC energy (E_{Total}) is as expressed in Equation (3.4).

$$E_{Total} = E_{Electricity} + E_{Gas} \quad (3.4)$$

Where the energy consumed in electricity form ($E_{Electricity}$) can be expressed in Equation (3.5).

$$E_{Eletricity} = E_{SF} + E_{RF} + E_{OAF} + E_{CHL} + E_{PUMP} \quad (3.5)$$

The energy consumed in natural gas form (E_{Gas}) is derived from Equations (3.6) – (3.7).

$$E_{Gas} = 0.293 \times Q_{Gas} \quad (3.6)$$

$$Q_{Gas} = 500 \times LPGPM \times (LSWT - LRWT) \times T \quad (3.7)$$

Where E_{Gas} is measured in Watt-hour (Wh) and Q_{Gas} is the natural gas measured in British thermal unit (BTU), LPGPM is the water flow rate of a loop pump (gallon/min), LSWT is the supply water temperature (°F), LRWT is the return water temperature (°F), T is the time span (hour), 0.293 is the conversion factor from BTU to Wh, 500 is the conversion factor (BTU·min/gallon· °F · h) for pure water used in the pump. To minimize the total energy consumption, two functions should be first established: the function for predicting the energy consumption and the function for predicting indoor temperature with relevant parameters of the HVAC system as inputs.

3.3 HVAC Predictive Model

3.3.1 Data description

The data set used in this research was collected from an experiment conducted at the Energy Resource Station (ERS) operated by the Iowa Energy Center. The ERS is an energy laboratory for testing and demonstration of commercial HVAC systems. It has two test areas, A and B, equipped with identical devices and four thermal zones. Each thermal zone has a variable air volume (VAV) box connected to the corresponding air handling unit (AHU) to maintain the thermal comfort of the zone. Weather data has been collected by sensors installed around the building. The control of the HVAC system involves two set points, the AHU static pressure set point (SA-SPSPT) and the supply air temperature set point (SAT-SPT) that were adjusted in the data collection experiment to reflect a range of the HVAC system states. In particular the SP-SPT set point was varied from 1.2 in. WG (0.3 kPa) to 1.8 in. WG (0.45 kPa) at 0.2 in. WG (0.05 kPa) increments, while the SAT-SPT varied from 50 ℉ (10 ℃) to 65 ℉ (18.33 ℃) at 1 ℉ (0.556 ℃) increment. The data on more than 300 parameters was recorded at one-minute sampling intervals. The experiment was conducted between July 31 to August 15, 2010, and September 21 to October 7, 2010. The data used in this research includes three subsets. Data set 2 of 2065 instances was used to train the predictive models, while data set 3 and

data set 4, each with 442 instances, was used to test and validate the models. These data sets are summarized in Table 3.1. (Note that the data in Table 3.1 is expressed in 30-min intervals derived from the original 1-min data).

Table 3.1 Description of data sets

Data Set No.	Data Set Type	Time Period	Number of Instances
1	Entire data set	07/31-08/15/2010 & 09/21-10/07/2010	2949
2	Training data set	Randomly selected from data set 1	2065
3	Test data set	Randomly selected from data set 1	442
4	Validation data set	Randomly selected from data set 1	442

3.3.2 Parameter selection

Parameter selection is performed to eliminate parameters of less importance to the model to enhance comprehensibility, scalability, and often the accuracy of the resulting models [48]. Table 3.2 includes 21 parameters that were selected as the candidates for building the models discussed later in this chapter. Boosting tree is a learning algorithm for ranking the importance of parameters for prediction. According to [49, 50], the boosting tree algorithm has demonstrated good performance in parameter selection and therefore it is utilized in this chapter for selecting parameters. Furthermore, since the HVAC system is dynamic, the system state and energy consumption are significantly influenced by past values and the system parameters. Correlation analysis has been used to determine the relationship between the system state and energy consumption with their past values at different time steps. Figures 3.1 and 3.2 illustrate the relationships between energy consumption and indoor room temperature with their previous values. Figure 3.3 shows the relationship between energy consumption and indoor room temperature at different time steps. Correlation analysis has determined the relationship between the system state and the energy consumption with the system inputs at different time steps.

Figure 3.4 shows the relationship between the energy consumption and the supply fan speed at different time steps. By combining the correlation analysis with the boosting tree algorithm, the parameters, listed in Tables 3.3 and 3.4, at different states have been selected to build the energy consumption model and the indoor room temperature model.

Table 3.2 Candidate parameters selected based on domain knowledge

Parameter Type	Parameter Name	Description	Unit
Optimized input parameter	SAT-SPT	AHU supply air temperature set point	℉ (℃)
	SASP-SPT	Supply air duct static pressure set point	in. WG (kPa)
Input parameter	CHWC-VLV	Chilled water coil valve position	% Open
	SA-HUMD	Supply air humidity	% RH
	MA-TEMP	Mixed air temperature	℉ (℃)
	CHWC-EWT	Chilled water coil entering water temperature	℉ (℃)
	SA-CFM	Supply air fan speed	CFM
	RA-CFM	Return air fan speed	CFM
	RM-TEMP	Room temperature	℉ (℃)
	OA-TEMP	Outside air temperature	℉ (℃)
	OA-HUMD	Outside air humidity	% RH
	OA-CO2	Outside air CO2 concentration	PPM
	IR-RADIA	Infrared radiation	B/HFt2
	SOL-HORZ	Solar normal flux	B/HFt2
	SOL-BEAM	Solar beam	B/HFt2
	BAR-PRES	Barometric pressure	mBar
	WIND-VEL	Outside wind velocity	MPH
	WIND-DIR	Outside wind direction	Deg
System state	RM-HUMD	Room humidity	% RH
	RM-TEMP	Room temperature	℉ (℃)
System output	ENERGY	Energy consumed by the HVAC system	Wh

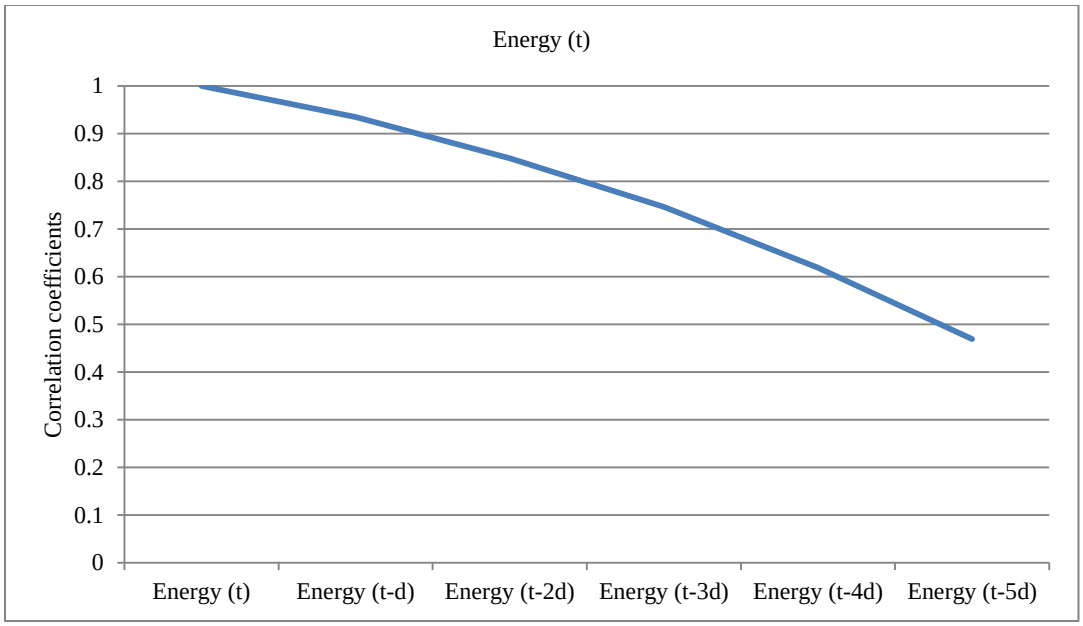

Figure 3.1 Correlation coefficient between energy consumption and its previous values at different time steps

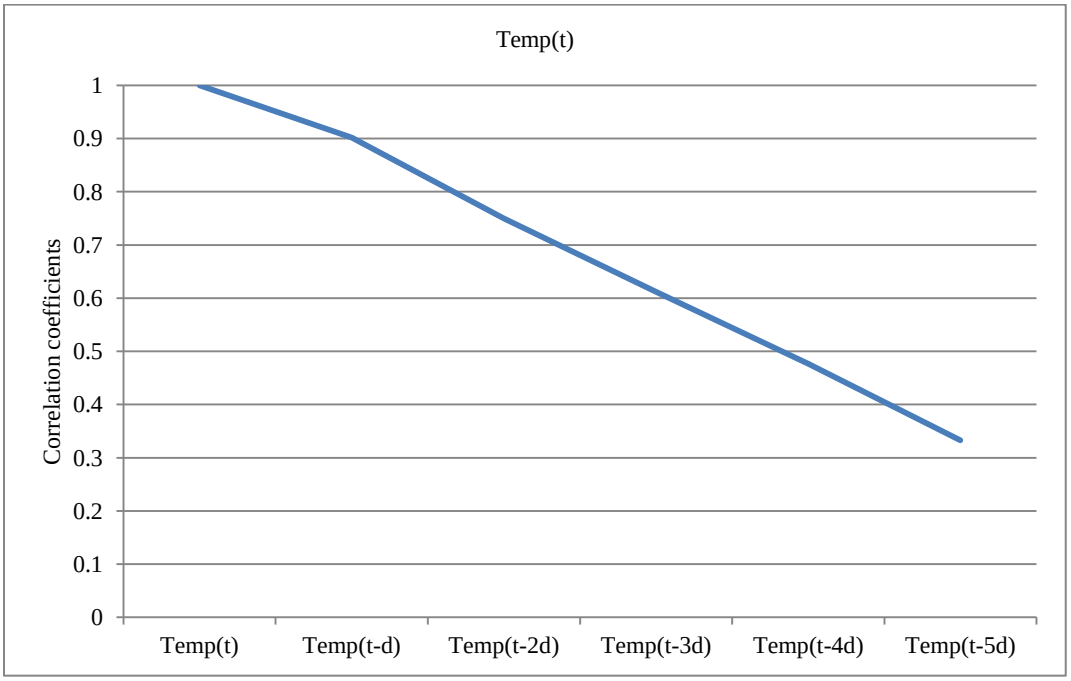

Figure 3.2 Correlation coefficient between room temperature and its previous values at different time steps

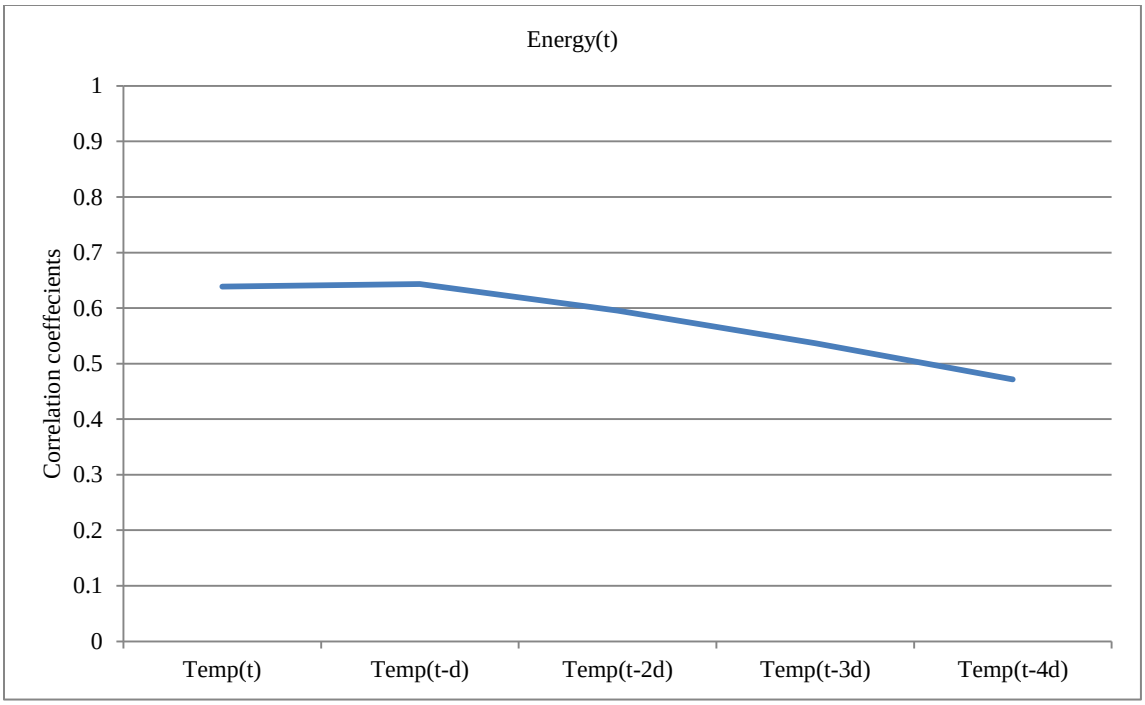

Figure 3.3 Correlation coefficient between energy consumption and room temperature at different time steps

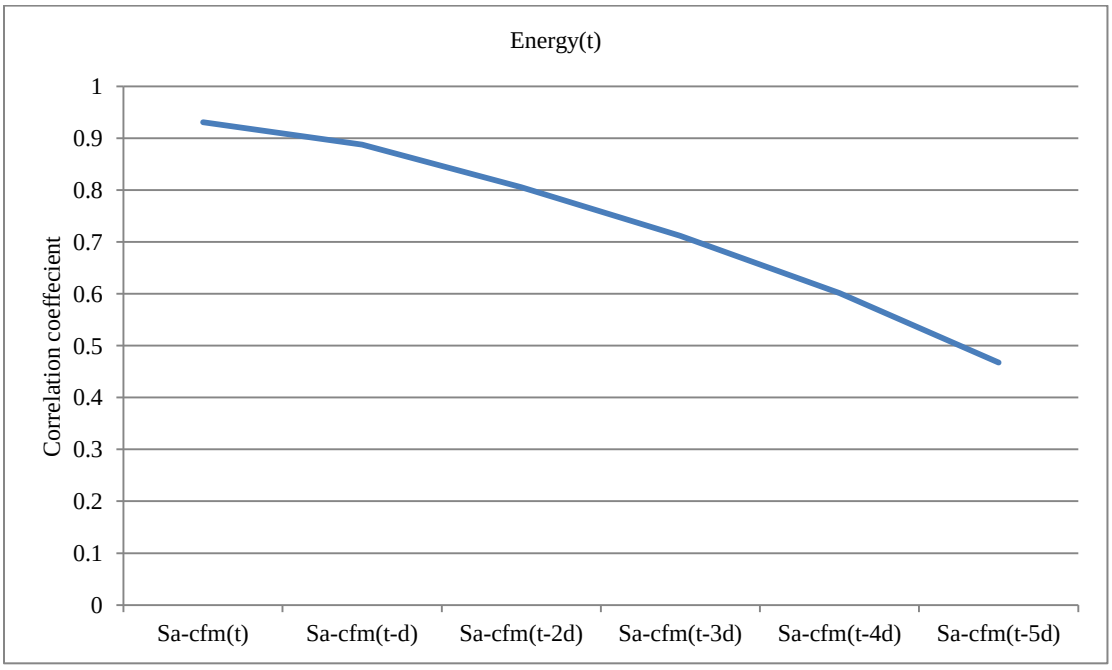

Figure 3.4 Correlation coefficient between energy consumption and supply air fan speed at different time steps

Table 3.3 Parameters selected for building energy consumption model at time $t + d$

Parameter	Parameter Name	Description
$y(t)$	Energy consumption	Energy consumption at time t
$y(t-d)$	Energy consumption	Energy consumption at time t - d
$y(t-2d)$	Energy consumption	Energy consumption at time t - 2d
$x(t+d)$	RM-TEMP	Estimated room temperature at time t + d
$x(t)$	RM-TEMP	Room temperature at time t
$x(t-d)$	RM-TEMP	Room temperature at time t - d
$v_{y1}(t)$	OA-HUMD	Outside air humidity at time t
$v_{y2}(t)$	OA-TEMP	Outside air temperature at time t
$v_{y3}(t)$	SA-HUMD	Supply air humidity at time t
$v_{y4}(t)$	SOL-HORZ	Solar normal flux at time t
$v_{y5}(t)$	RA-CFM	Return air fan speed at time t
$v_{y5}(t-d)$	RA-CFM	Return air fan speed at time t - d
$v_{y5}(t-2d)$	RA-CFM	Return air fan speed at time t 2d
$v_{y6}(t)$	SA-CFM	Supply air fan speed at time t
$v_{y6}(t-d)$	SA-CFM	Supply air fan speed at time t - d
$v_{y6}(t-2d)$	SA-CFM	Supply air fan speed at time t- 2d
$c_1(t+d)$	SAT-SPT	Supply air temperature set point at time t + d
$c_2(t+d)$	SASP-SPT	Supply air duct static pressure set point at time t + d

3.3.3 Model construction

In this section, a multi-layer perception (MLP) ensemble algorithm is used to build the predictive models for energy consumption and indoor room temperature as it outperforms other algorithms including the chi-squared automatic interaction detector (CHAID), classification and regression tree (C&RT) algorithm, support vector machine (SVM), multi-layer perception (MLP), boosting tree, random forest, and multivariate adaptive regression spline (MARSpline) algorithms [34]. The models constructed by the MLP ensemble are expressed as Equations (3.8) – (3.9):

$$x(t+d) = f_1(x(t), x(t-d), x(t-2d), y(t), v_{x1}(t), v_{x2}(t), v_{x3}(t), v_{x4}(t), v_{x5}(t), v_{x6}(t), v_{x7}(t), c_1(t+d), c_2(t+d)) \quad (3.8)$$

$$y(t+d) = f_2(y(t), y(t-d), y(t-2d), x(t+d), x(t), x(t-d), v_{y1}(t), v_{y2}(t), v_{y3}(t), v_{y4}(t), v_{y5}(t), v_{y5}(t-d), v_{y5}(t-2d), v_{y6}(t), v_{y6}(t-d), v_{y6}(t-2d), c_1(t+d), c_2(t+d)) \quad (3.9)$$

where $\hat{y}(t+d)$ is the energy consumption of the HVAC system (objective function), $\hat{x}(t+d)$ is the room temperature (objective function); $c_1(t+d)$ and $c_2(t+d)$ represent the supply air temperature set point and the supply air duct static pressure set point (decision variables).

Table 3.4 Parameters selected for building the indoor temperature model at time *t* + *d*

Parameter	Point Name	Description
$x(t)$	RM-TEMP	Room temperature at time *t*
$x(t-d)$	RM-TEMP	Room temperature at time *t* - d
$x(t-2d)$	RM-TEMP	Room temperature at time *t* 2d
$y(t)$	Energy consumption	Energy consumption at time *t*
$v_{x1}(t)$	RA-CFM	Return air fan speed at time *t*
$v_{x2}(t)$	SA-CFM	Supply air fan speed at time *t*
$v_{x3}(t)$	MA-TEMP	Mixed air temperature at time *t*
$v_{x4}(t)$	SA-HUMD	Supply air humidity at time *t*
$v_{x5}(t)$	OA-TEMP	Outside air temperature at time *t*
$v_{x6}(t)$	OA-CO2	Outside air CO2 concentration at time *t*
$v_{x7}(t)$	CHWC-VLV	Chilled water coil valve position at time *t*
$c_1(t+d)$	SAT-SPT	Supply air temperature set point at time *t* + d
$c_2(t+d)$	SASP-SPT	Supply air duct static pressure set point at time *t* + d

In order to obtain the concrete form of $f_1(\cdot)$ and $f_2(\cdot)$ in Equations (3.8) and (3.9), data set 1 (2949 data instances) was divided into three parts: training data set (2065 data instances), test data set (442 data instances), and validation data set (442 data instances) as shown in Table 3.1. In the next sub-section, the performance of the predictive models will be validated.

3.3.4 Model validation

To evaluate the performance of the predictive models built by the MLP ensemble algorithm, the metrics in Chapter 2 (Equations (2.17) – (2.22)) are used. The data in Table 3.5 shows the performance of the predictive models built by the MPL ensemble algorithm. Figure 3.5 compares the predicted and observed values of the energy consumption of HVAC systems on 442 30-min data instances drawn from data set 3. The values obtained from the energy consumption predictive model in Figure 3.6 follow closely to the observed values. Figure 3.7 compares the predicted and observed values of the room temperature on the same data instances with the energy consumption generated by the predictive model. The detailed measurement of the performance for the two models is summarized in Table 3.5. As shown in Table 3.5, the accuracy for the energy consumption predictive model on validation data set is 91.7%. For the temperature predictive model, the accuracy on the validation data set is 99.6%. Therefore, the two predictive models are selected to construct the overall optimization model.

Table 3.5 Prediction accuracy of the MLP ensemble algorithm of energy consumption and room temperature

Objective	Data Set	MAE	MAPE	Std_AE	Std_MAPE
Energy consumption	Training	153.975	0.064	143.086	0.166
	Test	179.836	0.067	217.791	0.083
	Validation	213.398	0.083	311.036	0.200
Room temperature	Training	0.269	0.004	0.263	0.004
	Test	0.287	0.004	0.285	0.004
	Validation	0.308	0.004	0.312	0.004

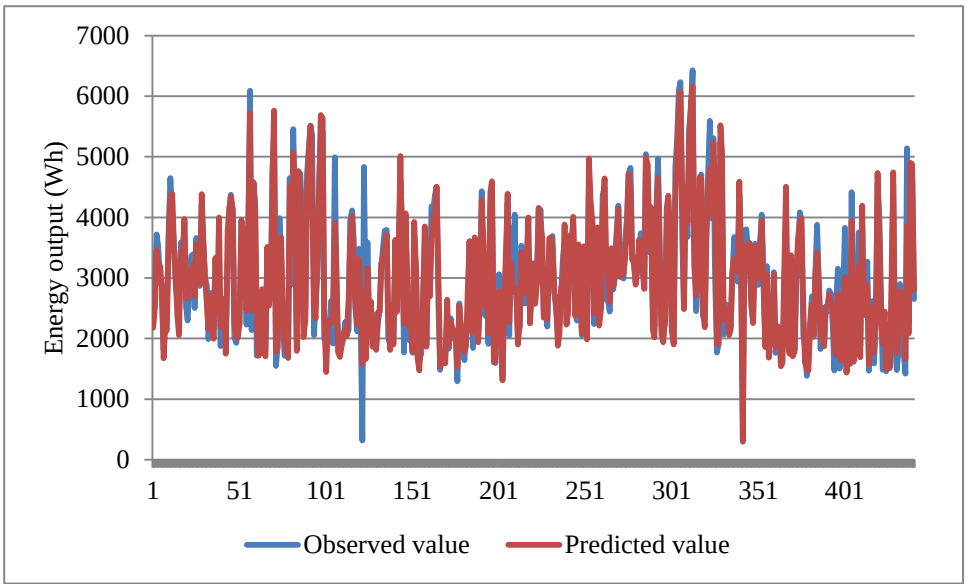

Figure 3.5 Validation of the energy consumption model with 442 data instances

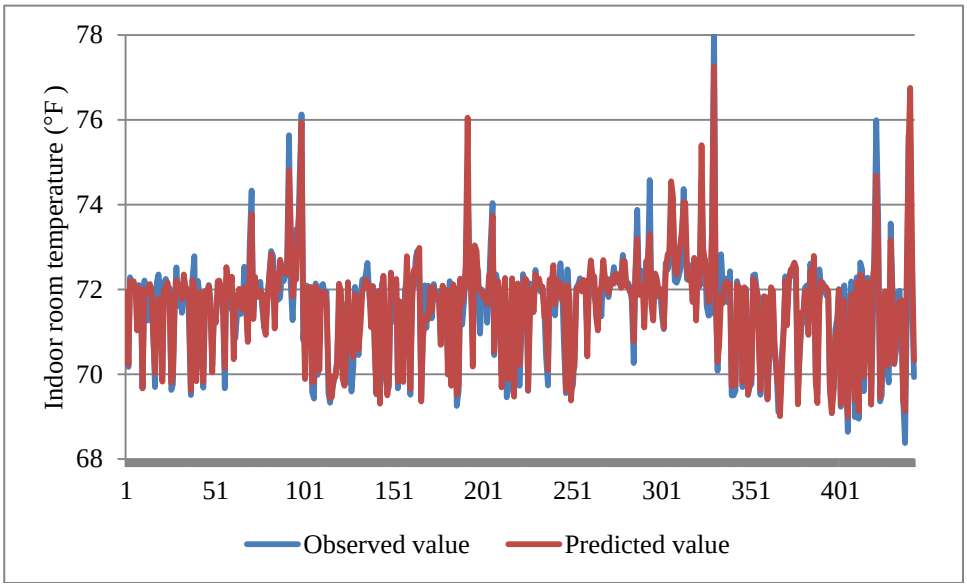

Figure 3.6 Validation of the room temperature model with 442 data instances

3.4 Model Optimization

3.4.1 Optimization model formulation

To minimize the energy consumption of the HVAC system, the objective function in Equation (3.9) is minimized while maintaining the value of in Equation (3.8) within an

acceptable range in search of the optimal supply air temperature and the supply air duct static pressure set points at the time $t + d$. The observed room temperature can be calibrated by the sensors originally installed in the system while the observed energy consumption can be computed from Equations (3.4)-(3.7). The constraints in the model are identified by setting the lower and upper bounds of the control parameters and assigning an acceptable range for room temperature. These settings are restricted within the following limits:

- The supply air temperature set point varies from 50 ℉ (10 ℃) to 64 ℉ (17.7 ℃).
- The supply air duct static pressure set point varies between 1.2 in. WG (0.3 kPa) to 1.8 in. WG (0.45 kPa).
- The room temperature is maintained between 70.5 ℉ (21.39 ℃) and 71.5 ℉ (21.94 ℃).

These three limits are determined by the design of the HVAC system and preferences of the occupants. Therefore, the optimization model is formulated as Equation (3.10):

$$\begin{gathered}\min_{c_1(t+d),c_2(t+d)} y(t+d) \\ \text{subject to:} \\ x(t+d) = f_1(x(t), x(t-d), x(t-2d), y(t), v_{x1}(t), v_{x2}(t), v_{x3}(t), v_{x4}(t), v_{x5}(t), v_{x6}(t), v_{x7}(t), c_1(t+d), c_2(t+d)) \\ y(t+d) = f_2(y(t), y(t-d), y(t-2d), x(t+d), x(t), x(t-d), v_{y1}(t), v_{y2}(t), v_{y3}(t), v_{y4}(t), v_{y5}(t), \\ v_{y5}(t-d), v_{y5}(t-2d), v_{y6}(t), v_{y6}(t-d), v_{y6}(t-2d), c_1(t+d), c_2(t+d) \\ 50 \le c_1(t+d) \le 64 \\ 1.2 \le c_2(t+d) \le 1.8 \\ 70.5 \le \widehat{x(t+d)} \le 71.5\end{gathered} \tag{3.10}$$

where $\hat{x}(t + d)$ is the predicted value of indoor room temperature by applying the original supply air temperature set point $c_1(t + d)$ and the supply air duct static pressure set point $c_2(t + d)$. In minimizing the energy consumption at time stamp t +

d, the room temperature is maintained within a pre-set range. The constrained model (3.10) is transformed to a bi-objective optimization model with the objective functions (3.11) and (3.12):

$$Obj1 = \hat{y}(t+d) \tag{3.11}$$

$$Obj2 = \max\{0, 70.5 - \hat{x}(t-d)\} + \max\{0, \hat{x}(t+d) - 71.5\} \tag{3.12}$$

Then the bi-objective optimization model is presented as Equation (3.13):

$$\begin{gathered}
\min_{c_1(t+d), c_2(t+d)} (Obj1, Obj2) \\
\text{subject to:} \\
\begin{aligned}
x(t+d) = f_1(&x(t), x(t-d), x(t-2d), y(t), v_{x1}(t), v_{x2}(t), v_{x3}(t), v_{x4}(t), v_{x5}(t), v_{x6}(t), v_{x7}(t), c_1(t+d), c_2(t+d)) \\
y(t+d) = f_2(&y(t), y(t-d), y(t-2d), x(t+d), x(t), x(t-d), v_{y1}(t), v_{y2}(t), v_{y3}(t), v_{y4}(t), v_{y5}(t), \\
&v_{y5}(t-d), v_{y5}(t-2d), v_{y6}(t), v_{y6}(t-d), v_{y6}(t-2d), c_1(t+d), c_2(t+d)
\end{aligned} \\
50 \le c_1(t+d) \le 64 \\
1.2 \le c_2(t+d) \le 1.8
\end{gathered} \tag{3.13}$$

Note that when Obj2 is equal to 0, all constraints of the model in Equation (3.13) are satisfied.

3.4.2 Multi-objective particle swarm optimization algorithm

Since the optimization model derived from the MLP ensemble algorithm is complex, it is difficult to solve it with traditional algorithms. Particle swarm optimization (PSO) inspired by natural bird flocks is a suitable optimization algorithm [36]. The PSO algorithm is easy to implement and there are few parameters to adjust. In recent years, many modifications have been made to the original algorithm [58]. Among those modifications, constant inertia weight particle swarm optimization (CIWPSO), constricted particle swarm optimization (CPSO), and decreasing inertia weight particle swarm optimization (DIWPSO) have good performance in most cases. Hence, these three PSO variants were applied in this research. The PSO in its original form [58] is presented next:

Step 1: Initialize a group of particles with random positions $x_i \in R^D$ and velocities $v_i \in R^D$ in the search space;

Perform the next steps until the pre-set requirements are satisfied.

Step 2: For each particle, compute fitness for each particle by using function $f_1(.)$.

Step 3: Compare each particle' fitness with its past best value, $pbest_i$. If current value is better than $pbest_i$, then using current value instead of and update $p_i \in R^D$ with current location x_i; compare all of the particles' and find the best one assigned as and set its current location as $p_g \in R^D$.

Step 4: Update the particles' velocities and positions based on the following Equation (3.14):

$$\begin{aligned} v_i &\leftarrow v_i + U(0,\varphi_1)\cdot(p_i - x_i) + U(0,\varphi_2)\cdot(p_g - x_i) \\ x_i &\leftarrow x_i + v_i \end{aligned} \tag{3.14}$$

Step 5: If the stop criterion is satisfied, p_g is the final solution and the final optimal fitness.

Note that $U(0,a)$ represents the uniform distribution in $[0,a]$; and v_i should be within the range $[-v_{max}, v_{max}]$.

In order to get CIWPSO, CPSO, and DIWPSO, the concrete modifications to the original PSO are listed in the following:

1) For constant inertia weight particle swarm optimization Equation (3.14) is transformed into Equation (3.15).

$$\begin{aligned} v_i &\leftarrow \omega v_i + U(0,\varphi_1)\cdot(p_i - x_i) + U(0,\varphi_2)\cdot(p_g - x_i) \\ x_i &\leftarrow x_i + v_i \end{aligned} \tag{3.15}$$

Where$\omega$is the inertia weight that can reduce the importance of v_{max} to satisfy the requirement of controlling the scope of the search? For constant inertial particle swarm optimization $\omega$is a constant.

2) For constricted particle swarm optimization Equation (3.14) is expresses as Equation (3.16).

$$\begin{aligned} v_i &\leftarrow \chi(v_i + U(0,\varphi_1)\cdot(p_i - x_i) + U(0,\varphi_2)\cdot(p_g - x_i)) \\ x_i &\leftarrow x_i + v_i \end{aligned} \tag{3.16}$$

where χ is the constriction coefficient that can control the convergence of the particle and prevent explosion of the particle's velocity. Usually this constriction coefficient is set to 0.7298.

3) For decreasing inertia weight particle swarm optimization Equation (3.14) is expressed as Equation (3.17).

$$\begin{aligned} v_i^{t+1} &\leftarrow \omega^t v_i^t + U(0,\varphi_1)\cdot(p_i^t - x_i^t) + U(0,\varphi_2)\cdot(p_i^t - x_i^t) \\ x_i^{t+1} &\leftarrow x_i^t + v_i^{t+1} \end{aligned} \tag{3.17}$$

In equation (3.17), ω^t is a time function. It is updated based on Equation (3.18).

$$\omega^t = \frac{\omega t_{\max} - t}{\omega t_{\max}}(\omega_{\max} - \omega_{\min}) + \omega_{\min} \tag{3.18}$$

To adopt the above three algorithms for solving a multi-objective optimization model, the following modifications are made according to [59].

Modification 1: Create a set $S_i$to store the non-dominated solutions for i^{th} particle up to the current time.

Modification 2: Create a set G to store the non-dominated solutions from all S_i at each iteration.

Modification 3: Create an external set E to store the non-dominated solutions from G at each iteration.

Modification 4: Process to updateS_i: At each iteration, compare the current particle solution with the stored solutions. Dominated solutions are removed while non-dominated solutions are kept.

Modification 5: Process to update G: At each iteration, copy all to G where dominated solutions are removed.

Modification 6: Process to update external non-dominated set E: At each iteration, copy solutions from G to E. Remove the dominated solutions from E.

Modification 7: Process to generate local and global best solution: For each particle at each iteration, the Euclidean distance among solutions from the corresponding local non-dominated set and global non-dominated set are measured. The pair with minimum distance in the search space is selected as the local and global best for this particle in under-taking the later velocity and position updating process.

In contrast to CIWPSO, DIWPSO, and CPSO that were designed for solving single objective models, multi-objective CIWPSO (MO-CIWPSO), multi-objective DIWPSO (MO-DIWPSO), and multi-objective CPSO (MO-CPSO) are aimed at solving multi-objective models. Figure 3.7 shows the flow chart for the multi-objective particle swarm optimization algorithm.

3.4.3 Optimization results and analysis

To solve the optimization model represented by (3.10), the above-mentioned three multi-objective PSO variants are applied and the detailed parameters for the algorithms are listed in Table 3.6.

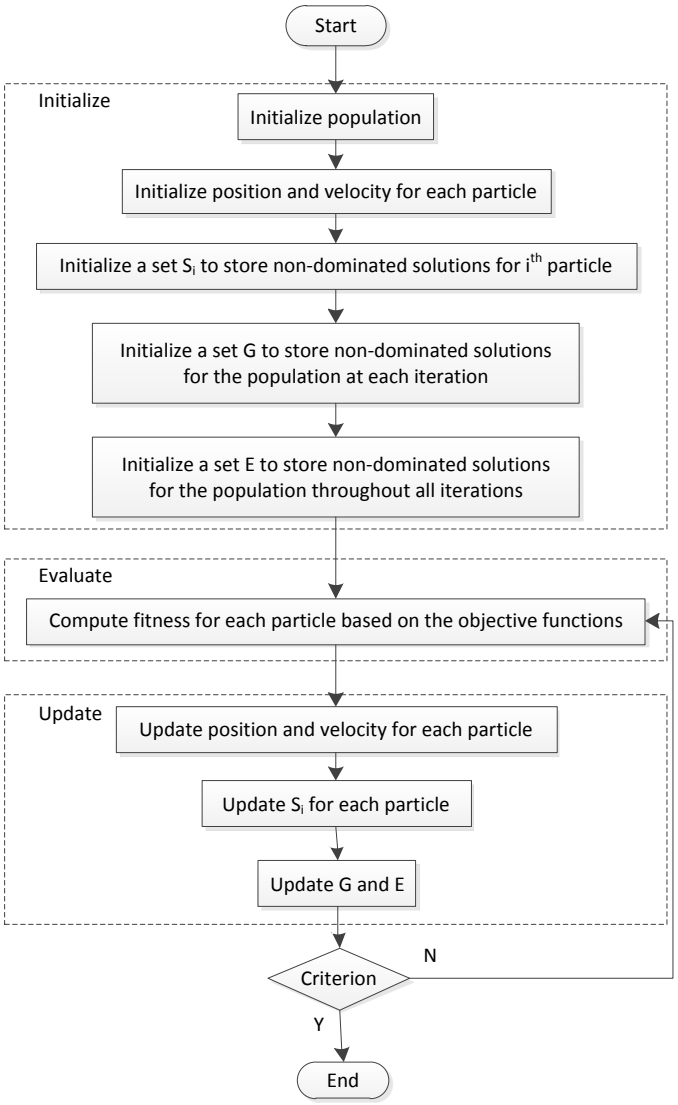

Figure 3.7 The flow chart of multi-objective particle swarm optimization algorithm

Data set 4 in Table 3.1 is used to run the variants of the PSO algorithm defined in Table 3.6. The optimal solution is selected from the final elite set based on the weighted normalized objective function (3.19).

$$Obj = w_1 \frac{Obj1 - Obj1_{\min}}{Obj1_{\max} - Obj1_{\min}} + w_2 \frac{Obj2 - Obj2_{\min}}{Obj2_{\max} - Obj2_{\min}} \tag{3.19}$$

where ω_1 and ω_2 are the user-defined weights indicating the preference of the corresponding objective, $Obj1_{max}$ and $Obj1_{min}$ are the maximum and the minimum

values of Obj1 in the final elite set. Similar notation is used for $Obj2_{max}$ and $Obj2_{min}$. Note that $\omega_1 + \omega_2 = 1$, with $\omega_1$and $\omega_2$being either constants or functions of other objectives.

Table 3.6 Settings for the three multi-objective PSO variants

Algorithm	Settings
MO-CIWPSO	Acceleration coefficients are set to $\phi1=\phi2=2.05$. Inertia weight is set to 0.95. Population size and the number of iterations are set to 100 and 50, respectively.
MO-DIWPSO	Acceleration coefficients are set to $\phi1=\phi2=2.05$. Linearly decreasing inertia weight from 0.9 to 0.4 and the final value is reach at the end of the run. Population size and iteration number are set to 100 and 50, respectively.
MO-CPSO	Acceleration coefficients $\phi=4.1$. Constriction factor $\chi=0.729$. Population size and the number of iterations are set to 100 and 50, respectively.

Table 3.7 presents two scenarios that represent different preferences to the objectives. Scenario 1 means that energy consumption is the only criterion to be considered when selecting the single best solution among the non-dominated solutions. Scenario 2 means energy consumption and room temperature are both important criterion when selecting the single best solution among the non-dominated solutions.

Table 3.7 Two scenarios involving different weight values

Scenario	Weights	Description
1	$w_1 = 1, w_2 = 0$	No AQI constraints
2	$w_1 = \begin{cases} 1 & if\ y_2 \in [70.5, 71.5] \\ 0.5 & otherwise \end{cases}, w_2 = \begin{cases} 0 & if\ y_2 \in [70.5, 71.5] \\ 0.5 & otherwise \end{cases}$	Consider room temperature as constraint

In order to eliminate the bias of the algorithms, each of the three multi-objective PSO variants was run ten times and the average values and the corresponding standard

deviation were calculated. The results provided by the three variants of the PSO algorithm are listed in Table 3.8 that illustrates the multi-objective DIWPSO outperforms other two multi-objective PSO variants, and therefore, the DIWPSO is used in the following analysis.

Table 3.8 Performance of the three multi-objective PSO variants

Algorithm	Energy Savings in Scenario 1	Energy Savings in Scenario 2
MO-CIWPSO	22.77% ± 0.12%	21.83% ± 0.13%
MO-DIWPSO	23.00% ± 0.06%	22.04% ± 0.13%
MO-CPSO	22.86% ± 0.13%	21.89% ± 0.12%

Figures 3.8- 3.9 compare the observed and the optimized values on data set 4 for Scenario 1 and 2. In most cases, the energy consumption of the optimized process is less than the observed one, which means the proposed model can save energy. Figures 3.10-3.11 illustrate the room temperature for Scenario 1 and 2. In most cases, the indoor room temperature can be kept in the range from 68 ℉ (20 ℃) to 72 ℉ (22.22 ℃) (desired room temperature range). Since Scenario 2 considers the room temperature as a constraint when selecting the single best solution among the non-dominated solutions, the number of the points which room temperature violates the desired room temperature range is less than the one in Scenario 1. Figures 3.12-3.13 present the supply air temperature set point and the supply air duct static pressure set point. Based on these set points, the energy savings which is the difference between the observed and optimized energy consumption shown in Figures 3.8 and 3.9 can be achieved.

The actual implementation and validation of the DIWPSO algorithm for Scenario 2 is discussed in the next section

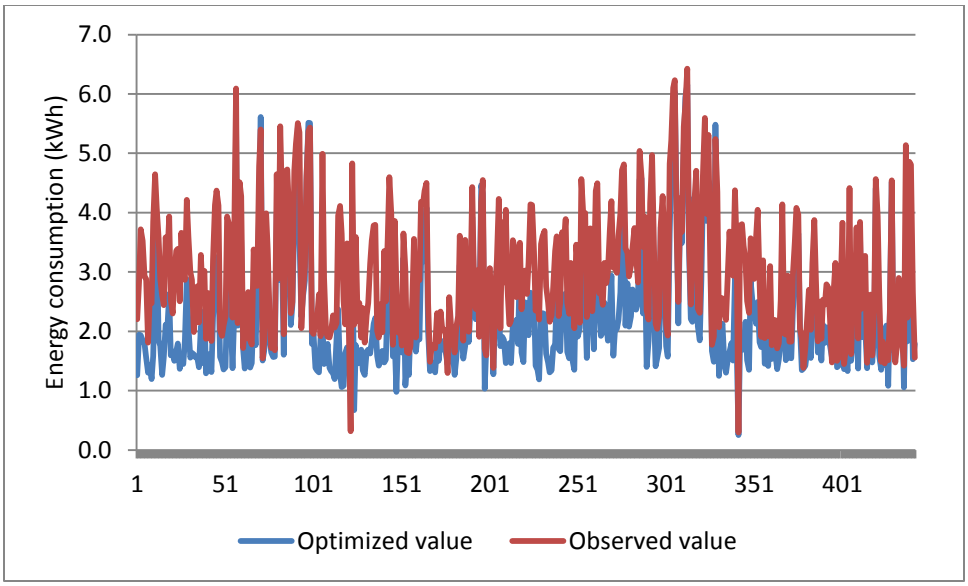

Figure 3.8 Comparison between the observed and optimized energy consumption in Scenario 1

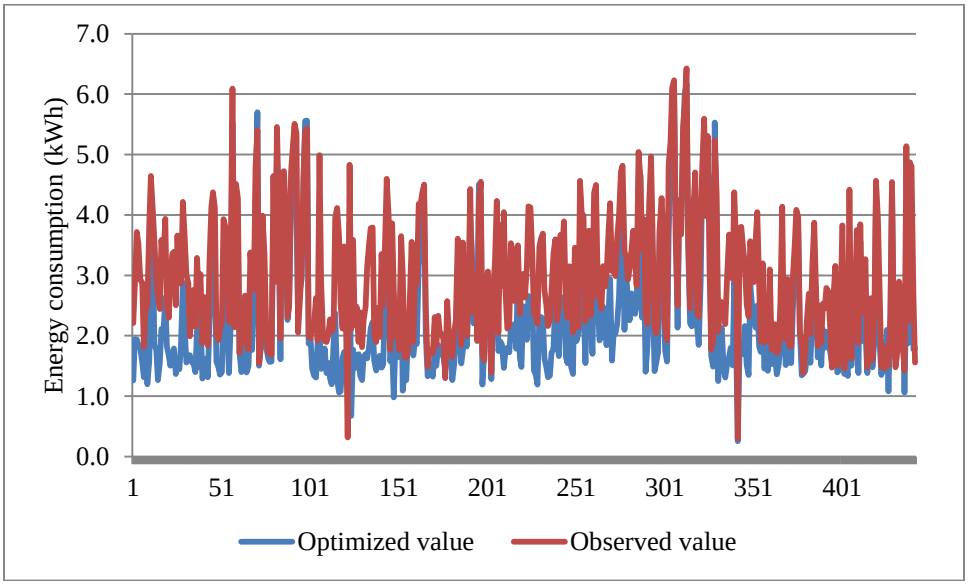

Figure 3.9 Comparison between the observed and optimized energy consumption in Scenario 2

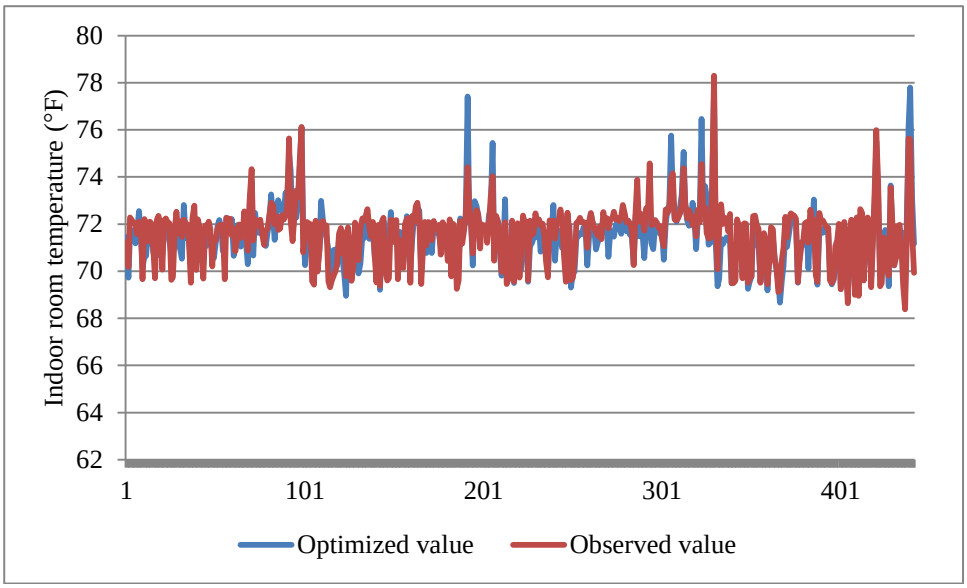

Figure 3.10 Comparison between the observed and optimized room temperature in Scenario 1

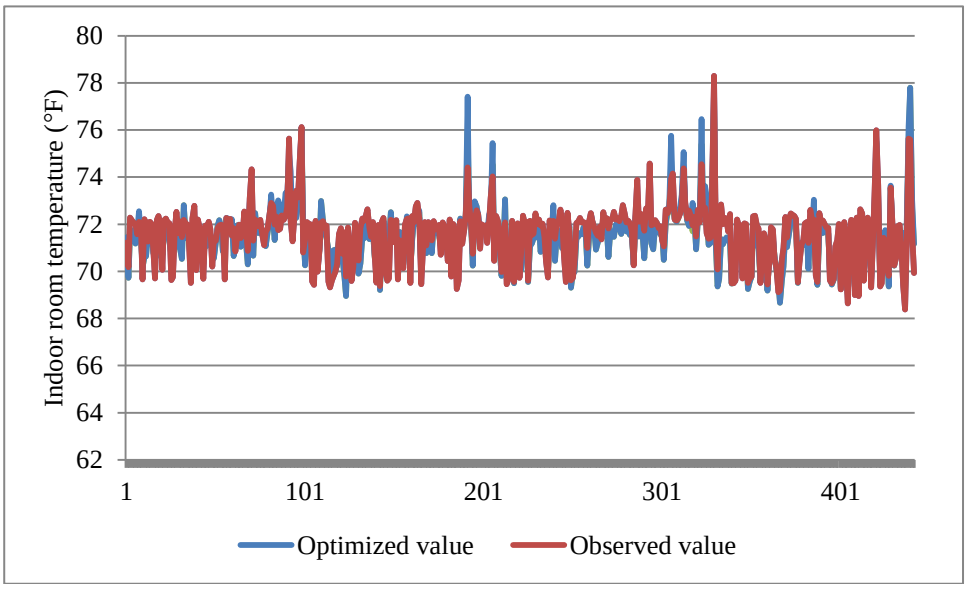

Figure 3.11 Comparison between the observed and optimized room temperature in Scenario 2

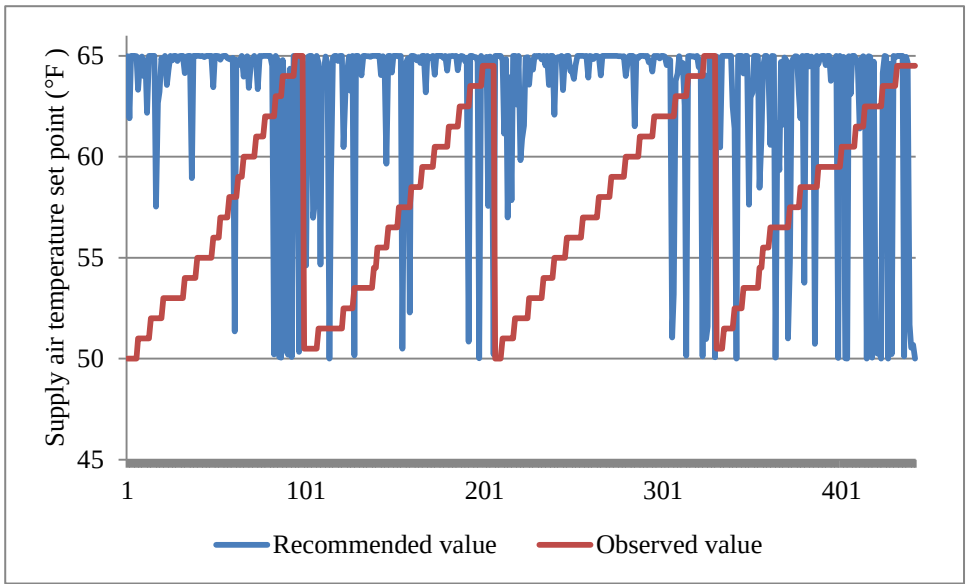

Figure 3.12 Recommended supply air temperature set point compared to the observed value in Scenario 1

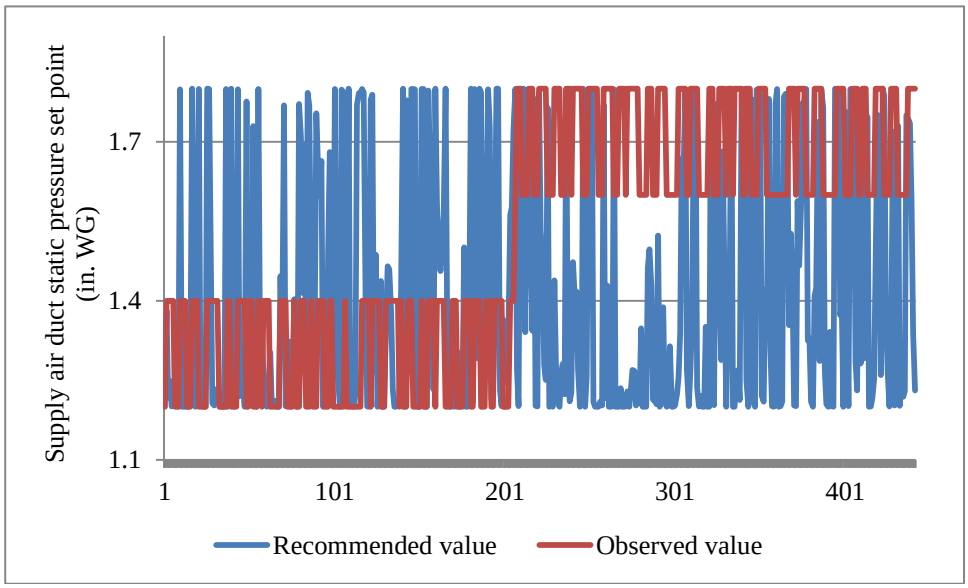

Figure 3.13 Recommended supply air duct static pressure set point compared to the observed value in Scenario 1

3.5 Model Implementation and Result Analysis

To validate the energy savings produced by the model presented in this chapter, an experiment was designed at the Energy Resource Station (ERS) of the Iowa Energy

Center from May 15 to 22, 2011. In the experiment, AHU-A and AHU-B were operated simultaneously. The AHU-A and AHU-B serve four identical thermal areas. The only difference between the two systems was that the AHU-A was controlled by the proposed approach while the AHU-B was controlled by the traditional approach. The experiment included two stages. The first stage from May 15 to 20, 2011 aimed at collecting data from the two systems while the second stage from May 21 to 22, 2011 was to establish the energy consumption bias between the two systems controlled by the traditional approach. At the first stage, AHU-A was controlled by the optimization model while AHU-B operated with fixed set points: the supply air temperature set at 55 ℉ (12.78 ℃) and the supply air duct static pressure set at 1.4 in. WG (0.35 kPa). Since these two systems use identical devices and they serve identical test areas, the difference in energy consumption points to the effectiveness of the proposed optimization approach. As shown in Figure 3.14, the energy consumption for AHU-A and AHU-B are 568.88and 781.16 kWh, respectively. AHU-A therefore consumed less energy than AHU-B, thus producing an energy savings of 27.18%. Figure 3.15 illustrates the room temperature for AHU-A and AHU-B. Although the range of indoor room temperature of AHU-A is larger than for AHU-B, it usually falls in the normal range of 68 ℉ (20 ℃) to 72 ℉ (22.22 ℃). Only for a limited time does it exceed the present constraints. Thus, the indoor room temperature is considered to be at an acceptable level. In the second stage, the two systems were operated with identical fixed set points: the supply air temperature was set at 55 ℉ (12.78 ℃) and the supply air duct static pressure was set at 1.4 in. WG (0.35 kPa). As shown in Figure 3.16, the energy consumption of AHU- A and AHU-B are 277.22 and 266.49 kWh, respectively. AHU- A therefore consumes 3.87% more energy than AHU-B for the same control settings. Considering for the bias between the two systems, the energy savings provided by the optimization model are adjusted to 29.99%. Figure 3.17 show the adjusted energy comparison after the adjustment.

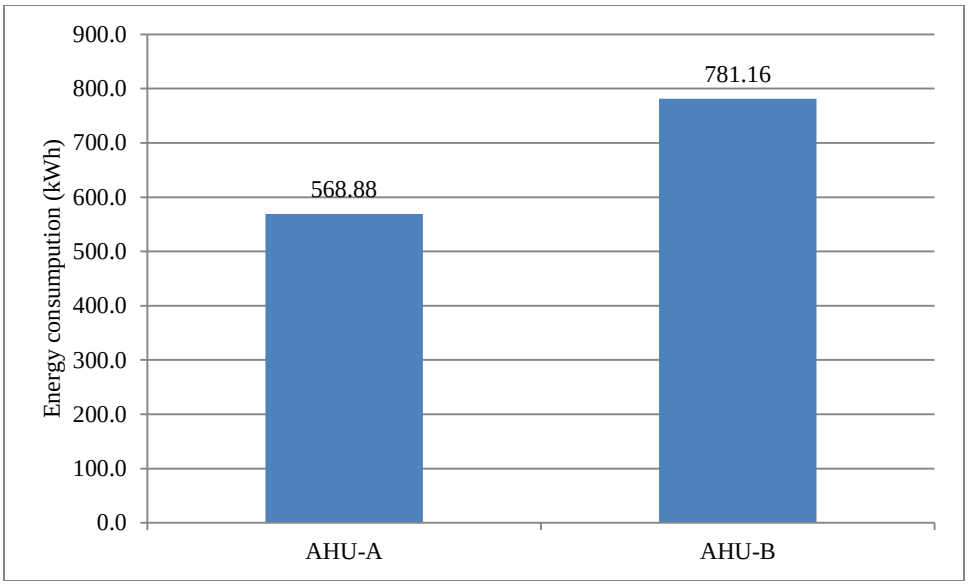

Figure 3.14 Energy consumption of AHU-A and AHU-B at the first stage

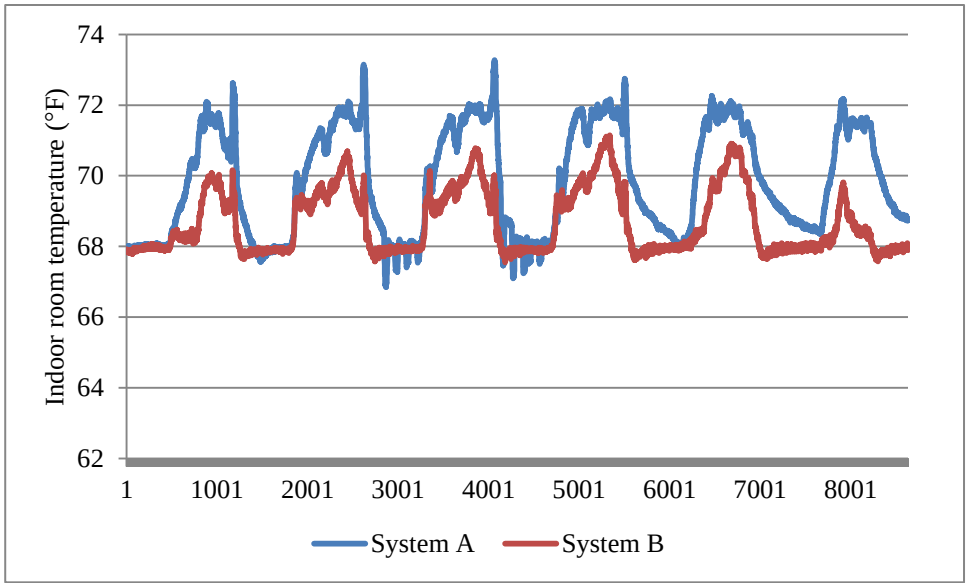

Figure 3.15 Room temperature of AHU-A and AHU-B at the first stage

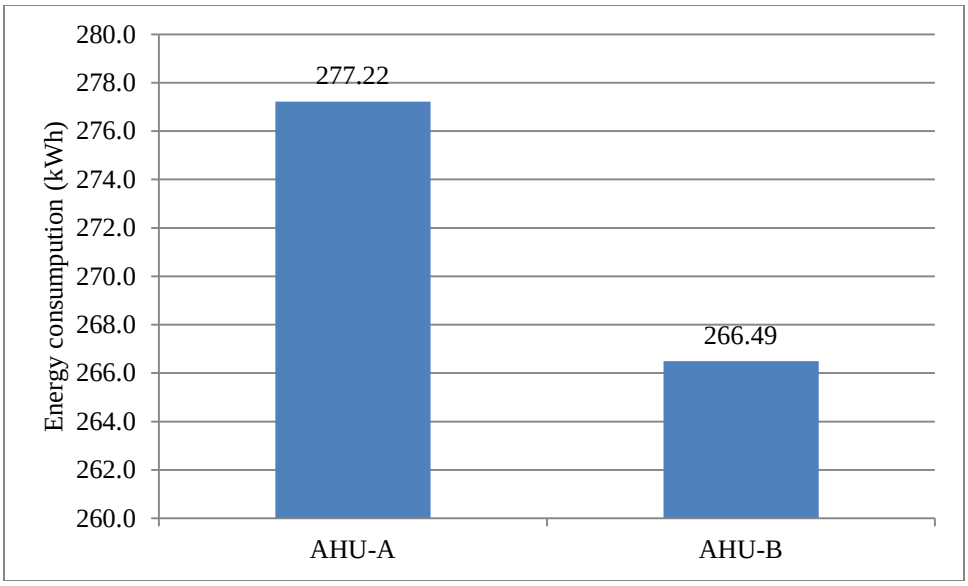

Figure 3.16 Comparison of energy consumption of AHU-A and AHU-B for the same set points at the second stage

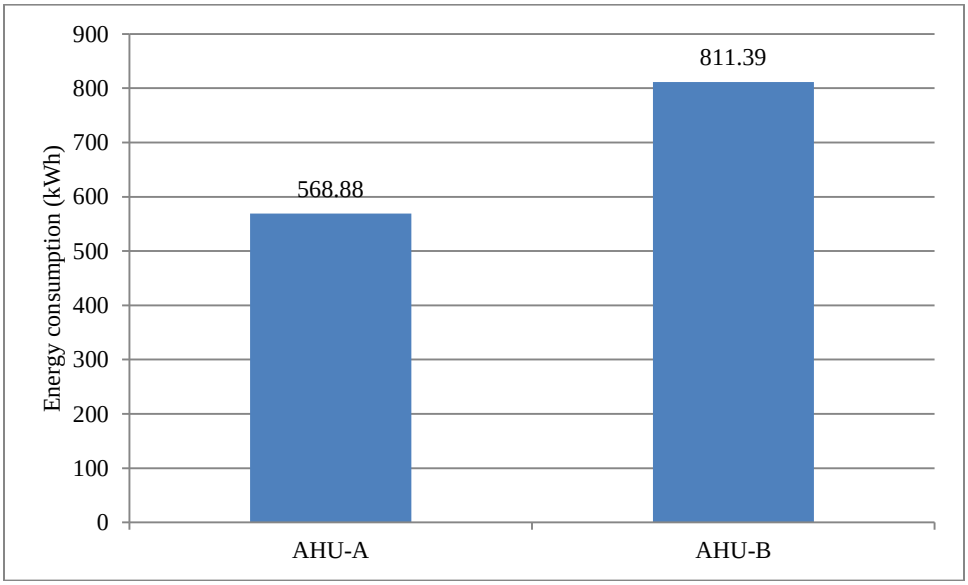

Figure 3.17 Comparison of the bias-adjusted energy consumption of AHU-A and AHU-B

3.6 Summary

In this chapter, the energy consumption of a heating ventilation and air conditioning (HVAC) system was optimized with a dynamic neural network. A model was built with data mining algorithms to optimize the controllable set points of the

HVAC system in order to provide energy savings while maintaining the room temperature within an acceptable range. Three modified multi-objective particle swarm optimization (MO-PSO) algorithms were applied to solve the optimization model. The computational results indicated that the multi-objective decreasing inertia weight particle swarm optimization (MO-DIWPSO) outperformed two other variants of the same algorithm. The MO-DIWPSO algorithm was implemented on the actual HVAC system. The experiments demonstrated that the optimization model saved 29.99% in energy consumption. Future research will focus on improving the accuracy of the model and approaches to improve handling of user preferences.

CHAPTER 4

CONTROLLING AN HVAC SYSTEM WITH SWARM INTELLIGENCE AND DATA-DRIVEN APPROACH

4.1 Introduction

In this chapter, a robust control strategy for an HVAC system, shown in Figure 4.1, is presented. A time-series approach is used to describe the system, and then a neural network is applied to develop a predictive model of energy consumption, which includes the energy consumed by chillers, pumps, fans, and reheating natural gas. The model involves optimization of two set points, the supply air static pressure and the supply air temperature, with a multi-objective particle swarm optimization algorithm. It is noted that the changes of the supply air temperature are constrained to small increments due to the considerable time needed to arrive at a steady state. In addition, the two set points minimize the energy consumption while maintaining the indoor temperature at an acceptable interval. To meet these requirements, a particle swarm optimization algorithm is integrated with fuzzy rules for solving the optimization models. The proposed approach has been validated on an industrial HVAC system.

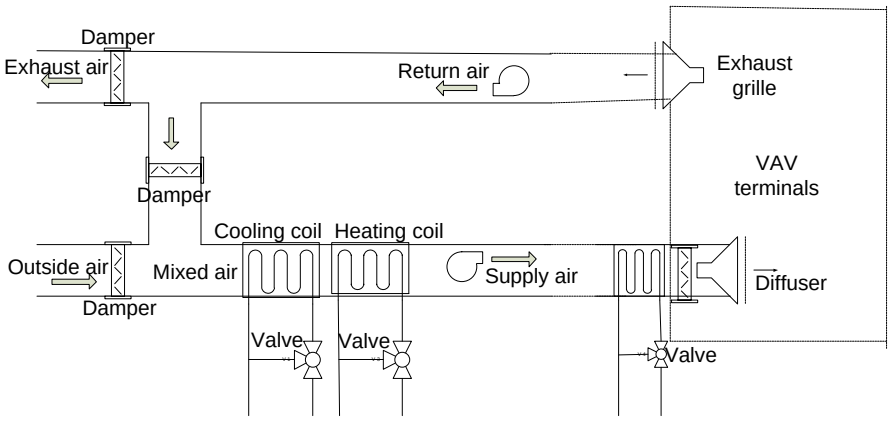

Figure 4.1 Schematic diagram of a typical HVAC system

4.2 Data Description

The data set in this research was obtained from an experiment conducted by the Energy Resource Station (ERS) in Ankeny, Iowa, which is an energy laboratory for testing and demonstrating commercial HVAC systems. The experiment aimed to assess the relationship between the states of the HVAC system, such as energy consumption and indoor temperature, and two of the system's controllable set points – supply air static pressure set point (SA-SPSPT) and supply air temperature set point (SAT-SPT). In particular, SA-SPSPT varied from 0.4 in. WG (0.1 kPa) to 1.8 in. WG (0.45 kPa) with 0.2 in. WG (0.05 kPa) increments; whereas SAT-SPT varied from 50 ℉ (10 ℃) to 65 ℉ (18.33 ℃) at 1 ℉ (0.556 ℃) increments over the course of the experiment. Corresponding to the change of the two set points, more than 300 parameters, including weather conditions, energy consumption, and indoor temperature, was recorded at 1-minute intervals by sensors installed in the systems. The data was collected July 31–August 16, 2009; September 21 – October 7, 2009; August 17 – September 6, 2010; and June 22 to July 27, 2011, respectively. Table 4.1 describes the experimental data in detail. The data set used in this research uses a 30-min sampling interval. It was derived from the originally collected 1-min data.

Table 4.1 Description of data sets

Number of data set	Data Set Type	Time Period	Number of Instances
1	Entire data set	07/31-08/15/2010; 09/21-10/07/2010; 08/01-09/06/2010; 06/22-07/27/2011	3532
2	Training data set	Randomly selected from data set 1	2472
3	Test data set	Randomly selected from data set 1	529
4	Validation data set	Randomly selected from data set 1	527

4.3 Control of the HVAC System

In this research, the HVAC system is controlled by adjusting supply air duct static pressure set point (SASP-SPT) and supply air temperature set point (SAT-SPT); however, the working characteristics of the chillers and fans contribute to the time lag needed for the actual supply air duct static pressure and supply air temperature to achieve the values dictated by the set points. Figure 4.2 indicates that the time for the actual supply air temperature entering a steady state of the new set point, in the case of 65 ℉ to 50 ℉, would be about 12 minutes while the case of 50 ℉ to 65 ℉, about 32 minutes. Unlike supply air temperature, supply air duct static pressure can achieve a steady state much faster (see Figure 4.3).

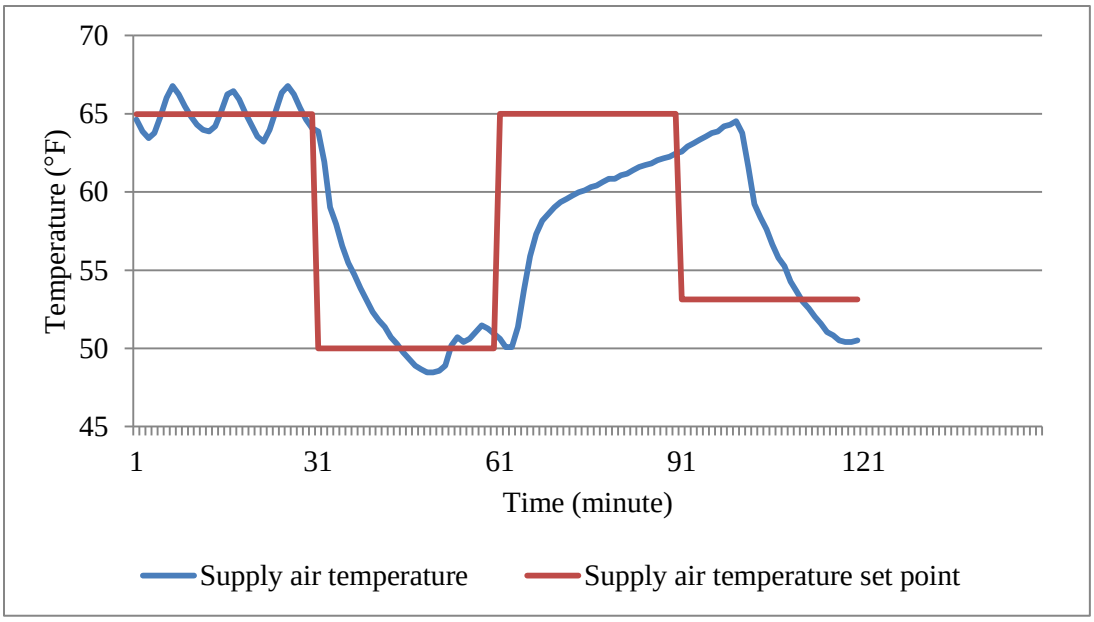

Figure 4.2 Set point and actual supply air temperature

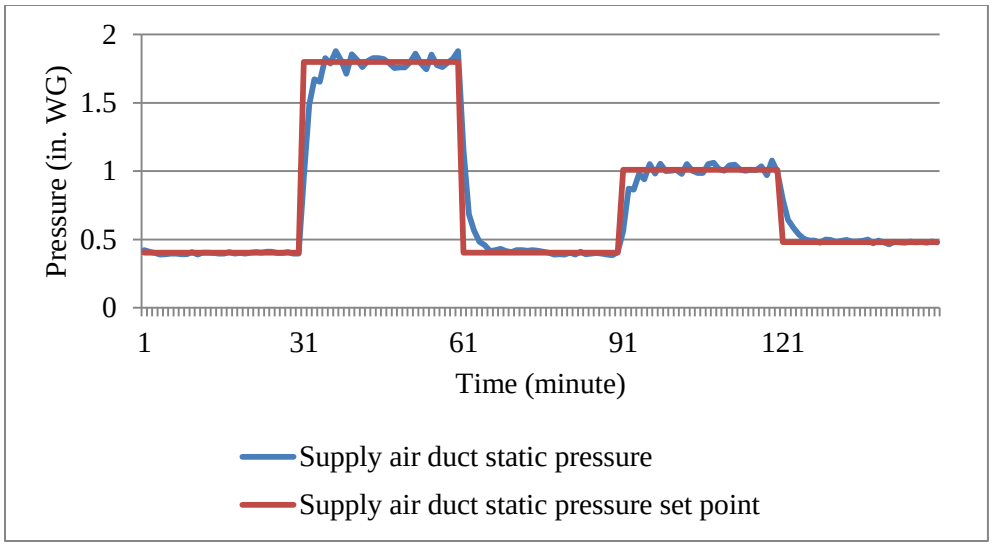

Figure 4.3 Set point and actual static pressure in supply air duct

To mitigate the impact of the time lag of the supply air temperature, a control strategy combining a data-driven approach and a rule-based particle swarm optimization is used in this research. As illustrated in Figure 4.4, two predictive models (i.e., the energy consumption prediction model and the indoor temperature prediction model) are built by data mining algorithms. The two models are then used in the optimization model.

To mitigate the impact of the system time lag on achieving a steady state, two approaches are applied:

- The supply air temperature changes once per hour, while the supply air duct static pressure set point changes every 30 min (the energy consumption is predicted 1-time increment and 2-time increments ahead for the same value of the supply air temperature, while the indoor temperature is predicted 1-time increment and 2-time increments ahead for different values of the supply air duct static pressure set point);
- A set of rules is used by the particle swarm optimization algorithm to reduce the increments for updating the supply air temperature set point.

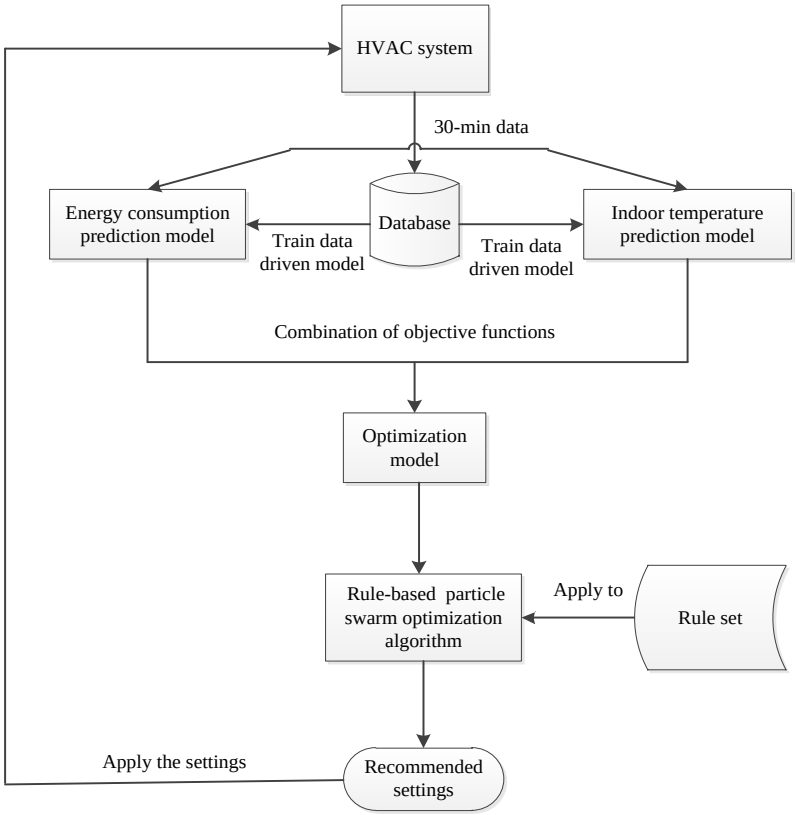

Figure 4.4 Diagram of the HVAC system control

In this research, fuzzy logic [60, 61] is used to model the supply air temperature set point. Based on the domain knowledge and expert experience, intervals of the parameter used by fuzzy rules are defined (see Table 4.2). Figures 4.5 and 4.6 illustrate the membership functions for the supply air temperature set point and the indoor temperature, respectively. For instance, if the current supply air temperature is 55 ℉ (13 ℃) and the current indoor temperature is 69 ℉ (21 ℃), the following rule listed in Table II is fired: IF SAT-SPT IS medium AND indoor temperature IS medium, THEN the change interval for next SAT-SPT IS [-3, 3]. The fuzzy transformation process is expressed in Equation (4.1).

$$|x_{SAT-SPT}(t+T) - x_{SAT-SPT}(t)| = F(x_{SAT-SPT}(t), y_{TEMP}(t)) \quad (4.1)$$

Table 4.2 Rules for deciding the intervals of the supply air temperature set point

Parameter	Low Indoor Temperature	Medium Indoor Temperature	High Indoor Temperature
Low SAT-SPT	[-10, 10]	[-6, 6]	[-3, 3]
Medium SAT-SPT	[-6, 6]	[-3, 3]	[-6, 6]
High SAT-SPT	[-3, 3]	[-6, 6]	[-10,10]

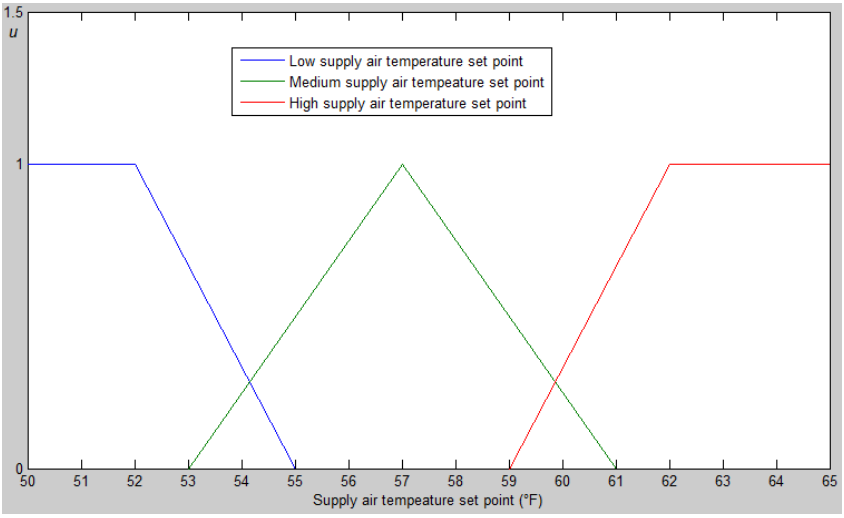

Figure 4.5 The membership function of the supply air temperature set point

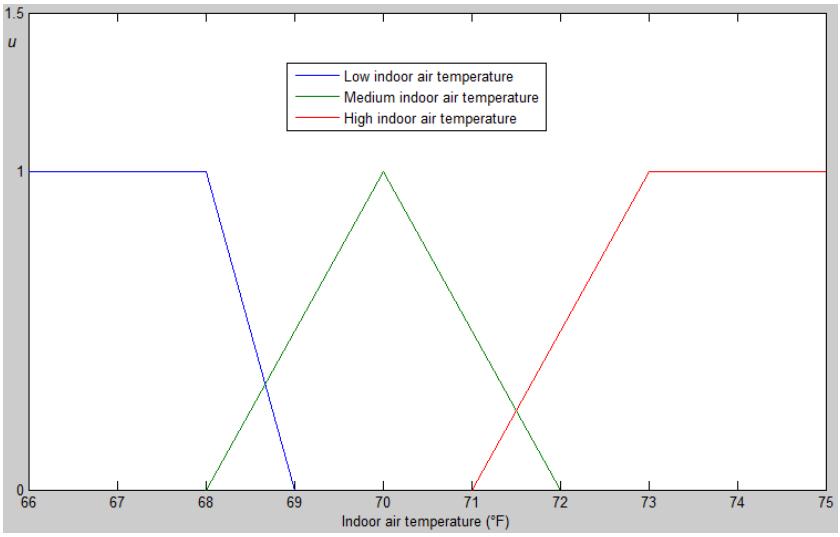

Figure 4.6 The membership function of the indoor temperature

4.4 Model Development

4.4.1 Parameter selection

Before a predictive model is developed, it is essential to select most important parameters to ensure comprehensibility, scalability, and accuracy of the resulting models [48]. The boosting tree algorithm is applied for parameter selection as it has demonstrated good performance [49]. Tables 4.3 and 4.4 include the parameters used as the inputs to the energy consumption prediction model and the indoor temperature prediction model selected by the correlation coefficient analysis approach and the boosting tree algorithm.

Table 4.3 Parameters selected for building the energy consumption model

Parameter	Parameter Name	Description	Unit
y_{Energy}	Energy Consumption	HVAC-consumed Energy in 30 min	kWh
$x_{SASP-SPT}$	SASP-SPT	Supply air duct static pressure set point	in.WG (kPa)
$x_{SAT-SPT}$	SAT-SPT	AHU supply air temperature set point	℉ (℃)
$v_{OAI-TEMP}$	OAI-TEMP	Outside air inlet temperature	℉ (℃)
$v_{CHWC-VLV}$	CHWC-VLV	Chilled water coil valve position	% Open
$v_{MA-TEMP}$	MA-TEMP	Mixed air temperature	℉ (℃)
$v_{CHWC-MWT}$	CHWC-MWT	Chilled water coil mixed water temperature	℉ (℃)
$v_{IR-RADIA}$	IR-RADIA	Infrared radiation	B/h ft^2 (W/m^2)
$v_{OA-TEMP}$	OA-TEMP	Outside air temperature	℉ (℃)
$v_{SOL-HORZ}$	SOL-HORZ	Solar normal flux	B/h ft^2 (W/m^2)
v_{SA-CFM}	SA-CFM	Supply air fan speed	CFM
$v_{SA-HUMD}$	SA-HUMD	Supply air humidity	% RH
y_{TEMP}	RM-TEMP	Indoor temperature	℉ (℃)

4.4.2 Predictive model formulation

A typical HVAC system includes components such as fans, cooling coil, heating coil, humidifier, filter and ductwork. Due to the physical properties of these components

and the structure of the building, HVAC is a dynamic, complex, and time-delayed system. A time-series approach – namely, nonlinear auto-regression with external inputs – is applied to model the dynamic HVAC system. In model development, 1-time increment and 2-time increment predictions are adopted. The boosting tree algorithm is also applied to determine the time lag of each parameter and to decide the time increment with the greatest impact on the system state. The energy consumption and the indoor temperature prediction models are expressed in Equations (4.2) - (4.5).

$$\begin{aligned} y_{Energy}(t+T) = f_1(&x_{SASP-SPT}(t+T), x_{SAT-SPT}(t+T), y_{Energy}(t), y_{Energy}(t-T), \\ &y_{TEMP}(t), v_{CHWC-VLV}(t), v_{CHWC-VLV}(t-T), v_{SA-CFM}(t), \\ &v_{OAI-TEMP}(t), v_{OAI-TEMP}(t-T), v_{OAI-TEMP}(t-2T), v_{MA-TEMP}(t), \\ &v_{MA-TEMP}(t-T), v_{CHWC-MWT}(t), v_{CHWC-MWT}(t-T), v_{IR-RADIA}(t), \\ &v_{IR-RADIA}(t-T), v_{OA-TEMP}(t), v_{OA-TEMP}(t-T), v_{SOL-HORZ}(t), \\ &v_{SOL-HORZ}(t-T), v_{SA-HUMD}(t)) \end{aligned} \tag{4.2}$$

$$\begin{aligned} y_{Energy}(t+2T) = f_2(&x_{SASP-SPT}(t+2T), x_{SAT-SPT}(t+2T), y_{Energy}(t+T), y_{Energy}(t), \\ &y_{TEMP}(t), v_{CHWC-VLV}(t), v_{CHWC-VLV}(t-T), v_{SA-CFM}(t), \\ &v_{OAI-TEMP}(t), v_{OAI-TEMP}(t-T), v_{OAI-TEMP}(t-2T), v_{MA-TEMP}(t), \\ &v_{MA-TEMP}(t-T), v_{CHWC-MWT}(t), v_{CHWC-MWT}(t-T), v_{IR-RADIA}(t), \\ &v_{IR-RADIA}(t-T), v_{OA-TEMP}(t), v_{OA-TEMP}(t-T), v_{SOL-HORZ}(t), \\ &v_{SOL-HORZ}(t-T), v_{SA-HUMD}(t)) \end{aligned} \tag{4.3}$$

$$\begin{aligned} y_{TEMP}(t+T) = f_3(&x_{SASP-SPT}(t+T), x_{SAT-SPT}(t+T), y_{TEMP}(t), y_{TEMP}(t-T), \\ &y_{Temp}(t-2T), y_{Energy}(t), v_{OAI-CFM}(t), v_{OAI-CFM}(t-T), \\ &v_{OAI-CFM}(t-2T), v_{RA-TEMP}(t), v_{RA-TEMP}(t-T), v_{RA-TEMP}(t-2T), \\ &v_{SA-CFM}(t), v_{SA-CFM}(t-T)) \end{aligned} \tag{4.4}$$

$$\begin{aligned} y_{TEMP}(t+2T) = f_4(&x_{SASP-SPT}(t+2T), x_{SAT-SPT}(t+2T), y_{TEMP}(t+T), y_{TEMP}(t), \\ &y_{Temp}(t-T), y_{Energy}(t), v_{OAI-CFM}(t), v_{OAI-CFM}(t-T), \\ &v_{OAI-CFM}(t-2T), v_{RA-TEMP}(t), v_{RA-TEMP}(t-T), v_{RA-TEMP}(t-2T), \\ &v_{SA-CFM}(t), v_{SA-CFM}(t-T)) \end{aligned} \tag{4.5}$$

Table 4.4 Parameters selected for building the indoor temperature model

Parameter	Parameter Name	Description	Unit
y_{TEMP}	RA-TEMP	Indoor temperature	℉ (℃)
$x_{SASP-SPT}$	SASP-SPT	Supply air duct static pressure set point	in.WG (kPa)
$x_{SAT-SPT}$	SAT-SPT	AHU supply air temperature set point	℉ (℃)
y_{Energy}	Energy consumption	Energy consumed by HVAC systems in 30 min	kWh
v_{SA-CFM}	SA-CFM	Supply air fan speed	CFM
$v_{RA-TEMP}$	RA-TEMP	Return air temperature	℉ (℃)
$v_{OAI-CFM}$	OAI-CFM	Outside air injection air flow	CFM

The multi-layer perception (MLP) ensemble approach is used to build predictive models of energy consumption and indoor temperature. Since it has supervised-learning pattern recognition and parallel distributed processing ability, MLP can approximate system with complex and nonlinear problems. The MLP ensemble performs better than other algorithms, such as the chi-squared automatic interaction detector (CHAID), classification and regression tree (C&RT) algorithm, support vector machine (SVM), boosting tree, random forest, and the multivariate adaptive regression spline (MARSpline) algorithm [31]. To derive the model expressed in Equations (4.2)-(4.5), data set 1 (3,532 data instances) was divided into three parts: a training data set (2,472 data instances), a test data set (529 data instances), and a validation data set (527 data instances).

4.4.3 Model validation

The fourth metrics in Chapter 2 (Equations (2.17) – (2.22)) are also applied here to validate the predictive models in the above section. The data in Table 4.5 illustrates performance of the energy consumption and the indoor temperature models built by the MLP ensemble algorithm. The MAPE values for the indoor temperature prediction model in Table V indicate satisfactory accuracies of 99.6% and 99.3% using the predictive

models for 1-time increment and 2-time increment predictions, respectively. The MAPE value of the energy consumption for 1-time increment predictions is 92.3% for validation data set. The 2-time increment prediction of energy consumption is 88.2% accurate. As shown in Figures 4.7-4.10, the correlation coefficients between the predicted values and the corresponding observed values are 0.965, 0.937, 0.976, and 0.951 for energy consumption 1-time increment and 2-time increment models, indoor temperature 1-time increment and 2-time increment models, respectively. Therefore, the four predictive models, including the 1-time increment and 2-time increment predictions, are employed to construct the overall HVAC system optimization model.

Table 4.5 Performance of the MLP ensemble models of energy consumption and indoor temperature

Objective		Data Set	MAE	MAPE	Std_AE	Std_APE
Energy consumption	1	Train	141.2	0.067	130.1	0.119
		Test	167.5	0.076	181.25	0.099
		Valid.	213.4	0.083	311.0	0.200
	2	Train	196.9	0.093	189.8	0.126
		Test	213.3	0.114	284.3	0.294
		Valid.	211.7	0.118	254.2	0.418
Indoor Temperature	1	Train	0.263	0.004	0.310	0.004
		Test	0.263	0.004	0.294	0.004
		Valid.	0.298	0.004	0.343	0.005
	2	Train	0.447	0.006	0.474	0.007
		Test	0.422	0.006	0.417	0.006
		Valid.	0.474	0.007	0.467	0.006

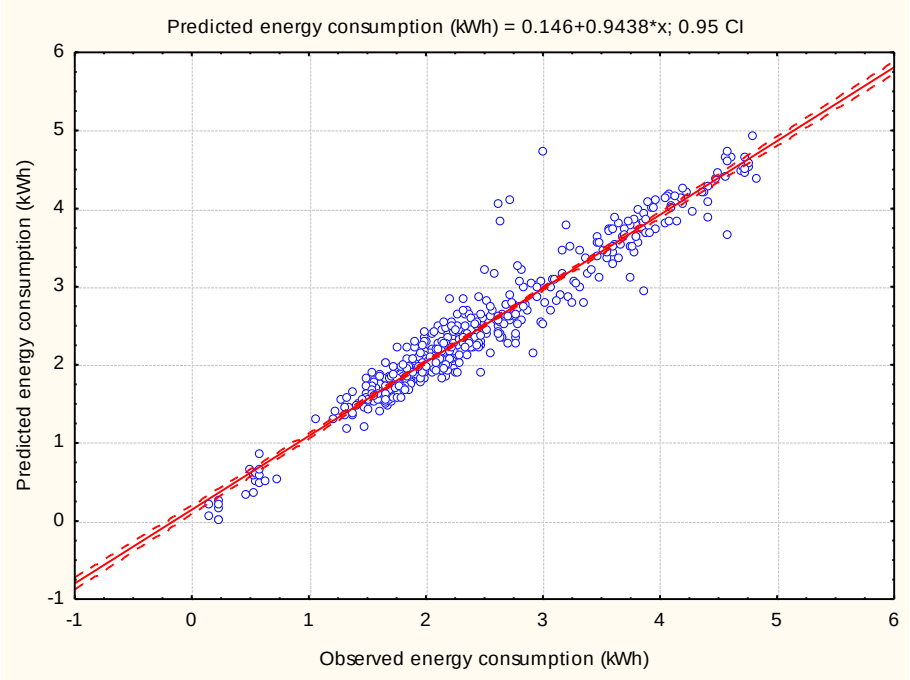

Figure 4.7 The correlation coefficient between predicted and observed values for 1-increment ahead prediction of energy consumption

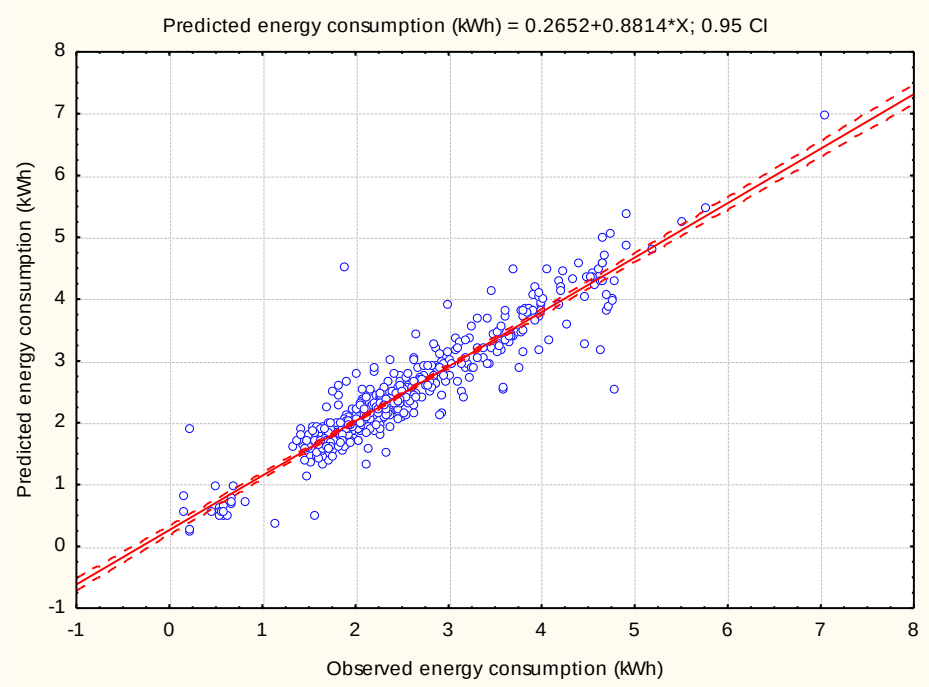

Figure 4.8 The correlation coefficient between predicted and observed values for 2-increment ahead prediction of energy consumption

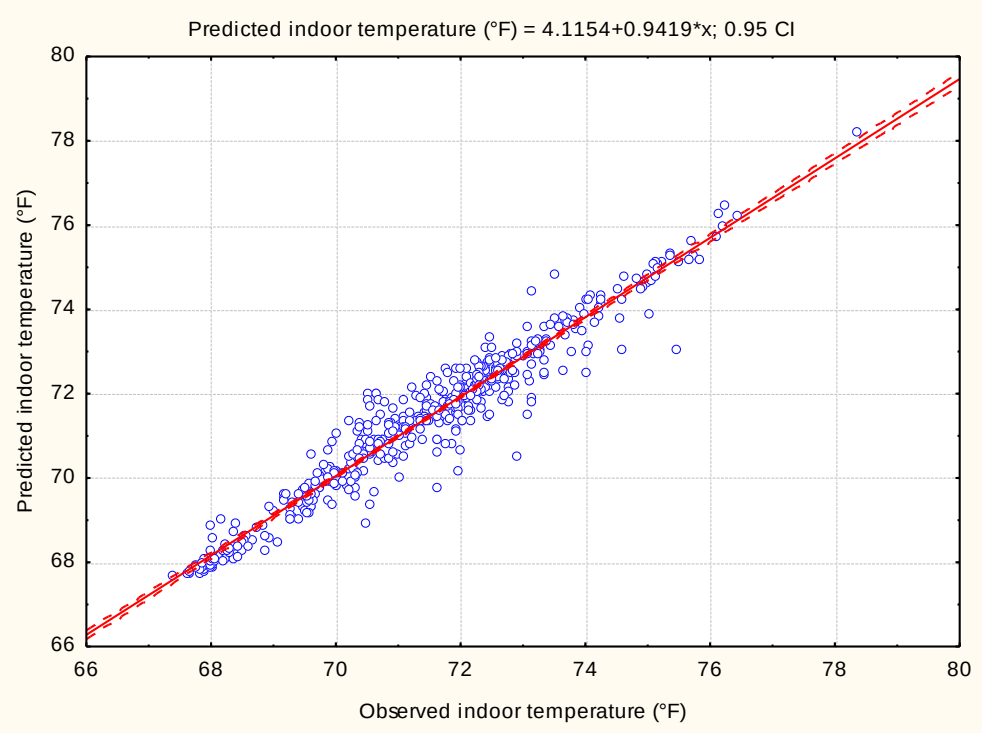

Figure 4.9 The correlation coefficient between predicted and observed values for 1-increment ahead prediction of indoor temperature

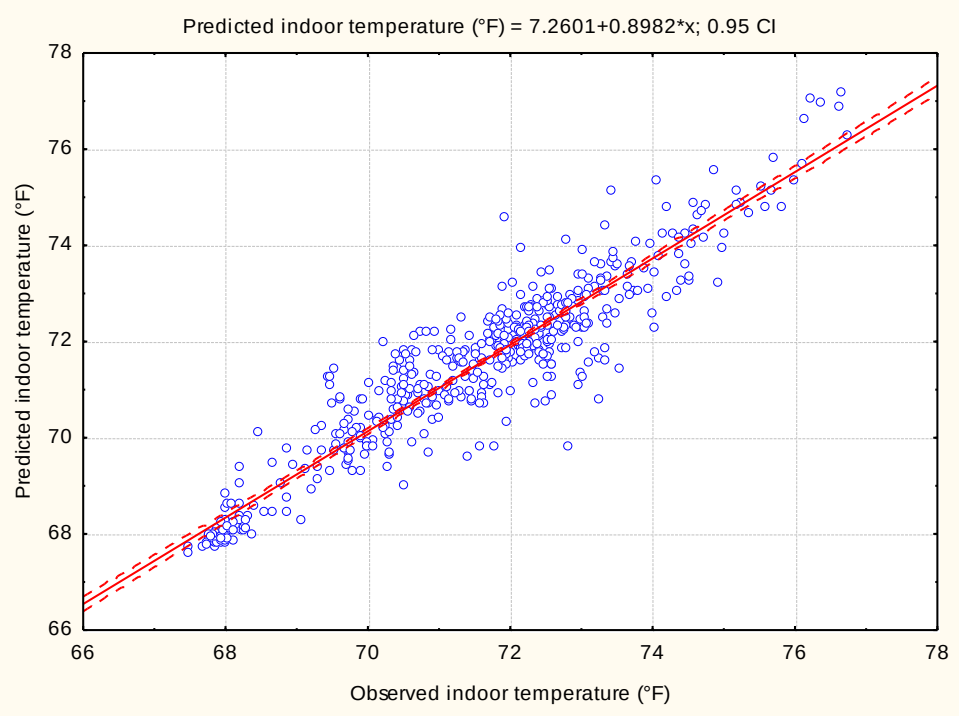

Figure 4.10 The correlation coefficient between predicted and observed values for 2-increment ahead prediction of indoor temperature

4.5 Multi-objective Optimization Model

4.5.1 Optimization model formulation

To optimize and control the HVAC system, Equations (4.2) and (4.3) are used in the model objective. Equations (4.4) and (4.5) are used as the constraints. Two values of two set points – the supply air temperature set point and the supply air duct static pressure set point – at time t + T and t + 2T are the decision variables of the HVAC optimization model. Lower and upper bounds of the control parameters and the constraint functions are imposed as follows:

- The supply air temperature set point varies from 50 ℉ (10 ℃) to 65 ℉ (18.3 ℃);
- The change interval of the supply air temperature set point should refer to the fuzzy function expressed in Equation (4.1);
- The supply air duct static pressure set point varies between 0.6 in. WG (0.1 kPa) and 1.8 in. WG (0.45 kPa);
- The indoor temperature is maintained between 68 ℉ (20 ℃) and 72 ℉ (22.2 ℃).

The above four constraints depend on the actual design of the HVAC system and the preferences of the occupants. The constraints are classified as hard or soft constraints. Hard constraints need to always be respected, while soft constraints can, to some degree, be violated. The HVAC optimization model is expressed in (4.6)-(4.18). Note that (4.16) and (4.17) can be considered as soft constraints:

$$\min_{x_{SASP-SPT}(t+T),x_{SASP-SPT}(t+2T),x_{SAT-SPT}(t+T),x_{SAT-SPT}(t+2T)} y_{Energy}(t+T)+y_{Energy}(t+2T) \tag{4.6}$$

$$y_{Energy}(t+T) = f_1(x_{SASP-SPT}(t+T), x_{SAT-SPT}(t+T), y_{Energy}(t), y_{Energy}(t-T), y_{TEMP}(t), v_{CHWC-VLV}(t), v_{CHWC-VLV}(t-T), v_{SA-CFM}(t), v_{OAI-TEMP}(t), v_{OAI-TEMP}(t-T), v_{OAI-TEMP}(t-2T), v_{MA-TEMP}(t), v_{MA-TEMP}(t-T), v_{CHWC-MWT}(t), v_{CHWC-MWT}(t-T), v_{IR-RADIA}(t), v_{IR-RADIA}(t-T), v_{OA-TEMP}(t), v_{OA-TEMP}(t-T), v_{SOL-HORZ}(t), v_{SOL-HORZ}(t-T), v_{SA-HUMD}(t))$$

Subject to: (4.7)

$$y_{Energy}(t+2T) = f_2(x_{SASP-SPT}(t+2T), x_{SAT-SPT}(t+2T), y_{Energy}(t+T), y_{Energy}(t), y_{TEMP}(t), v_{CHWC-VLV}(t), v_{CHWC-VLV}(t-T), v_{SA-CFM}(t), v_{OAI-TEMP}(t), v_{OAI-TEMP}(t-T), v_{OAI-TEMP}(t-2T), v_{MA-TEMP}(t), v_{MA-TEMP}(t-T), v_{CHWC-MWT}(t), v_{CHWC-MWT}(t-T), v_{IR-RADIA}(t), v_{IR-RADIA}(t-T), v_{OA-TEMP}(t), v_{OA-TEMP}(t-T), v_{SOL-HORZ}(t), v_{SOL-HORZ}(t-T), v_{SA-HUMD}(t)) \quad (4.8)$$

$$y_{TEMP}(t+T) = f_3(x_{SASP-SPT}(t+T), x_{SAT-SPT}(t+T), y_{TEMP}(t), y_{TEMP}(t-T), y_{Temp}(t-2T), y_{Energy}(t), v_{OAI-CFM}(t), v_{OAI-CFM}(t-T), v_{OAI-CFM}(t-2T), v_{RA-TEMP}(t), v_{RA-TEMP}(t-T), v_{RA-TEMP}(t-2T), v_{SA-CFM}(t), v_{SA-CFM}(t-T)) \quad (4.9)$$

$$y_{TEMP}(t+2T) = f_4(x_{SASP-SPT}(t+2T), x_{SAT-SPT}(t+2T), y_{TEMP}(t+T), y_{TEMP}(t), y_{Temp}(t-T), y_{Energy}(t), v_{OAI-CFM}(t), v_{OAI-CFM}(t-T), v_{OAI-CFM}(t-2T), v_{RA-TEMP}(t), v_{RA-TEMP}(t-T), v_{RA-TEMP}(t-2T), v_{SA-CFM}(t), v_{SA-CFM}(t-T)) \quad (4.10)$$

$$0.6 \le x_{SASP-SPT}(t+T) \le 1.8 \quad (4.11)$$

$$0.6 \le x_{SASP-SPT}(t+2T) \le 1.8 \quad (4.12)$$

$$50 \le x_{SAT-SPT}(t+T) \le 65 \quad (4.13)$$

$$50 \le x_{SAT-SPT}(t+2T) \le 65 \quad (4.14)$$

$$x_{SAT-SPT}(t+T) = x_{SAT-SPT}(t+2T) \quad (4.15)$$

$$68 \le y_{TEMP}(t+T) \le 72 \quad (4.16)$$

$$68 \le y_{TEMP}(t+2T) \le 72 \quad (4.17)$$

$$x_{SAT-SPT}(t) - F(x_{SAT-SPT}(t), y_{TEMP}(t)) \le x_{SAT-SPT}(t+T) \le x_{SAT-SPT}(t) + F(x_{SAT-SPT}(t), y_{TEMP}(t)) \quad (4.18)$$

Where $y_{Energy}(t+T) + y_{Energy}(t+2T)$ is the sum of the predicted energy consumption at t + T and t + 2T, $y_{TEMP}(t+T)$ and $y_{TEMP}(t+2T)$ are the predicted values of indoor temperature at t + T and t + 2T. Applying the optimal supply air temperature set point $x_{SAT-SPT}(t+T) = x_{SAT-SPT}(t+2T)$ and the supply air duct static pressure set point $x_{SASP-SPT}(t+T)$ and $x_{SASP-SPT}(t+2T)$. In minimizing the energy consumption at time stamp t + T and t + 2T, the indoor temperature at time stamp t + T and t + 2T is maintained within a pre-set range. The constrained model (4.6)-(4.18) is transformed into a multi-objective optimization model with the objective functions (4.19)-(4.21) by converting the soft constraints into objective functions:

$$Obj1 = y_{Energy}(t+T) + y_{Energy}(t+2T) \quad (4.19)$$

$$Obj2 = \max\{0, 68 - y_{Energy}(t+T)\} + \max\{0, y_{Energy}(t+T) - 72\} \quad (4.20)$$

$$Obj3 = \max\{0, 68 - y_{Energy}(t+2T)\} + \max\{0, y_{Energy}(t+2T) - 72\} \quad (4.21)$$

The multi-objective optimization model is presented in (4.22). Note that, when Obj2 and Obj3 are equal 0, constraints (4.11)-(4.18) are all satisfied:

$$\min_{x_{SASP-SPT}(t+T),x_{SASP-SPT}(t+2T),x_{SAT-SPT}(t+T),x_{SAT-SPT}(t+2T)} (Obj1, Obj2, Obj3)$$

subject to:

$$\begin{aligned}
y_{Energy}(t+T) = f_1(&x_{SASP-SPT}(t+T), x_{SAT-SPT}(t+T), y_{Energy}(t), y_{Energy}(t-T),\\
&y_{TEMP}(t), v_{CHWC-VLV}(t), v_{CHWC-VLV}(t-T), v_{SA-CFM}(t),\\
&v_{OAI-TEMP}(t), v_{OAI-TEMP}(t-T), v_{OAI-TEMP}(t-2T), v_{MA-TEMP}(t),\\
&v_{MA-TEMP}(t-T), v_{CHWC-MWT}(t), v_{CHWC-MWT}(t-T), v_{IR-RADIA}(t),\\
&v_{IR-RADIA}(t-T), v_{OA-TEMP}(t), v_{OA-TEMP}(t-T), v_{SOL-HORZ}(t),\\
&v_{SOL-HORZ}(t-T), v_{SA-HUMD}(t))\\
\widehat{y_{Energy}}(t+2T) = f_2(&x_{SASP-SPT}(t+2T), x_{SAT-SPT}(t+2T), \widehat{y_{Energy}}(t+T), y_{Energy}(t),\\
&y_{TEMP}(t), v_{CHWC-VLV}(t), v_{CHWC-VLV}(t-T), v_{SA-CFM}(t),\\
&v_{OAI-TEMP}(t), v_{OAI-TEMP}(t-T), v_{OAI-TEMP}(t-2T), v_{MA-TEMP}(t),\\
&v_{MA-TEMP}(t-T), v_{CHWC-MWT}(t), v_{CHWC-MWT}(t-T), v_{IR-RADIA}(t),\\
&v_{IR-RADIA}(t-T), v_{OA-TEMP}(t), v_{OA-TEMP}(t-T), v_{SOL-HORZ}(t),\\
&v_{SOL-HORZ}(t-T), v_{SA-HUMD}(t))\\
\widehat{y_{TEMP}}(t+T) = f_3(&x_{SASP-SPT}(t+T), x_{SAT-SPT}(t+T), y_{TEMP}(t), y_{TEMP}(t-T),\\
&y_{Temp}(t-2T), y_{Energy}(t), v_{OAI-CFM}(t), v_{OAI-CFM}(t-T),\\
&v_{OAI-CFM}(t-2T), v_{RA-TEMP}(t), v_{RA-TEMP}(t-T), v_{RA-TEMP}(t-2T),\\
&v_{SA-CFM}(t), v_{SA-CFM}(t-T))\\
\widehat{y_{TEMP}}(t+2T) = f_4(&x_{SASP-SPT}(t+2T), x_{SAT-SPT}(t+2T), \widehat{y_{TEMP}}(t+T), y_{TEMP}(t),\\
&y_{Temp}(t-T), y_{Energy}(t), v_{OAI-CFM}(t), v_{OAI-CFM}(t-T),\\
&v_{OAI-CFM}(t-2T), v_{RA-TEMP}(t), v_{RA-TEMP}(t-T), v_{RA-TEMP}(t-2T),\\
&v_{SA-CFM}(t), v_{SA-CFM}(t-T))
\end{aligned} \tag{4.22}$$

$$0.6 \le x_{SASP-SPT}(t+T) \le 1.8$$

$$0.6 \le x_{SASP-SPT}(t+2T) \le 1.8$$

$$50 \le x_{SAT-SPT}(t+T) = x_{SAT-SPT}(t+2T) \le 65$$

$$x_{SAT-SPT}(t) - F(x_{SAT-SPT}(t), y_{TEMP}(t)) \le x_{SAT-SPT}(t+T)$$
$$\le x_{SAT-SPT}(t) + F(x_{SAT-SPT}(t), y_{TEMP}(t))$$

4.5.2 Multi-objective rule-based particle swarm optimization algorithm

The HVAC optimization model derived from data-driven approach is non-parametric and non-convex complex and therefore cannot be easily solved by traditional gradient-descent-based algorithms. Rather, a particle swarm optimization (PSO) algorithm inspired by the social behavior of flocks of birds and schools of fish is used [62]. To solve multi-objective optimization problems, the general single objective PSO

algorithm is extended to multi-objective PSO algorithm by integrating a Pareto optimal set. Since the Pareto optimal set includes many non-dominated solutions, the leader in the general single objective PSO has to be changed. In MOPSO, every non-dominated solution can be considered as a new leader, then one leader is selected using a quality measure reflecting the goodness of the leader. The nearest neighbor density estimator is used as the quality measure. It corresponds to the perimeter of the cuboid formed by the nearest neighbors as the vertices. The larger value of the perimeter is preferred. An external archive is used in MOPSO to retain non-dominated solutions. A solution enters the archive provided that it meets the following two standards:

- It is non-dominated with respect to the content of the archive or
- It dominates all the solutions in the archive.

The steps of the MOPSO are shown next:

Begin
Initialize swarm in the search space R^n
Initialize leaders in an external archive *A*
Quality leaders
gen = 0
While *gen* < *gen_max*
For each particle
Select leader
Update position
Evaluation
Update *pbest*
EndFor
Update leaders in the external archive
Quality leaders
gen = *gen* + 1
EndWhile
Report results in the external archive
End

To control the HVAC system, the rules shown in Table 4.2 are embedded in a multi-objective particle swarm optimization, thus leading to the multi-objective rule-based particle swarm optimization (MORBPSO) algorithm. These rules manage the

update interval of the supply air temperature set point. The steps of MORBPSO are as follows:

Begin
Initialize search space based on rule set *S*
Initialize swarm in the search space R^n
Initialize leaders in an external archive *A*
Quality leaders
gen = 0
While *gen* < *gen_max*
For each particle
Select leader
Update position
Evaluation
Update *pbest*
EndFor
Update leaders in the external archive
Quality leaders
gen = gen + 1
EndWhile
Report results in the external archive

End

4.6 Computational Results

4.6.1 Representative points used in optimization

In this section, the multi-objective rule-based PSO algorithm is demonstrated with the nine representative points selected from the validation data set of Table 4.1. Each of these nine representative points listed in Table 4.6 reflects one of the rules listed in Table 4.2. Since the multi-objective rule-based PSO algorithm provides a set of non-dominated solutions, a user-defined weight vector is applied to the non-dominated solutions. The weighted normalized objective function is expressed in Equation (4.23):

$$OBJ = w_1 \frac{OBJ1 - OBJ1_{\min}}{OBJ1_{\max} - OBJ1_{\min}} + w_2 \frac{OBJ2 - OBJ2_{\min}}{OBJ2_{\max} - OBJ2_{\min}} + w_3 \frac{OBJ3 - OBJ3_{\min}}{OBJ3_{\max} - OBJ3_{\min}} \quad (4.23)$$

Where ω_1, $\omega_2$and $\omega_3$are the user-defined weights indicating the preference of the corresponding objective, and $OBJ1_{max}$ and $OBJ1_{min}$ are the maximum and the minimum values of the final non-dominated set. Similar notation is used for $OBJ2_{max}$, $OBJ2_{min}$, $OBJ3_{max}$, and $OBJ3_{max}$. Note that $w_1 + w_2 + w_3 = 1$, with w_1, w_2 *and* w_3 being either constants or functions of other objectives. In this chapter, three scenarios listed in Table 4.7 are considered to demonstrate the impact of the user preferences on the optimized solutions. Figure 4.11 shows a comparison between the observed energy consumption and the optimized one at *t* + *T* and *t* + *2T*. It indicates that in most cases, the optimized energy consumption for three scenarios have the same values. This is because the corresponding optimized indoor temperature falls between 68 ℉ (20 ℃) and 72 ℉ (22.2 ℃) as shown in Figures 4.12 – 4.13, and in this situation the values of Obj1 and Obj2 are zero. Therefore, in the three scenarios, only the energy consumption is optimized; however, for data points 2 and 4, the optimized indoor temperature is outside the 68 ℉ (20 ℃) - 72 ℉ (22.2 ℃) interval. As the user-defined weights vary for the three scenarios, the corresponding optimal solutions differ. As shown in Figure 4.11 and Table 4.7, the higher the weight assigned to the indoor temperature, the smaller the energy savings. For example, for data point 2, the optimized energy consumption for scenario 1, 2, and 3 is 4.04, 4.80, and 5.16 kWh, respectively.

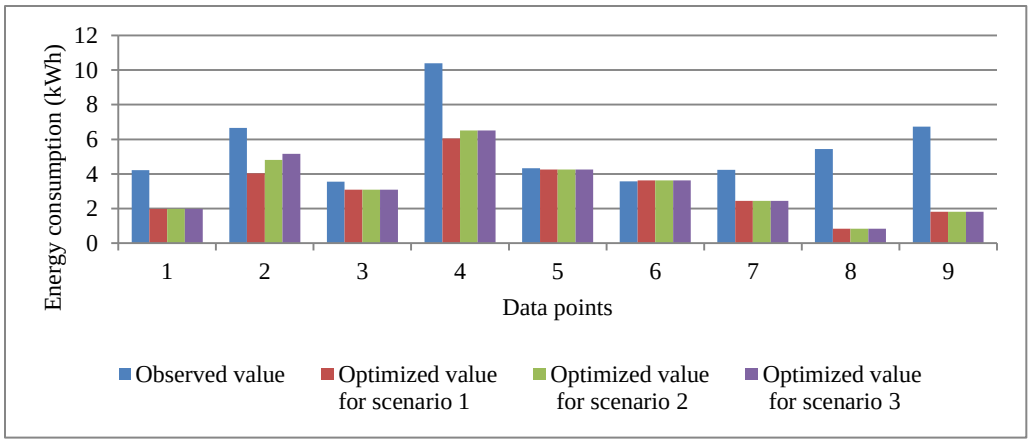

Figure 4.11 The observed and optimized energy consumption for the three scenarios

Table 4.6 Nine representative points selected from the validation data set

No.	Current SAT-SPT	Current Indoor Temp.	Energy ($t + T$)	Energy ($t + 2T$)	Indoor Temp. ($t + T$)	Indoor Temp. ($t + 2T$)
1	55	67.9	2119.2	2098.2	68	68
2	55	72.7	2805.6	3857.4	72.4	72.5
3	55	70.5	1596.1	1954.3	69.7	71.6
4	50.2	71.9	4527.4	5850	71.9	72.7
5	50.2	70.4	1830.8	2487	72.0	72.1
6	64.9	72.1	2393.1	2301.1	71.6	70.9
7	64.9	70.8	2865.7	1363.7	69.9	68.5
8	61.1	68.1	1994.3	3431.2	71.2	73
9	53	68	2461.2	4273.6	71.6	70.7

Table 4.7 Three weight scenarios for energy consumption and indoor temperature preference

Scenario No.	Weight assigned to energy at $t + T$ and $t + 2T$	Weight assigned to indoor temperature at $t + T$	Weight assigned to indoor temperature at $t + 2T$
1	1	0	0
2	0.4	0.3	0.3
3	0	0.5	0.5

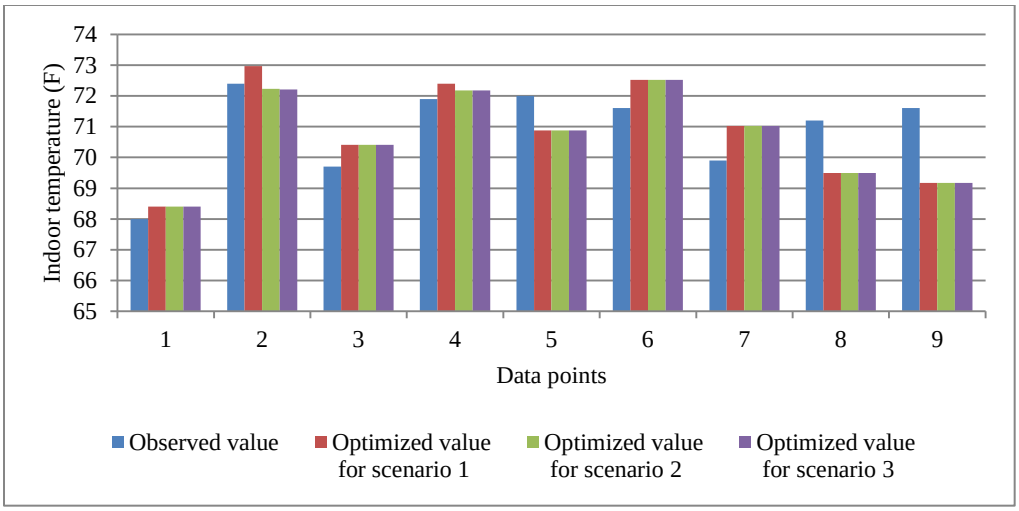

Figure 4.12 The observed and optimized indoor temperature at time $t + T$ for the three scenarios

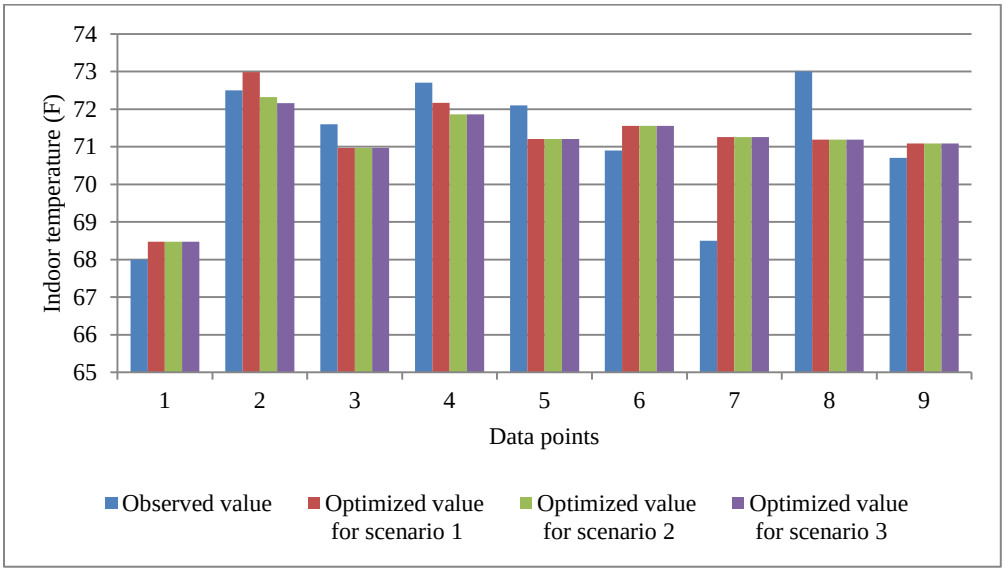

Figure 4.13 The observed and optimized indoor temperature at time $t + 2T$ for the three scenarios

4.6.2 Optimization of multiple data points

In this section, 100 data points from the validation data set in Table 4.1 are selected to demonstrate performance of the multi-objective rule-based PSO algorithm, and three scenarios from Table 4.7 are considered. Figure 4.14 compares the sum of

observed and optimized energy consumption of the 100 points for these three scenarios. Note that the energy consumption in Figure 4.14 is expressed as the sum of energy at time increments: t + T and t + 2T. The optimized energy consumption in scenario 1 is the lowest as this scenario considers only the energy consumed while choosing the optimized solution from the non-dominated set; however, since scenario 3 is only concerned with indoor temperature, the corresponding optimized energy consumption is the highest. The optimization algorithm, therefore, saves 34.4%, 28.5%, and 26.2% for scenarios 1, 2, and 3, respectively. Figures 4.15 – 4.16 illustrate the indoor room temperature at t + T and t + 2T for the three scenarios. In most cases, the indoor temperature remains within the desired interval from 68 ℉ (20 ℃) to 72 ℉ (22.2 ℃), in the three scenarios. In a limited number of cases, the indoor temperature falls outside of the desired interval. The optimization algorithm selects different values for each of the three scenarios based on the weights. Figures 4.17 – 4.18 illustrate the recommended set points for scenario 3, which is concerned with the indoor temperature violating the constraint.

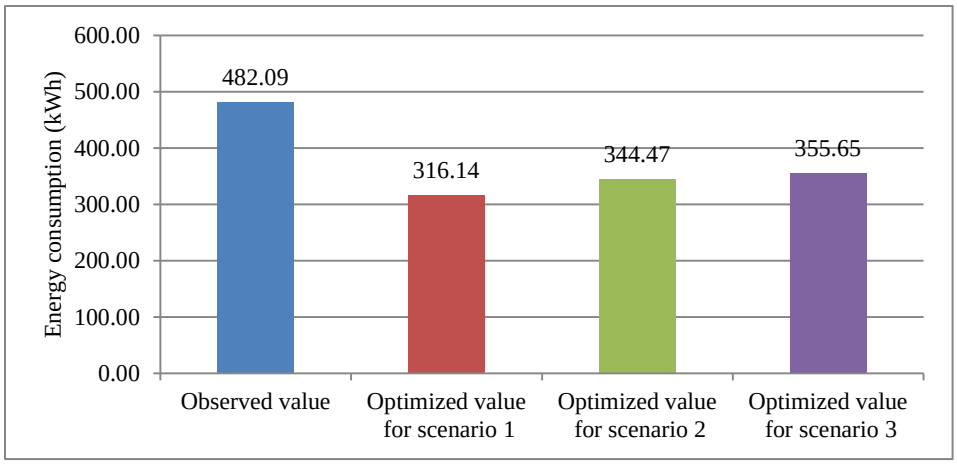

Figure 4.14 The sum of the observed and optimized energy consumption of the 100 points for the three scenarios

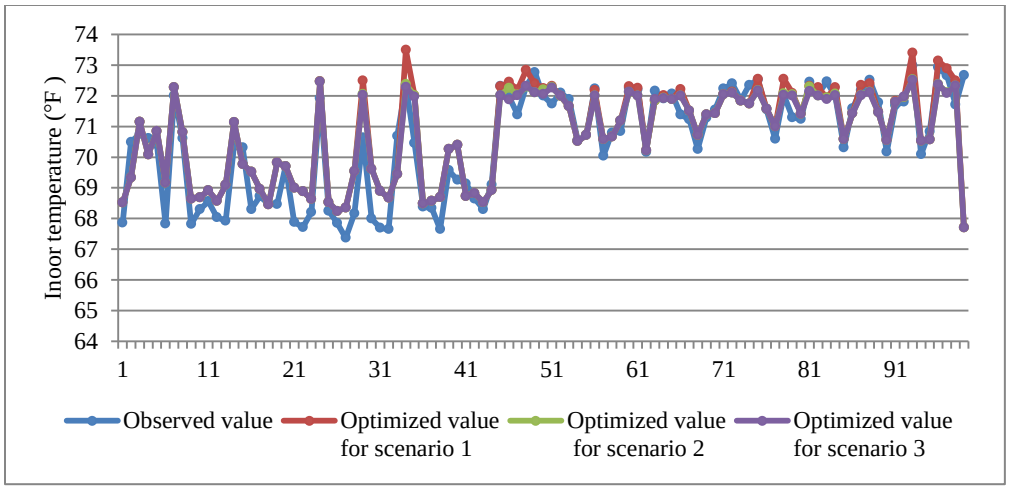

Figure 4.15 The observed and optimized indoor temperature at time $t + T$ for the three scenarios

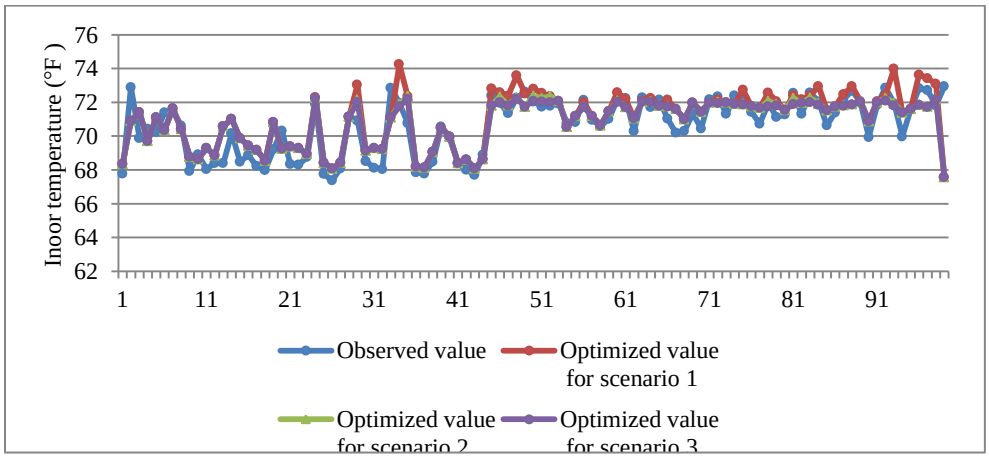

Figure 4.16 The observed and optimized indoor temperature at $t + 2T$ for the three scenarios

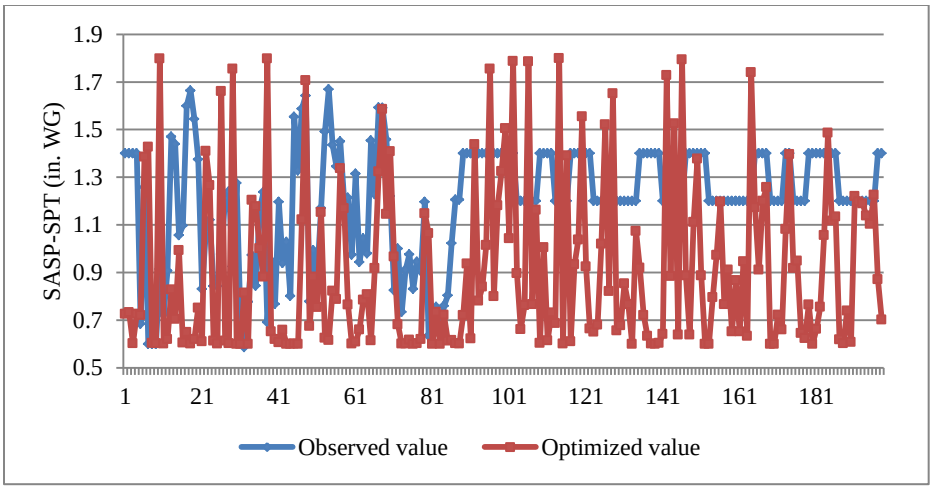

Figure 4.17 The recommended set point of the supply air static pressure at $t + T$ and $t + 2T$

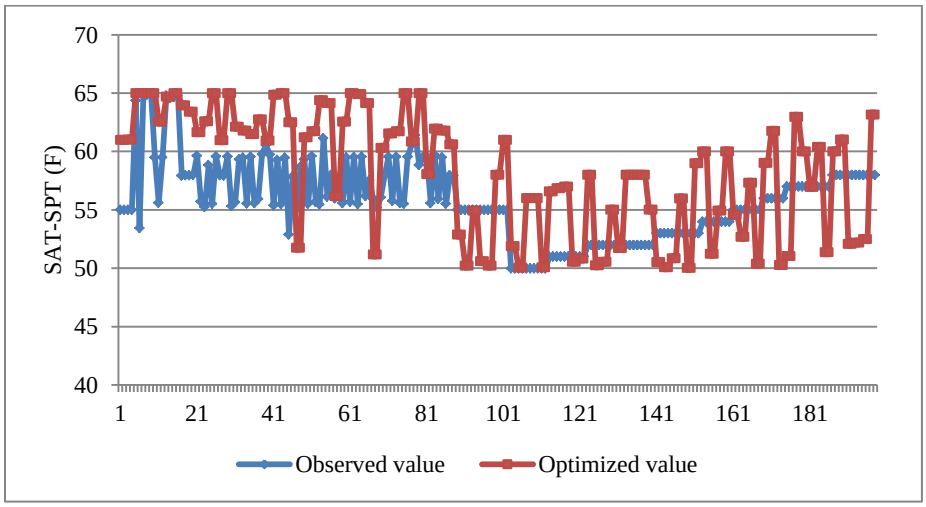

Figure 4.18 The recommended set point of the supply air temperature at $t + T$ and $t + 2T$

4.7 Summary

In this chapter, a model was developed to optimize energy consumption of an HVAC system. The model and an optimization algorithm were applied on an industrial-grade HVAC system. To control the system, a set of rules updating the set points was integrated into the optimization algorithm. An experiment was designed to collect data utilized to build, train, and validate the optimization model. Computational experience

with representative single- and multi-point case studies demonstrated that energy savings ranging from 26.2% to 34.4% can be achieved by the proposed data-driven approach. The approximate 8% margin of energy savings is determined by the user comfort preferences.

CHAPTER 5

CONCLUSION

A data-driven methodology to model heating, ventilating, and air-conditioning (HVAC) systems was studied. It included analysis of experimental data, parameter selection, building HVAC models, and investigating optimization of system performance by considering energy consumption and thermal comfort. The research reported in the Thesis shed light on a new perspective of saving energy in building energy area.

In Chapter 2, a predictive model and a simulation model were built. The predictive model was used to predict the energy consumption and indoor temperature of an HVAC system, while the simulation model is to simulate the HVAC system behavior. Then the predictive model was converted to an optimization model. A nonlinear interior-point algorithm was employed to optimize the proposed optimization model. A comparison between the optimized and simulated result was analyzed in the end.

In Chapter 3, a time series based neural network was applied to build models for an HVAC system. After converting the data-approach model into an optimization model, three multi-objective particle swarm optimization algorithm were proposed and the best one was chosen to solve the optimization model. The proposed data-driven approach was implemented and was proved to save energy up to 30%.

In Chapter 4, a robust control strategy for an HVAC system was presented. A time series approach was used to describe the system and neural network was employed to build models with two set points as controllable variables. A fuzzy rule was adopted to control the set points in the model when applying a multi-objective particle swarm optimization algorithm to solve the optimization model. The proposed approach was validated with two cases: representative single data points and multiple data points.

One of the challenges for future research is to develop hybrid model based on the combination of physical equations and data-driven approach. Some components which have simple physical principle can apply mathematical equation to describe. For the

complex process, data-driven approach can be utilized to simplify the description without sacrificing accuracy.

REFERENCES

[1] L. Perez-lombard, J. Ortiz, and C. Pout, "A review on buildings energy consumption information," *Energy and Buildings*, American Society of Mechanical Engineers, Solar Energy Division (Publication) SED, Vol. 40, No. 3, pp. 394-398, 2008.

[2] W. Huang, M. Zaheeruddin, and S. H. Cho, "Dynamic simulation of energy management control functions for HVAC systems in buildings," *Energy Conversion and Management*, Vol. 47, No. 7-8, pp. 926-943, 2006.

[3] F. Tang, "HVAC system modeling and optimization: a data-mining approach", thesis, University of Iowa, 2010.

[4] F. C. Winkelmann and S. Selkowitz , "Daylighting simulation in the DOE-2 building energy analysis program," *Energy and Buildings*, Vol. 8, No. 4, pp. 271-286, 1985.

[5] P. Cui, H. Yang, J. D. Spitler, and Z. Fang, "Simulation of hybrid ground-coupled heat pump with domestic hot water heating systems using HVACSIM+," *Energy and Buildings*, Vol. 40, No. 9, pp. 1731-1736, 2008.

[6] Y. P. Zhou, J. Y. Wu, R. Z. Wang, S. Shiochi, and Y. M. Li, "Simulation and experimental validation of the variable-regrigerant-volume (VRV) air-conditioning system in EnergyPlus," *Energy and Buildings*, Vol. 40, No. 6, pp. 1041-1047, 2008.

[7] T. P. McDowell, J. W. Thornton, S. Emmerich, and G. Walton, "Integration of airflow and energy simulation using CONTAM and TRNSYS," *ASHRAE Transactions*, Vol. 109, No. 1, pp. 1-14, 2003.

[8] E. F. Sowell and P. Haves, "Efficient solution strategies for building energy system simulation," *Energy and Buildings*, Vol. 33, pp. 309-317, 2001.

[9] D. B. Crawley, J. W. Hand, M. Kummert, and B. T. Griffith, "Contrasting the capabilities of building energy performance simulation programs," *Building and Environment*, Vol. 43, No. 4, pp. 661-673, 2008.

[10] F. W. Yu and K. T. Chan, "Condensing temperature control to enhance the efficiency of air-cooled chillers," *Builing Services Engineering Research & Technology*, Vol. 25, No. 4, pp. 279-294, 2004.

[11] W. Z. Huang, M. Zaheeruddin, and S. H. Cho, "Dynamic simulation of energy management control functions for HVAC systems in buildings," *Energy Conversion and Management*, Vol. 47, No. 7-8, pp. 926-943, 2006.

[12] J. A. Clarke, J. Cockroft, S. Conner, J. W. Hand, N. J. Kelly, R. Moore, T. O'Brien, and P. Strachan, "Simulation-assisted control in building energy management systems," *Energy and Buildings*, Vol. 34, No. 9, pp. 933-940, 2002.

[13] X. D. He, S. Liu, and H. H. Asada, "Modeling of vapor compression cycles for multivariable feedback control of HVAC systems," *Journal of Dynamic Systems, Measurement, and Control*, Vol. 119, No. 2, pp. 183-191, 1997.

[14] Y. W. Wang, W. J. Cai, Y. C. Soh, S. J. Li, L. Lu, and L. Xie, "A simplified modeling of cooling coils for control and optimization of HVAC systems," *Energy Conversion and Management*, Vol. 45, No. 18-19, pp. 2915-2930, 2004.

[15] G. Y. Jin, W. J. Cai, L. Lu, E. L. Lee, and A. Chiang, "A simplified modeling of mechanical cooling tower for control and optimization of HVAC systems," *Energy Conversion and Management*, Vol. 48, No. 2, pp. 355-365, 2007.

[16] B. Yu and A. H. C. van Paassen, "Simulink and bond graph modelling of an air-conditioned room," *Simulation Modeling Practice and Theory*, Vol. 12, No. 1, pp. 61-76, 2004.

[17] A. K. Sen and J. Darabi, "Modeling and optimization of a microscale capacitive humidity sensor for HVAC applications," *IEEE Sensors Jounral*, Vol. 8, No. 4, pp. 333-340, 2008.

[18] M. Liu and D. E. Claridge, "Use of calibrated HVAC system models to optimize system operation," *Journal of Solar Energy Engineering*, Vol. 120, No. 2, pp. 131-138, 1998.

[19] G. R. Zheng, "Dynamic modeling and global optimal operation of multizone variable air volume HVAC systems," thesis, Concordia University, 1997.

[20] M. R. Kulkarni and F. Hong, "Energy optimal control of a residential space-conditioning system based o sensible heat transfer modeling," *Building and Environment*, Vol. 39, No.1, pp. 31 – 38, 2004.

[21] G. Platt, J. Li, R. Li, G. Poulton, G. James, and J. Wall, "Adaptive HVAC zone modeling for sustainable buildings," *Energy and Buildings*, Vol. 42, No. 4, pp. 412-421, 2010.

[22] B. Tashtoush, M. Molhim, and M. Al-Rousan, "Dynamic model of an HVAC system for control analysis," *Energy*, Vol. 30, No. 10, pp. 1729-1745, 2005.

[23] D. F. Specht, "A general regression neural network," *IEEE Transaction on Neural Network*, Vol. 2, No. 6, pp. 568 – 576, 1991.

[24] L. K. Hansen and P. Salamon, "Neural network ensembles," *IEEE Transaction on Pattern Analysis and Machine Intelligence*, Vol. 12, No. 10, pp. 993-1001, 1990.

[25] S. Katipamula, T. A. Reddy, and D. E. Claridge, "Multivariate regression modeling," *Journal of Solar Energy Engineering*, Vol. 120, No. 3, pp. 177-184, 1998.

[26] A. Abbassi and L. Bahar, "Application of neural network for the modeling and control of evaporative condenser cooling load," *Applied Thermal Engineering*, Vol. 25, No. 17-18, pp. 3176-3186, 2005.

[27] J. Teeter and M. Y. Chow, "Application of functional link neural network to HVAC thermal dynamic system identification," *IEEE Transactions on Industrial Electronics*, Vol. 45, No. 1, pp. 170-176, 1998.

[28] S. Soyguder and H. Alli, "An expert system for the humidity and temperature control in HVAC systems using ANFIS and optimization with fuzzy modeling approach," *Energy and Buildings*, Vol. 41, No. 8, pp. 814-822, 2009.

[29] X. C. Xi, A. N. Poo, and S. K. Chou, "Support vector regression model predictive control on a HVAC plant," *Control Engineering Practice*, Vol. 15, No. 8, pp. 897-908, 2007.

[30] M. Kumar and I. N. Kar, "Non-linear HVAC computations using least square support vector machines," *Energy Conversion and Management*, Vol. 50, No. 6, pp. 1411-1418, 2009.

[31] A. Kusiak, M. Y. Li, and Z. Zhang, "A data-driven approach for steam-load prediction in buildings," *Applied Energy*, Vol. 87, No. 3, pp. 925-933, 2010.

[32] A. Andrew and M. Y. Li, "Cooling output optimization of an air handling unit," *Applied Energy*, Vol. 87, No. 3, pp. 901-909, 2010.

[33] A. Kusiak and M. Y. Li, "Reheat optimization of the variable-air-volume box," *Energy*, Vol. 35, No. 5, pp. 1997-2005, 2010.

[34] A. Kusiak, M. Y. Li, and F. Tang, "Modeling and optimization of HVAC energy consumption," *Applied Energy*, Vol. 87, No. 10, pp. 3092-3102, 2010.

[35] A. Kusiak, M. Y. Li, and H. Y. Zheng, "Virtual models of indoor-air-quality sensors," *Applied Energy*, Vol. 87, No. 6, pp. 2087-2094, 2010.

[36] J. Kennedy and R. Eberhart, "Particle swarm optimization," *Proceedings of IEEE International Conference on Neural Networks*, Vol. 4, pp. 1942-1948, 1995.

[37] K. Deb, A. Pratap, S. Agarwal, and T. Meyarivan, "A fast and elitist multiobjective genetic algorithm: NSGA-II," *IEEE Transactions on Evolutionary Computation*, Vol. 6, No. 2, pp. 182-197, 2002.

[38] M. Dorigo, M. Birattari, and T. Stutzle, "Ant colony optimization," *IEEE Computational Intelligence Magazine*, Vol. 1, No. 4, pp. 28-39, 2006.

[39] J. A. Wright, H. A. Loosemore, and R. Farmani, "Optimization of building thermal design and control by multi-criterion genetic algorithm," *Energy and Buildings*, Vol. 34, No. 9, pp. 959-972, 2002.

[40] L. Lu, W. Cai, L. Xie, S. Li, and Y. C. Soh, "HVAC system optimization—in building section," *Energy and Buildings*, Vol. 37, No. 1, pp. 11-22, 2005.

[41] K. F. Fong, V. I. Hanby, and T. T. Chow, "HVAC system optimization for energy management by evolutionary programming," *Energy and Buildings*, Vol. 38, No. 3, pp. 220-231, 2006.

[42] M. Hadjiski, V. Sgurev, and V. Boishina, "HVAC control via hybrid intelligent systems," *Cybernetics and Information Technologies*, Vol. 7, No. 1, pp. 77-94, 2007.

[43] K. F. Fong, V. I. Hanby, T. T. Chow, "System optimization for HVAC energy management using the robust evolutionary algorithm," *Applied Thermal Engineering*, Vol. 29, No. 11-12, pp. 2327-2334, 2009.

[44] A. J. Ardakani, F. F. Ardakani, and S. H. Hosseinian, "A novel approach for optimal chiller loading using particle swarm optimization," *Energy and Buildings*, Vol. 40, No. 12, pp. 2177-2187, 2008.

[45] R. J. Vanderbei and D. F. Shanno, "An interior-point algorithm for nonconvex nonlinear programming," *Computational Optimization and Applications*, Vol. 13, No. 1, pp. 231-252, 1997.

[46] D. F. Shanno and R. J. Vanderbei, "Interior methods for nonconvex nonlinear programming: orderings and higher-order methods," *Mathematical Programming*, Vol. 87, No. 2, pp. 301-316, 2000.

[47] F. E. Curtis, O. Schenk, and A. Wachter, "An interior-point algorithm for large-scale nonlinear optimization with inexact step computations," *SIAM Journal on Scientific Computing*, Vol. 32, No. 6, pp. 3447-3475, 2010.

[48] J. Wang. *Data Mining: Opprortunities and Challenges*. North Sydney: Idea Group. 2003.

[49] J. Friedman. *Stochastic gradient boosting*. Stanford University Statistics Department, 1999.

[50] T. Hastie, R. Tibshirani, and J. H. Friedman. *The Elements of Statistical Learning*. New York: Springer, 2001.

[51] F. Rosenblatt. Principles of Neurodynamics: Perceptron and the Theory of Brain Mechanisim. Washington DC: Spartan Books, 1961.

[52] G. Casella and R. Berger. *Statistical Inference*. Pacific Grove, CA: Duxbury Press, 1990.

[53] J. Nocedal and S. J. Wright. *Numerical Optimization*. New York: Springer, 1999.

[54] K. S. Narendra and K. Parthasarathy, "Identification and control of dynamical systems using neural network," *IEEE Transactions on Neural Network*, Vol. 1, No. 1, pp. 4-27, 1990.

[55] A. U. Levin and K. S. Narendra. "Control of nonlinear dynamical systems using neural network: controllability and stabilization," *IEEE Transactions on Neural Network*, Vol. 4, No. 2, pp. 192-206, 1993.

[56] A. U. Levin and K. S. Narendra, "Control of nonlinear dynamical systems using neural network – part II: observability, identification, and control," *IEEE Transactions on Neural Network*, Vol. 7, No. 1, pp. 30-42, 1996.

[57] J. Maria, P. Menezes Jr., and G. A. Barreto, "Long-term time series prediction with the NARX network: An empirical evaluation," *Neurocomputing*, Vol. 71, No. 16-18, pp. 3335-3343, 2008.

[58] R. Poli, J. Kennedy, and T. Blackwell, "Particle swarm optimization: An overview," *Swarm Intelligence*, Vol. 1, No. 1, pp. 33-57, 2007.

[59] M. A. Abido, "Two-level of non-dominated solutions approach to multi-objective particle swarm optimization," in *Genetic and Evolutionary Computation Conference*, 2007, pp. 726-733.

[60] L. A. Zadeh, "Fuzzy sets," *Information and Control*, Vol. 8, pp. 338-353, 1965.

[61] T. J. Ross. *Fuzzy logic with engineering application*. Chichester: Wiley, 2004.

[62] M. Reyes-Sierra and C. A. Coello, "Multi-objective particle swarm optimizer: A survey of the state-of-art," *Internal Journal of Computational Intelligence Research*, Vol. 2, pp. 287-308, 2006.